UNIVERSITÀ
DEGLI STUDI
DI PADOVA

Head Office: Università degli Studi di Padova

Department of Cardiac, Thoracic, Vascular Sciences and Public Health

Ph.D. COURSE IN TRANSLATIONAL SPECIALISTIC MEDICINE "G. B. MORGAGNI"

CURRICULUM: Cardiovascular Sciences

SERIES XXXV

USE OF ZEBRAFISH MODELS FOR STUDYING ARRHYTHMOGENIC CARDIOMYOPATHY

Coordinator: Ch.mo Prof.ssa Annalisa Angelini

Supervisor: Ch.mo Prof.ssa Cristina Basso

Co-Supervisor: Ch.mo Prof.ssa Natascia Tiso

Ph.D. student: Dott. Giovanni Risato

INDEX

ABSTRACT

Arrhythmogenic Cardiomyopathy (AC) is a rare inherited cardiac disorder characterized by fibro-fatty replacement and progressive loss of the ventricular myocardium causing life-threatening arrhythmias, syncope and sudden cardiac death in young and athletes. Based on genotype-phenotype correlation, the spectrum of the AC phenotype was shown to be broader than previously believed. About 50% of AC cases carry one or more mutations in genes encoding for desmosomal proteins, including Desmoplakin (Dsp). However, also mutations in non-desmosomal genes have been identified in 1-3% of AC patients, such as Galcetin-3 (Gal-3), recently associated with the disease. I present here a stable Dsp knock-out (KO) zebrafish line able to model cardiac abnormalities and cell signalling dysregulation, characteristic of the AC disease, on which environmental factors and candidate drugs can be tested. In addition, I describe also a Gal-3 KO zebrafish line that reproduces the correlated cardiac phenotype and other observed dysregulations, for a better understanding of its role in AC pathogenesis. Our stable Dsp KO zebrafish line was characterized by structural abnormalities, pericardial effusion and/or hemopericardium, related with bradycardia and inflammatory response at larval stage. Histological analysis of mutated adult hearts showed reduced contractile structures and abnormal shape of the ventricle, with thinning of the myocardial layer, vessels dilation and adipose infiltration in the myocardium. Moreover, Transmission Electron Microscopy (TEM) analysis revealed “pale”, disorganized and delocalized desmosomes. Intensive physical training protocol caused a global worsening of the cardiac phenotype, accelerating the progression of the disease. Of note, we detected a dysregulation of the Wnt/β-catenin pathway, recently associated with AC pathogenesis. Pharmacological treatment of mutated larvae with SB216763, a Wnt/β-catenin agonist, rescued pathway expression and cardiac abnormalities, stabilizing the heart rhythm. The stable Gal-3 KO zebrafish line also presented a clear cardiac phenotype, like the Dsp mutant, showing the same types of structural changes associated with bradycardic phenotype, ventricular dilation and signalling pathway dysregulations. Cell death and inflammation were observed in the cardiac region of this mutant line, connecting it with these phases of the disease. Overall, our Dsp KO zebrafish line recapitulates many AC features

observed in human patients, pointing at zebrafish as a suitable system for *in vivo* analysis of environmental modulators, such as the physical exercise, and the screening of pathway-targeted drugs. The Gal-3 KO zebrafish line confirms also in zebrafish the strict connection between mutations in this gene and cardiac alterations, attributable to AC. Moreover, cell death and inflammation, known to be involved in the remodelling of the myocardium, were observed and place this model at the centre of future more in-depth studies of the pathogenesis of the disease.

RIASSUNTO

La cardiomiopatia aritmogena (AC) è una rara malattia cardiaca ereditaria caratterizzata da sostituzione fibro-adiposa e progressiva perdita del miocardio ventricolare, che causa aritmie potenzialmente letali, sincope e morte cardiaca improvvisa nei giovani e negli atleti. Sulla base della correlazione genotipo-fenotipo, lo spettro del fenotipo AC si è dimostrato più ampio di quanto si credesse in precedenza. Circa il 50% dei casi di AC presentano una o più mutazioni nei geni che codificano proteine desmosomiali, inclusa la Desmoplachina (Dsp). Tuttavia, nell'1-3% dei pazienti con AC sono state identificate anche mutazioni in geni non desmosomiali, come Galectina-3 (Gal-3), recentemente associata alla malattia. In questa tesi presento una linea zebrafish knock-out (KO) stabile mutata nel gene Dsp capace di riprodurre alterazioni morfo-funzionali cardiache e sregolazioni di vie di segnale, tipiche della malattia, su cui testare la possibile influenza di fattori ambientali e farmaci. Inoltre, descrivo anche una linea zebrafish KO per Gal-3 che presenta un particolare fenotipo cardiaco correlato ad AC e ad altre sregolazioni osservate, per cercare di comprendere meglio il suo ruolo nella patogenesi della malattia. La nostra linea di zebrafish Dsp KO ha presentato allo stadio larvale alterazioni cardiache, versamento pericardico e/o emopericardico, associati a un fenotipo bradicardico e una risposta infiammatoria. L'analisi istologica dei cuori adulti mutati ha mostrato strutture contrattili ridotte e forma anormale del ventricolo, con assottigliamento dello strato miocardico, dilatazione dei vasi e infiltrazione adiposa. Inoltre, l'analisi al microscopio ottico a trasmissione (TEM) ha rivelato desmosomi “pallidi”, disorganizzati e delocalizzati. Un allenamento fisico intensivo ha inoltre causato un peggioramento generale del fenotipo cardiaco, accelerando la progressione della malattia. Abbiamo infine rilevato una sregolazione della via Wnt/β-catenina, recentemente associata alla patogenesi dell'AC. Un trattamento farmacologico allo stadio larvale con SB216763, un agonista della via Wnt/β-catenina, ha mostrato un recupero dell’espressione della via e delle alterazioni cardiache, stabilizzando anche il ritmo cardiaco. Anche la linea stabile zebrafish KO per Gal-3 è stata contraddistinta da un chiaro fenotipo cardiaco, simile a quello della linea Dsp, mostrando gli stessi tipi di alterazioni associate ad un fenotipo bradicardico, alla dilatazione ventricolare e a sregolazioni

delle vie di segnale. La morte cellulare e l'infiammazione sono state osservate nella regione cardiaca di questa linea mutante, collegandola chiaramente a queste fasi della malattia. Nel complesso, la nostra linea zebrafish Dsp-KO ricapitola molte caratteristiche AC osservate nei pazienti umani, indicando questo modello come un sistema adatto per l'analisi *in vivo* di fattori ambientali, come l'esercizio fisico, e lo screening di farmaci. La linea zebrafish Gal-3-KO conferma la stretta connessione tra le mutazioni trovate in questo gene e le alterazioni cardiache attribuibili a AC. Inoltre, sono state osservate morte cellulare e infiammazione, notoriamente coinvolte nel rimodellamento del miocardio, che pongono questo modello al centro di futuri studi più approfonditi sulla patogenesi della malattia.

1. INTRODUCTION

1.1. Cardiomyopathies

In accordance with the American Heart Association (AHA), cardiomyopathies are defined as a heterogeneous group of diseases that affect the myocardium and are linked to mechanical and/or electrical dysfunctions; they often manifest as abnormal ventricular dilation or hypertrophy and are caused by several factors, many of which are genetics (Maron et al., 2006; McCartan et al., 2012). Initially, cardiomyopathies were classified as a cardiac muscle disorder of undetermined aetiology and considered separate from diseases due to known cause (Report of the WHO/ISFC task force on the definition and classification of cardiomyopathies, 1980; Goodwin, 1982; Marcus et al., 1982). These heart muscle pathologies were firstly divided into three groups based on their pathophysiological characteristics: dilated cardiomyopathy (DCM), hypertrophic cardiomyopathy (HCM) and restricted cardiomyopathy (RCM). Since this, significant advancements have made it necessary for this too basic categorization to include additional clinical entities such arrhythmogenic right ventricular dysplasia (ARVD) (Marcus et al., 1982; Thiene et al., 1988). Therefore, in 1995 the World Health Organization/International Society and Federation of Cardiology Task Force (WHO/ISFC) updated these clinical guidelines integrating the new ARVD, specific cardiomyopathies such as inflammatory cardiomyopathy and other still unclassified forms of the disease (Richardson et al., 1996). In 2006, the AHA divided cardiomyopathies into a more complete classification, composed of two main categories: primary cardiomyopathies (genetic, acquired, or mixed), in which the myocardium is involved primarily or exclusively, and secondary cardiomyopathies, in which myocardial defects are only a part of a widespread systemic disorders (**Table 1**) (Maron et al., 2006). However, it still might be challenging to distinguish between primary and secondary cardiomyopathies, since primary disorders can have extra-cardiac implications whereas secondary ones can primarily or completely affect the heart (Maron et al., 2006; Elliott et al., 2008).

Table 1: Summary of 2006 classification (AHA) (McCartan et al., 2012).

Primary cardiomyopathies	Secondary cardiomyopathies
Genetic (hypertrophic cardiomyopathy; conduction abnormalities: prolonged QT syndrome; Brugada syndrome)	Infiltrative (amyloidosis and Gaucher disease)
Mixed (dilated cardiomyopathy; restrictive cardiomyopathy)	Storage (haemochromatosis and Fabry's disease)
Acquired (inflammatory myocarditis, peripartum, stress cardiomyopathy—"broken heart syndrome" or tako-tsubo)	Toxicity (drugs, alcohol, heavy metals, and chemicals/chemotherapy)
	Inflammatory (sarcoidosis) endocrine (diabetes mellitus; thyroid disorders; hyperparathyroidism), cardiofacial (Noonan syndrome, lentiginosis) neuromuscular/neurological, nutritional deficiencies, and autoimmune and collagen disorders

Although several types of cardiomyopathies have been classified and put into these two main categories over years, ARVD, HCM, RCM, and DCM are still the four primary kinds (Maron et al., 2006; Elliott et al., 2008). At first, ARVD was identified using the word "dysplasia", supposing that was caused by a congenital cardiac development abnormality. Nevertheless, this wrong diagnosis was quickly overtaken by the term "cardiomyopathy", which refers to a hereditary heart muscle problem, due to the advancement of genetic and phenotypic characterization. Initially, the disease was thought to affect only the right ventricle, hence the name Arrhythmogenic Right Ventricular Cardiomyopathy (ARVC) (Thiene et al., 1988; Basso et al., 1996). Later, after the discovery of forms affecting the left ventricle or both ventricles, the name was changed to the more general Arrhythmogenic cardiomyopathy (AC), to summarize all phenotypic expressions of the disease (Sen-Chowdhry et al., 2008; Corrado et al., 2017). In light of the increased understanding of the genomic and molecular markers of these diseases, a novel approach based on the research of causative mutations, thought to be responsible for the disease's onset, had been proposed to overcome the criticized points in the previous classifications (Thiene et al., 2004; Maisch et al., 2012). Finally, in 2008 the European Society of Cardiology (ESC) defined "cardiomyopathy" as a myocardial disorder in which the heart muscle is structurally and functionally abnormal, in the absence of coronary artery disease, hypertension, valvular disease, and congenital heart disease sufficient to cause the observed myocardial phenotype (Elliott et al., 2008). Therefore, although the diagnosis of cardiomyopathies hardly begins with genetic screening and the mutations' identification, remains fundamental the genetic testing, which represents the base for this disease's prevention and treatment.

1.2. Arrhythmogenic cardiomyopathy

Arrhythmogenic cardiomyopathy (AC) (OMIM #107970; ORPHA247) is an inherited cardiac disorder characterized pathologically by progressive replacement of cardiomyocytes by fibrous and adipose tissue, starting from the epicardium and extending toward the endocardium (Thiene et al., 1988; Basso et al., 1996). Because of this transmural damage, thinning of the ventricular wall occurs with overt dilation of the cardiac chambers, myocardial atrophy, aneurysms, syncope, palpitations, prominent ventricular arrhythmias and impairment of ventricular systolic function that can lead to sudden cardiac death (SCD) in young people and athletes (Nava et al., 1988; Thiene et al., 1988; Basso et al., 1996, 2009, 2011). Physical exercise and competitive sports activity may in fact trigger life-threatening ventricular arrhythmias and accelerate the disease progression and the risk of SCD in patients with AC (Zorzi et al., 2021). Although the clinical physiology of this syndrome was reported four years earlier in France (Frank et al., 1978), Marcus and colleagues are credited with first describing this disorder in 1982. They identified 24 patients with significant replacement of the right ventricular (RV) myocardium by fatty and fibrous tissue (Marcus et al., 1982). This progressive loss of ventricular myocardial tissue causes the isolation of healthy cardiomyocytes within the fibro-adipose matrix, causing problems and alterations in depolarization and re-polarization of the cell membrane. From a histopathological point of view, two forms that differ in the type of tissue that replaces the myocardium are known: the adipose variant, in which adipose tissue prevails and ventricular wall thickness is normal or increased; the fibro-adipose variant in which both fibrous and adipose tissue are present with a thinner ventricular wall (Basso et al., 2006).

1.3. Epidemiology

The prevalence of AC in the population is approximately 1 case per 2000-5000 (Nava et al., 2000; Corrado and Thiene, 2006; Basso et al., 2009, 2011). However, this frequency could be an underestimation due to difficulty or errors in diagnosis (Thiene et al., 2007). This pathology was initially considered an endemic disease in Italy, especially in Veneto region, due to higher frequency with respect to the

worldwide population (20% vs 10 - 15%), estimated around 1:1000 through a deeper analysis of the causes of SCD mostly in young people and athletes (Thiene et al., 1988; Corrado et al., 2017). This meticulous, systematic investigation of SCD cases in this geographic region could erroneously lead to thinking of AC as a uniquely Venetian (or Italian) disease, somehow changing the perception of AC as a worldwide equally distributed pathology. Nowadays, AC is acknowledged in other countries as well and is readily recognizable in the population from many ethnic backgrounds. For example, in Netherlands there are large cohorts that share founder mutations, and the tracking of mutant haplotypes revealed the mutations presence also in North America. The majority of patients in the United States are white, although there are some people of Asian and African heritage in well-defined cohorts. Interestilngy, the first case of AC was identified in South America as part of a syndrome, named Carvajal syndrome, which also included palmoplantar keratoderma and woolly hair. Other nonsyndromic forms of AC are also found in Asia and Africa. (Corrado et al., 2017). It most frequently manifests clinically in the second to fourth decades of life (Nava et al., 2000; Basso et al., 2009, 2011) but, less commonly, symptoms might develop prior to puberty or in older people. Although the classical clinical symptoms can occasionally appear in individuals above the age of 70, the diagnosis is frequently overlooked because clinicians fail to recognize this morbid entity in this later age range (Basso et al., 2009). Males develop AC up to three times more frequently than females, which has been linked to either sex-related differences in exercise volume and intensity or the physiologic effects of sex hormones (James et al., 2013; Rigato et al., 2013; Choudhary et al., 2016; Akdis et al., 2017).

1.4. Pathogenesis

The identification of AC is very complex due to its peculiar pathogenesis. In fact, there are diseases that can show strong phenotypic similarities with AC, such as the Uhl disease, a congenital cardiac defect that involves the development of the right ventricle’s myocardium during embryonic life, resulting in the epicardium directly applied to the endocardium and myocyte loss starting from the childhood (Uhl, 1952). The "dysplasia triangle," which is described as the region between the right

ventricle's outflow track, the apex, and the tricuspid inflow, is where most AC alterations seem to be concentrated (**Figure 1**) (Fontaine et al., 1984).

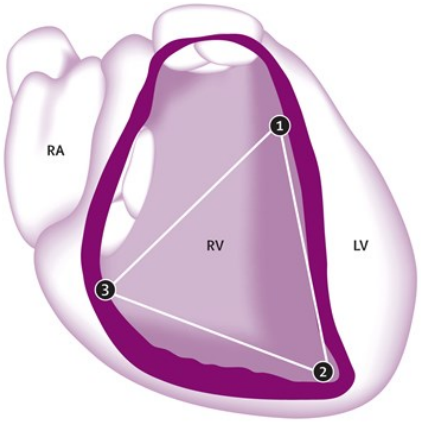

Figure 1: Triangle of dysplasia.
Characteristic areas called Triangle of dysplasia, typically located at the inferior, apical, and infundibular walls where most AC alterations seem to be concentrated. RA=right atrium. RV=right ventricle. LV=left ventricle. (Modified from Basso et al., 2009).

The main hallmark of AC is the fibro-fatty replacement of the ventricular myocardium (Marcus et al., 1982; Thiene et al., 1988; Basso et al., 1996), with the progressive tissue substitution from the epicardium towards the endocardium (**Figure 2 A-B-C-E**). This specific trademark of the disease seems to depend on the instability and disruption, due to genetic reasons, of desmosomes structure. Desmosomes are symmetrical multi-protein structures, that together with *fascia adherens* and gap junctions form the intercalated disks (ICD) (Zhao et al., 2019) allowing cells to adhere to each other and mediating mechanical anchorage by connecting the cytoskeleton to the cell membranes of adjacent cells. ICDs are specifically involved in the transmission of force, electrical continuity and chemical communication between adjacent cardiomyocytes and are composed by the *fascia adherens*, the gap junctions and the desmosomes (Estigoy et al., 2009). Another feature that can distinguish this type of cardiomyopathy from others, such as DCM, seems to depend on the differentiation of a specific type of progenitor cell, known as fibro-adipocyte progenitor cells (FAPs). FAPs originally identified as a dormant population of cells that quickly proliferate and contribute to adipocyte and fibroblast development if triggered by the structural destabilization of the cardiac

muscle (Joe et al., 2010; Uezumi et al., 2011). This gradual, genetically programmed myocardial atrophy provokes transmural lesions with thinning and weakening of the ventricular wall and frequent development of single or multiple aneurysms over time (**Figure 2 A-C-D**) (Marcus et al., 1982; Basso et al., 1996). Pathological features can range from a heart that is largely normal to a heart that has been severely affected by biventricular alterations. End-stage heart disease that results in cardiac failure typically manifests as massive biventricular chamber dilatation and many free-wall aneurysms (Basso et al., 1996; Corrado et al., 1997).

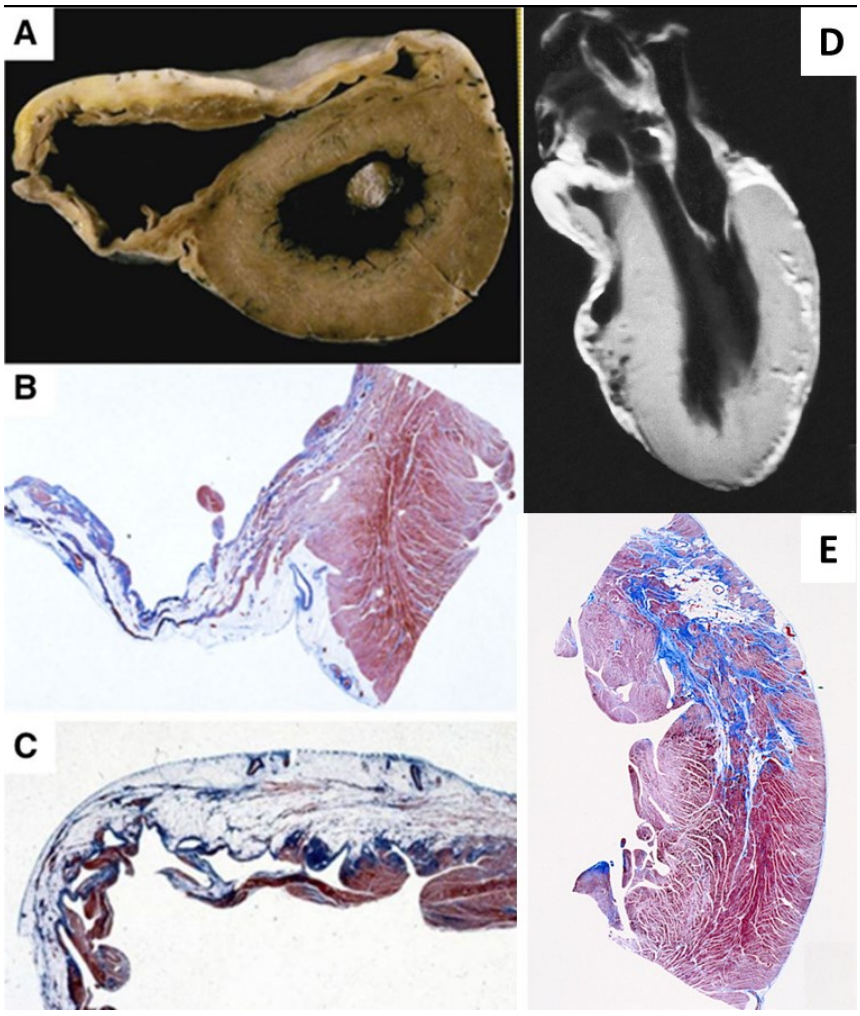

Figure 2: Pathologic features of arrhythmogenic cardiomyopathy.

A: Gross transverse section of the heart that shows anterior and posterior right ventricular (RV) wall thinning due to myocardial atrophy and a sub-tricuspid aneurysm. B-C: Full-thickness histology of the posterior (B) and anterior (C) RV free wall that shows fibro-fatty tissue replacement. There is thinning and residual myocardium confined to the endocardial trabeculae (trichrome stain). D**:** Nuclear magnetic resonance spectroscopy (NMR) scan in

the long-axis view showing extensive involvement of the anterior free wall of the right ventricle and patchy involvement of the posterior wall of the left ventricle; the interventricular septum is spared. E: Corresponding panoramic histological view of the left ventricle showing a spot of fibro-fatty replacement of the myocardium (Azan stain; original magnification, ×2.5) (Modified from Basso et al., 1996; Corrado et al., 2017).

The typical ventricular arrhythmias phenomenona may be explained by these pathological changes in the myocardial tissue that causes inhomogeneity and alters the normal conduction of the intraventricular impulse, leading to electrical instability and abnormal repolarization and depolarization of the action potential. Islands of healthy myocardial cells scattered throughout the fibro-adipose matrix can contribute to these effects (Marcus et al., 1982; Nava et al., 1988; Basso et al., 1996). Moreover, multifocal patchy inflammatory infiltrates, associated with myocyte degeneration and death, can be seen through myocardial biopsies in 67–75% of AC cases (Basso et al., 1996; Corrado et al., 1997; Thiene et al., 2007). These inflammatory responses, during the disease, do not show a chronic and continuous process but seem to occur through periodic acute responses mimicking myocarditis or myocardial infarction with normal coronary arteries (Lubos et al., 2020; Lin et al., 2021), accelerating the disease's progression rather than being a primary factor (Thiene et al., 1991). Increasing evidence underlines that inflammation occurs before overt histological and electrical abnormalities in AC (Patrianakos et al., 2012; Lopez-Ayala et al., 2015). Furthermore, necrotic and/or apoptotic myocyte death have also been included in the cascade of events that can lead to fibro-fatty replacement and therefore possibly connected to AC pathogenesis (Mallat et al., 1996; Valente et al., 1998; Pilichou et al., 2009; Rizzo et al., 2012). Dysregulated apoptosis in fact has been implicated in many diseases including cancer, autoimmune and degenerative disorders. Patients with end-stage cardiomyopathy present myocyte loss owing to both apoptosis and necrosis, which may contribute to the progression of cardiac dysfunction and degeneration (Mallat et al., 1996; Narula et al., 1996; Rayment et al., 1999; Pilichou et al., 2009), leading to fibrotic replacement of necrotic and/or apoptotic cardiomyocytes, trying to maintain the myocardium's structural integrity (de Jong et al., 2011). Unlike

necrosis, which is believed to be a mostly irreversible process, apoptosis occurs in stages and may be open to therapeutic intervention (Gill et al., 2002).

1.5. Clinical findings

AC-related fatalities are often due to a challenging and difficult early diagnosis. AC is a heterogeneous disease, both clinically and genetically, whose features can range from asymptomatic family members with concealed clinical profiles and no arrhythmias, to symptomatic patients going through arrhythmic cardiac arrest or requiring a cardiac transplant (Corrado et al., 1997; Bomma et al., 2004; Basso et al., 2009; Marcus et al., 2009; Groeneweg et al., 2015; Protonotarios et al., 2016; Zorzi et al., 2016). Precisely, the common clinical findings in patients with AC are characterized by ventricular arrhythmias due to electric instability, palpitations, systolic dysfunction, syncopal episodes, and cardiac arrest. SCD is also another important trademark of this disease that can occur as the first symptom in asymptomatic individuals, mostly young people and athletes (Nava et al., 1988; Corrado et al., 1990, 2003, 2006). Based on clinical and pathological conditions, the course of AC may be divided into four distinct phases (Corrado et al., 2000; Thiene et al., 2007; Basso et al., 2009): an initial concealed phase, an electrical disorder phase, a right ventricular dysfunction phase and a final bilateral phase. The "concealed" phase is defined by the initial absence of symptoms, with possible slight and imperceptible changes in ventricular structure and rare arrhythmia episodes that increase a lot the problems in diagnosis. In the second phase, the electrical disorder starts to be more detectable, with clear ventricular arrhythmias phenomena, palpitations, syncopes, and structural changes in the ventricular myocardial tissue, usually detectable by cardiac imaging techniques. The third phase is the continuation of the second one, in which the clinical symptoms become more severe and present, leading to ventricular dysfunction. The last phase comprehends ventricular failure in one or both ventricles, similar to DCM that can lead to heart functional instability (Sen-Chowdhry et al., 2008). The risk of SCD, despite being more frequent in the last more severe phases, can occur at any time, even in the first-asymptomatic stage, especially in athletes (Corrado et al., 1990, 2017).

1.6. Diagnostic criteria and therapeutic treatments

The diagnosis of AC is not based on a single diagnostic tool but is a combination of multiple criteria and sources of information, such as echocardiography, angiography and cardiac magnetic resonance, histopathological features on endomyocardial biopsy (EMB), abnormalities in the electrocardiogram (ECG), arrhythmias episodes, family history and genetics (McKenna et al., 1994; Marcus et al., 2010). Electrical defects generally precede structural defects; in fact, patients with AC are usually initially asymptomatic, and death can occur as first sign of the disease. Therefore, post-mortem autopsy analysis in subjects who died suddenly is very important to understand clearly the causes of death and to be able to monitor family members who are still alive by identifying subjects at risk to undergo any precautionary therapies (Marcus et al., 2010). Over years, these criteria were updated and ameliorated to increase the sensitivity to milder and less evident forms of AC, facilitating the recognition of possible pathological conditions among relatives of AC patients (Marcus et al., 2010). In contrast to other forms of cardiomyopathy, the diagnostic criteria for AC now include the presence of a pathogenic mutation in genes associated with the disease as a key factor needed to validate the diagnosis, being sufficient alone to classify the patients as potential AC cases. The "Padua criteria," which proposed new diagnostic criteria regarding tissue characterization findings by contrast-enhanced cardiac magnetic resonance (CE-CMR), depolarization/repolarization ECG abnormalities and ventricular arrhythmia features for diagnosis of the left ventricular (LV) phenotype, was introduced in 2020 by a multidisciplinary team of basic researchers and clinical cardiologists at the Medical School of the University of Padua (Corrado et al., 2020). Clinical investigations including a sizable patient cohort are required to validate these novel criteria during the next years. Once the disease has been diagnosed, the clinical treatment of AC patients depends on the stage and progression of the disease, being mainly focused on the prevention of SCD. These therapies are normally based on the administration of antiarrhythmic (AADs) and anti-heart failure drugs, such as β-blockers (Basso et al., 2009; Corrado et al., 2017), implantable cardiac defibrillator (ICD), catheter ablation and heart transplantation (HTX) if required (Groeneweg et al., 2015). Moreover, according to current

recommendations, carriers of desmosome gene variants should also avoid participating in competitive or endurance sports. Nevertheless, all these therapeutic approaches are palliative, aimed only at reducing the AC phenotype but are not focused on the genetic nature of the disease. For this reason, it is of fundamental importance to concentrate all efforts on the research for new therapies, aimed at preventing, and not just alleviating, the disease. A high-throughput drug screening made by Asimaki and colleagues in 2014 (Asimaki et al., 2014) identified a drug molecule able to recover electrophysiological alterations in cardiomyocytes, preventing heart failure and normalizing survival, in two different JUP-deficient models specifically expressing a human *JUP* mutation: zebrafish (*Danio rerio*) and neonatal rat ventricular myocytes (Asimaki et al., 2014). This drug molecule, called SB216763, by acting through the modulation of the Wnt/β-catenin signaling pathway, which was fund dysregulated in AC patients (Garcia-Gras et al., 2006), seemed to alleviate the progression of the disease, paving the way for a new therapeutic approach.

1.7. Genetics of AC

AC is currently thought to be a heterogeneous inherited cardiomyopathy transmitted as an autosomal dominant form with incomplete penetrance and variable expressivity (Nava et al., 1988, 2000; Corrado et al., 2000). Marcus and colleagues in 1982 endorsed the idea of the hereditary character of AC, describing two symptomatic adult patients who belonged to the same family (Marcus et al., 1982). Besides, compound/digenic heterozygotes and homozygous recessive forms of AC have frequently been described as severe forms of the disease, with complete penetrance and extra-cardiac and cutaneous anomalies (Alcalai et al., 2003; Simpson et al., 2009; Bauce et al., 2010; Cabral et al., 2010; Gerull et al., 2013; Rigato et al., 2013; Al-Sabeq et al., 2014; Lorenzon et al., 2015; Qadri et al., 2017), such as Naxos and Carvajal syndromes (Protonotarios et al., 1986; Carvajal-Huerta, 1998; McKoy et al., 2000; Norgett et al., 2000). In Mediterranean countries several hereditary palmoplantar keratosis were diagnosed during years, such as Meleda disease (Franceschetti et al., 1972), until cases of correlated cardiac abnormalities, ventricular arrhythmias and sporadic SCD, were observed in the Greek island of

Naxos (Protonotarios et al., 1986). The Naxos form of AC was the first familial autosomal recessive form of the disease studied and genetically characterized, very similar to the dominant forms according to the age and the manner in which the condition presents clinically, the distribution of right and left ventricular involvement, electrocardiographic signs and morphological and histological characteristics, with the only difference given by the presence at birth of a hereditary palmoplantar keratosis and woolly hair (Protonotarios et al., 1986; Fontaine et al., 1998). In 2000 Mckoy and colleagues (McKoy et al., 2000) identified by linkage analysis a genetic locus on the long arm of chromosome 17 (17q21.2) (Coonar et al., 1998), later associated by sequencing analysis to *Plakoglobin (JUP)*, a candidate gene for causing the disease, presenting a 2-bp deletion and a subsequent frame shift with the introduction of a premature stop codon after 11 amino acids (McKoy et al., 2000). The other recessive form discovered was originally identified in 3 Ecuador families in 1998 and was named Carvajal syndrome (Carvajal-Huerta, 1998). As in the Naxos one, hereditary palmoplantar keratoderma and woolly hair were hallmarks of this novel cardio-cutaneous condition that has been also linked to ventricular hypertrophy and dilation, aneurysms and abnormal ICDs structure (Kaplan et al., 2004). The linkage analysis and the direct sequencing resulted in the identification of a single-nucleotide deletion c.7901delG, which creates a premature stop codon depriving *Desmoplakin (DSP)* of its C-domain (Norgett et al., 2000; Kaplan et al., 2004). Both *DSP* and *JUP* have a fundamental role in adherens and desmosomal junctions, explaining the phenotypic conditions observed if mutated (Hatzfeld, 1999; Norgett et al., 2000). From these two AC recessive forms, it was possible to start the genetic understanding of the disease, detecting the first mutations in genes encoding for desmosomal proteins and revealing structural and functional alterations in the ICDs (Corrado et al., 2017). To date, about 50% of affected individuals carry a mutation in genes encoding for desmosomal proteins, thus AC is normally defined as a pathology of desmosomes or cell junctions (Calore et al., 2015; Pilichou et al., 2017; Giuliodori et al., 2018). Anyway, only in around 50-60% of patients, a comprehensive genetic analysis finds a rare variant as a possible disease-causing factor. This finding raises the possibility that further unidentified genes and undiscovered genome modifications may also exist (Bennett et al., 2019). The

genes implicated in the pathogenesis of AC can present nonsense mutations, frameshifts, and splicing modification in 83% of patients, whereas missense mutations constitute only 14% of the pathology's causes (Bennett et al., 2019). Despite being mostly a monogenic disorder, examples with several mutations in either the same gene or separate genes have been documented, with a prevalence ranging from 4% to 20% (Groeneweg et al., 2015). However, it is fair to remember that AC is caused principally by the genetic background of these patients, but also by other factors among which epigenetic, age, and environmental variables can play a significant role in the evolution of the disease (Bondue et al., 2018). Thus far, 26 genes have been associated with dominant AC forms since the first genetic tests in the Naxos patients (McKoy et al., 2000), mostly encoding ICDs proteins (**Table 2**) (Marcus et al., 2010; Groeneweg et al., 2015; James et al., 2021).

Table 2: Reported Genes for AC (James et al., 2021).

Gene	Protein	Cellular complex	HGNC ID*
ACTC1	Actin alpha cardiac muscle 1	Sarcomere	143
CDH2	Cadherin-2	Area composita	1759
CTNNA3	Catenin alpha 3	Area composita	2511
DES	Desmin	Intermediate filament	2770
DSC2	Desmocollin-2	Desmosome	3036
DSP	Desmoplakin	Desmosome	3052
DSG2	Desmoglein-2	Desmosome	3049
JUP	Junction plakoglobin	Desmosome	6207
LDB3	LIM domain binding 3	Sarcomere	15710
LMNA	Lamin A/C	Nuclear envelope	6636
MYBPC3	Myosin binding protein C3	Sarcomere	7551
MYH7	Myosin heavy chain 7	Sarcomere	7577
MYL2	Myosin light chain 2	Sarcomere	7583
MYL3	Myosin light chain 3	Sarcomere	7584
PKP2	Plakophilin-2	Desmosome	9024
PLN	Phospholamban	Calcium handling	9080
RYR2	Ryanodine receptor 2	Calcium handling	10484
SCN5A	Sodium voltage-gated channel alpha subunit 5	Sodium channel	10593
TGFB3	Transforming growth factor beta 3	Signaling pathways	11769
TJP1	Tight junction protein 1	Area composita	11827
TMEM43	Transmembrane protein 43	Nuclear envelope	28472
TNNI3	Troponin I3	Sarcomere	11947
TNNC1	Troponin C1	Sarcomere	11943
TNNT2	Troponin T2	Sarcomere	11949
TPM1	Tropomyosin 1	Sarcomere	12010
TTN	Titin	Sarcomere related	12403

* HUGO gene nomenclature committee at the European Bioinformatics Institute ID.

Among these pools of genes, the ones encoding desmosomal proteins DSP (Rampazzo et al., 2002), Plakophilin-2 (PKP2) (Gerull et al., 2004), Desmoglein-2 (DSG2) (Pilichou et al., 2006), Desmocollin-2 (DSC2) (Syrris et al., 2006) and JUP (Asimaki et al., 2007) have been consistently identified in AC patients (Thiene, 2015). However, also mutations in non-desmosomal genes have been recognized in 1-3% of AC patients, such as Galectin-3 (GAL-3) (Cason et al., 2021), transforming growth factor-β-3 (TGFβ3) (Beffagna et al., 2005), cardiac Ryanodine receptor (RYR2) (Tiso et al., 2001), Transmembrane protein 43 (TMEM43) (Merner et al., 2008), Lamin A/C (LMNA) (Quarta et al., 2012), Desmin (DES) (van Tintelen et al., 2009), Catenin alpha 3 (CTNNA3) (van Hengel et al., 2013), Titin (TTN) (Taylor et al., 2011), Phospholamban (PLN) (van der Zwaag et al., 2012), Filamin C (FLNC) (Ortiz-Genga et al., 2016; Celeghin et al., 2022) and N-cadherin (CDH2) (Mayosi et al., 2017). Nowadays, only the desmosomal genes are definitively associated with AC, while all the others show either limited or no evidence for AC causation and can be classified into two different groups: recently published genes with very limited data or genes detected only in few families with clear AC phenotype (i.e. CTNNA3). These genes could be kink to other cardiac disorders such as different types of cardiomyopathies or arrhythmia syndromes, where there is little or no evidence of AC (i.e RYR2, LMNA and TTN) (James et al., 2021).

1.8. Desmosome

Although cardiomyocyte's ICDs have historically been represented as a collection of distinct units, recent studies suggest that it should be viewed as a single functional unit in which macromolecular complexes interact mechanically and electrically to preserve cardiomyocyte's adhesion and synchrony (Zhao et al., 2019). Specifically, desmosomes allow cells to adhere to each other and mediate mechanical anchorage by connecting the cytoskeleton to the cell membranes of adjacent cells, conferring functional integrity in epithelial tissue and cardiac muscle under mechanical-associated stimuli, like friction, tension, and contraction (**Figure 3**) (North et al., 1999; Awad et al., 2008). Because of their close association with the intermediate filaments (IFs) of neighbouring cells, which transmits the signal to the cytoskeleton, they can confer such resistance to strong and continuous

mechanical stresses responding in a uniform and non-disruptive manner. The electrical input that drives the synchronous and uniform contraction defining the dynamics of the cardiac muscle can be affected by the possible disruption of this functional unit, causing arrhythmia episodes, which are one of the major symptoms of cardiac diseases including AC (Delmar and McKenna, 2010). Moreover, they are involved also in tissue differentiation, cell-to-cell communication, electrochemical coupling, and apoptosis. (Merritt et al., 2002). Disruption and instability of desmosomes, aside from the mechanical consequences in the contraction impairment, can promote indeed the dysregulation of signalling pathways involved in myocyte's replacement by fibro-adipose tissue, such as Wnt/β-catenin, Hippo/YAP-TAZ, and TGFβ pathways, recently associated with AC (Garcia-Gras et al., 2006; Asimaki et al., 2014; Giuliodori et al., 2018).

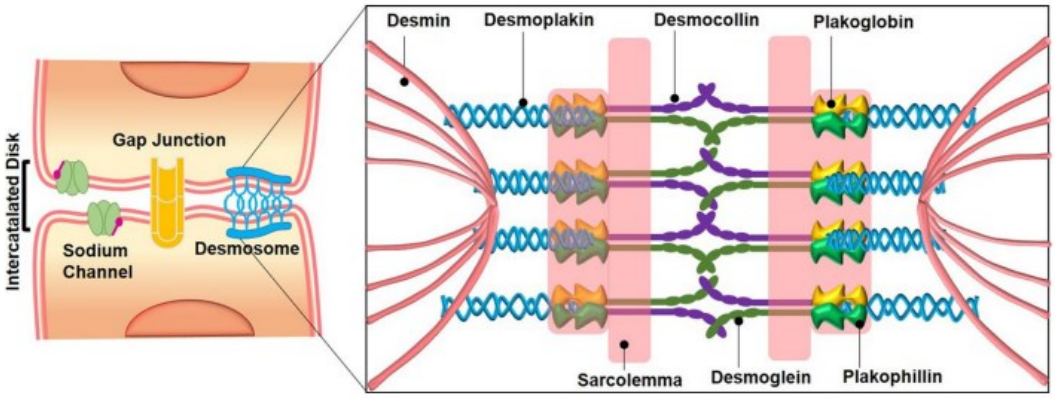

Figure 3: Representations of desmosome structure.

Structure of desmosomes and intercalated discs. The desmosome comprises cadherins (DSG and DSC), armadillo proteins (PKP and PG), and plakin (DSP). DSG and DSC extend in extracellular space and associate with their counterparts on the other side of the junction. Cadherins in intracellular space associate also with PKPs and PKGs. DSP connects the desmosome complex to the IFs, DES. Desmosomes work together with gap junctions and sodium channels as a function unit, which provides mechanical support and electrical coupling of myocardial tissue (From Lin et al., 2021).

From a structural point of view, desmosomes are often considered in combination with IFs such as DES in the cardiac tissue, forming the Desmosome intermediate filaments complexes (DIFC) (Garrod and Chidgey, 2008). Desmosome looks like a dense membrane-associated plaque that can be divided into 3 components: two

intracellular plaques split by a central mid-line of intercellular space, between 20 and 35 nm wide, called desmoglea. All these components are fundamental for the stability and the correct response to stress stimuli, due to their very strong association and interactions, and mutations in one of them can compromise all this delicate balance (Garrod and Chidgey, 2008). Specifically, two different types of proteins compose the desmosome structure: transmembrane adhesive glycoproteins (cadherin superfamily) and cytoplasmic proteins (plakin and armadillo families). While the intercellular part of this complex is characterized by the interaction between cadherin proteins (DSG2 and DSC2), the intracellular part is divided into two areas, the outer dense plaque, and a dense inner plaque, with DSP protein and two armadillo proteins, JUP and PKP2, that compose it. The DSG2 and DSC2 calcium-dependent cadherins are considered the central part of the structure, due to their role in the interaction with cadherins of desmosomes from adjacent cells. They can be found in a highly calcium-independent form, assuming a hugely organized-packed conformation, or in a weak calcium-dependent one (Garrod et al., 2005). In this weak form of interaction, calcium ion interposes itself between the cadherins of two different cells, allowing them to adhere and forming a homo/heterodimer, while the removal of it abolishes adhesive activity because the negative charges present on the N-terminal extracellular domains of cadherins would repel by electrostatic repulsion, preventing cell-cell adhesion (Nagar et al., 1996; Huber, 2003). Plakin DSP and the armadillo proteins JUP and PKP2 mediate the linkage between the IFs and the desmosomal adhesion molecules. In the inner dense plaque, DSP acts as a direct linker between IFs and the desmosomal complex. In the outer dense plaque instead, DSP interacts through the armadillo proteins PKP2 and JUP with the C-terminal domains of the desmosomal cadherins DSG2 and DSC2 (**Figure 3**) (North et al., 1999; Garrod and Chidgey, 2008). Therefore, we can comprehend why desmosomes, like any other type of protein complex with various responsibilities and related activities, play a crucial part in a variety of disorders, including AC.

1.9. Desmosomal proteins

1.9.1. Cadherins proteins

Four DSGs (DSG 1-4) and three DSC (DSC1-3) with a very similar structure characterized the group of the seven desmosomal cadherins found in humans. DSG mediates calcium-dependent cell-cell attachment and exists in four different isoforms (DSG 1-4), each of which it is expressed differently in various tissues (Green and Simpson, 2007). Although DSG2 seems to be the unique isoform expressed in the heart tissue, it is present also in all tissues containing desmosomes (Schäfer et al., 1994; Nuber et al., 1995). DSG2 has four extracellular cadherin domains, each with a calcium-binding site that stabilizes its shape and function, a transmembrane domain, an intracellular anchoring domain, and a small signal domain called RUD (repeated-unit domains), whose function is still not clear. DSC is another member of the cadherin superfamily that mediates calcium-dependent cell-cell adhesion. As already discussed, DSC has three known isoforms (DSC 1-3), although only DSC2 is found in heart tissue while being expressed also everywhere else (Green and Simpson, 2007). It is composed of four highly conserved extracellular domains, whit the first one named CAR that is responsible for the heterophilic interaction with the DSGs in the adjacent cells. A transmembrane domain connects them to an intracellular anchor domain at the N-terminus, which binds the intracellular portion of the desmosome in the inner dense plaque, making up the structure of DSC2. DSG2 and DSC2 were both described for the first time to be involved in AC only in 2006 (Syrris et al., 2006). Heterozygous DSC2 frameshift variants were found in 4 AC-affected probands without variants in other desmosomal genes (Syrris et al., 2006). Since then, less than 50 DSC2 nucleotide variants, which account for 1–3% of AC cases, have been reported (Heuser et al., 2006; Syrris et al., 2006; Beffagna et al., 2007; Fressart et al., 2010; Cox et al., 2011). Instead, DSG2 was connected to the disease with the discovery of 9 missense variants affecting highly conserved amino acids in 8 Italian families with AC. More than 50 DSG2 mutations have been discovered nowadays in 2–20% of AC patients (Pilichou et al., 2006; Fressart et al., 2010; Cox et al., 2011).

1.9.2. Armadillo Proteins

JUP is characterized by a N-terminal and C-terminal domain, linked by a central one that presents highly conserved armadillo repeats (12 arm repeats), characteristic of this protein family (Garrod and Chidgey, 2008). JUP exhibits dual localization in both adherents junctions, where it is interchangeable with the closely related armadillo protein β-catenin, and in desmosomes where interacts with strong affinity with cytoplasmic domain of DSG2 and DSC2 cadherins in the outer dense plaque, connecting them with the inner dense plaque trough the interaction with DSP, creating a sort of bridge which connects the extracellular portion of the desmosome to the IFs (Chitaev et al., 1996). PKP instead exists in various forms (PKP1-3), with the PKP2 predominately expressed in the cardiac tissue (Hatzfeld, 2007). As JUP, it has a structural role interacting with both desmosomal cadherins and DSP (Chen et al., 2002) and presents two isoforms, a shorter "a" variant and a longer "b" one, due to alternatively spliced mRNA transcripts. Transcript 2b (881 amino acid) differs from the 2a (837amino acid) by the insertion of 44 amino acids between arm repeats 2 and 3 (Mertens et al., 1996; Gandjbakhch et al., 2011). It presents 9 arm repeats in total in the central part of the protein, with a flexible loop in the middle (between 5 and 6 arm repeat) that allow its curved structure. Both JUP and PKP2 armadillo proteins are found in desmosome and were recently linked to the dominant AC form (Gerull et al., 2004; Asimaki et al., 2007). JUP was initially associated with disease due to its involvement in recessive forms, as described in the 1986 by Protonotarios and colleagues in the Greek island of Naxos (Protonotarios et al., 1986). A recently report of an in frame insertion of a serine residue (p.Ser39_Lys40insSer) at the N-terminus of the JUP protein, in a small German family, linked JUP protein also to the dominant form of AC (Asimaki et al., 2007). Nevertheless, approximately only 1% of AC patients present less than 20 JUP variations identified so far (Asimaki et al., 2007; Fressart et al., 2010; Cox et al., 2011). The first time PKP2 has been linked to AC was when 3 large PKP2 deletions were described in a 149 Dutch AC cases (Cox et al., 2011). Right now, between 10 and 45% of AC reported cases, are attributed to more than 120 PKP2 pathogenic variations (Gerull et al., 2004; Pilichou et al., 2006; Fressart et al., 2010; Cox et al., 2011). Although recessive and compound heterozygous variations have

also been found in several cases, most variants exhibit a dominant inheritance with lower penetrance, typical of AC.

1.9.3. Desmoplakin

DSP belongs to the plakin family and is the most abundant protein in desmosomes essential for normal adhesion, mediating the binding between the plasma membrane and the IFs (Yuan et al., 2021). Being part of the plakin family, DSP is divided into 3 parts: a globular N-terminal domain important for localization and heterophilic protein-protein interactions such as with PKP2, a central α-helical coiled-coil domain (rod domain) involved in protein dimerization, and a C-terminal domain composed by three plakin repeats domains (A-B-C), as well as a glycine-serine-arginine rich domain (GSR) that interacts directly with IFs (**Figure 4**) (Delva et al., 2009). Mutations in the C-terminal part of DSP can cause severe problems, due to the direct involvement of the phosphorylation in the GSR domain for the regulation and affinity of the interaction with IFs. DSP is expressed in all desmosome-containing tissues (Leung et al., 2002) and an alternative mRNA splicing produces two isoforms, which differ in the length of the central rod domain: DSP I, predominantly expressed in the myocardium and comprise 2871 amino acids, and DSP II, consisting of only 2271 amino acids. Recently DSP II has been found also in the ventricle and atrial tissues, changing another time AC's underlying beliefs (Yuan et al., 2021).

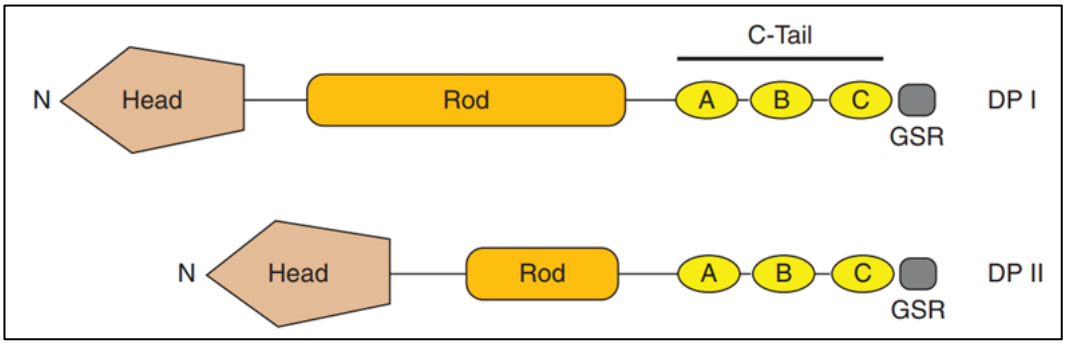

Figure 4: Different domains that form the two Desmoplakin isoforms, DSP (DP) I and II.

The two isoforms differ in the length of the central rod domain (Rod), with DSP II that is missing approximately two-thirds of it. The carboxy-terminal tail (C-Tail) contains three

plakin repeat domains (A, B, C), as well as a glycine-serine-arginine rich domain (GSR) thought to regulate DSP binding to intermediate filaments. The amino-terminal globular head domain (Head) mediates protein–protein interactions (From Delva et al., 2009).

Nowadays more than 100 pathological variants of the DSP gene have been detected in 10-15% of AC cases (Pilichou et al., 2006, 2016; Fressart et al., 2010; Cox et al., 2011). Moreover, other types of cardiomyopathies are linked to DSP gene mutations: DCM, which causes the heart's chambers to enlarge, and the Carvajal syndrome, another uncommon autosomal recessive type are two examples of this (Carvajal-Huerta, 1998; Corrado et al., 2017). A heterozygous nonsense variation, p.Gln331Ter, and a splicing site variant, c.939+1G>A, were the first autosomal dominant pathogenic nucleotide variants discovered in the DSP gene, located on the short arm of chromosome 6 (6p24.3), causing striated palmoplantar keratoderma (Armstrong et al., 1999), although cardiac changes were not investigated at that time. Later, six AC-affected subjects from an Italian family in the Veneto Region were found to carry an autosomal dominant heterozygous missense mutation c.897C>G in the DSP gene (Rampazzo et al., 2002). Even so, besides its established role in the heart's structural stability, DSP mutations were also connected with other clinical features present in AC, such as inflammation and adipogenesis. In particular, the specific activation of cellular mediators Nuclear factor kappa B (NF-kB) and Neurofibromin-2 (NF2), which are triggered by DSP mutation, stimulate the expression of their specific signalling pathways (NF-kB and Hippo), connecting DSP with inflammation and adipogenesis (Yuan et al., 2021). Lastly, DSP also affects the Wnt/β-catenin pathway, central in AC pathogenesis (Calore et al., 2015; Lorenzon et al., 2017), highlighting once again how crucial this protein is for the beginning and development of this disease.

1.10. Non-desmosomal proteins

A small percentage of AC patients (1-3%) have also been shown to have mutations in non-desmosomal genes. However, nowadays only the desmosomal genes are definitively associated with AC, while all the others show either limited or no evidence and are commonly link to other cardiomyopathies or arrhythmia syndromes. New findings could eventually reverse this classification in the future,

leading to an increase for evidence supporting these genes involvement. For example, TMEM43 was added to the pool of genes strongly correlated with AC in the last years, between the desmosomal ones (James et al., 2021). A founder variant that segregated in a well-characterized AC community in Newfoundland, with an extremely high SCD rates, led at first to the discovery of this gene, which was then confirmed also in populations in the UK, Denmark, and Germany as well as most recently in Spain (Merner et al., 2008; Haywood et al., 2013; Milting et al., 2015; Dominguez et al., 2020). Another protein lately strongly associated with AC is FLNC (Ortiz-Genga et al., 2016; Celeghin et al., 2022). FLNC, traditionally linked to HCM, is raising great interest given its possible involvement in the pathogenesis of a peculiar left ventricular phenotype found in 28 families, characterized by extensive fibrosis, life-threatening ventricular arrhythmias and SCD, resembling AC pathogenesis (Celeghin et al., 2022). Therefore, not only desmosomal components but also different proteins that play distinctive roles in the cell could be involved in AC.

1.10.1. Galectin-3

One of the genes most recently associated with the disease is the *LGALS3* gene (Cason et al., 2021). Galectins are glycan-binding proteins encoded by the *LGALS* gene family in humans and are involved in a wide range of physiological healthy processes, including signalling, cell migration, adhesion, apoptosis, and mRNA stability. On the other hand, pathological galectins have been correlated with cancer, fibrosis, chronic inflammation, and scarring affecting many different tissues (Nio-Kobayashi, 2017; Sciacchitano et al., 2018). Galectin-3 (aliases: Gal-3, Lgals3) is a 35 kDa protein, member of this lectin family, encoded by the *LGALS3* gene and prevalently found in many different organs, including the lungs, heart, stomach, colon, adrenals, uterus, and ovaries (Sygitowicz et al., 2021). Gal-3 includes in its C-terminal region a carbohydrate recognition domain (CRD) that allows it to bind oligosaccharides that contain glycoconjugates, by means of a highly-conserved Asp-Trp-Gly-Arg (NWGR) motif responsible also for the anti-apoptotic activity of this protein (Yang et al., 1996). The N-terminal region of this protein has instead a highly-conserved serine 6 that casein kinases (CK) 1 and 2 can

phosphorylate. This modification in the N-terminal portion of the protein contributes to its nuclear translocation and reduces also the affinity for its ligands, participating together with the CRD in oligosaccharide binding and anti-apoptotic signalling activity (Barboni et al., 2000; Mazurek et al., 2000; Yoshii et al., 2002). Furthermore, the N-terminal domain was also found to be crucial for the protein secretion outside of cells (Menon and Hughes, 1999). A tail of 100–150 amino acid residues, made up of repetitions of proline, glycine, tyrosine, and glutamine-rich sequence, connects the N-terminal to the C-terminal domain, participating in the oligomerization of Gal-3 molecules into a pentamer in the presence of ligands, and being involved in its interactions with other proteins (Mehul et al., 1995; Yang et al., 1998; Ippel et al., 2016). However, in the absence of ligands, Gal-3 is mostly found as a monomer in solution and it can dimerize through its CRD domain to produce a homodimer (**Figure 5**) (Yang et al., 1998).

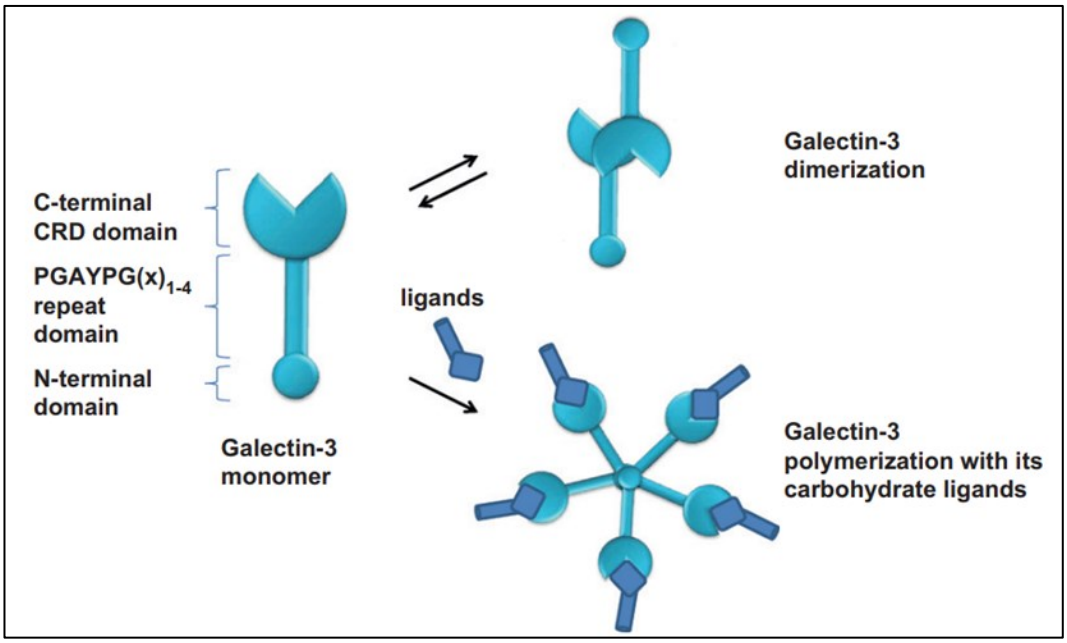

Figure 5: Gal-3 monomeric structure and dimerization process.
Schematic representations of the monomeric structure of Gal-3 and Gal-3 dimerization in the absence of binding ligand and polymerization through in the presence of carbohydrate-binding ligands (From Newlaczyl and Yu, 2011).

Gal-3 is known to be directly involved in the stabilization of intercellular junctions, mediating cell-to-cell adhesion through the interactions specifically with N-linked

β-galactosides on the extracellular domain of DSG2 proteins, as demonstrated by experiments in intestinal, corneal and conjunctival epithelia (Boscher et al., 2012; Jiang et al., 2014; Argüeso et al., 2015; Gross et al., 2018). Moreover, in primary squamous carcinomas, Gal-3 interacts also with DSP proteins (Argüeso et al., 2015). Additionally, recent research by Cason et al.(Cason et al., 2021) has shown that pharmacological suppression of Gal-3 in zebrafish model led to aberrant DSP localisation in epidermal cells where desmosomes seemed to be separated from the cytoskeletal complex and unevenly distributed (Cason et al., 2021). As briefly mentioned before, Gal-3 is believed to have an anti-apoptotic and anti-necroptotic activity (Cecchinelli et al., 2006; Nirmala and Lopus, 2020; Al-Salam et al., 2021). Co-immunoprecipitation experiments demonstrated its interaction in the cytosol with several molecules involved in the apoptotic signalling pathway, such as Nucling and CD95, both pro-apoptotic factors (Fukumori et al., 2004; Liu et al., 2004). Especially, Galectin-3 was found to be structurally very similar to the Bcl-2 protein, a well-known anti-apoptotic factor. They both have a highly rich proline, glycine, and alanine sequence in their N- termini region and a highly-conserved Asp-Trp-Gly-Arg (NWGR) motif in the C-terminal portion, very important for their anti-apoptotic activity, in addition to the carbohydrate-binding activity in Galectin-3 (Yang et al., 1998; Nangia-Makker et al., 2007). Just like Bcl-2, Galectin-3 can lead to an anti-apoptotic effect through the blocking of cytochrome c release from mitochondria followed by activation of the caspase cascade (Moon et al., 2001; Burlacu, 2003). Moreover, Galectin-3 and Bcl-2 were demonstrated to interact with each other, mimicking the homo-dimerization typical of the Bcl-2 proteins family (Dumic et al., 2006), indicating that the involvement of Galectin-3 in a cell death inhibition mechanism of Bcl-2 may control apoptosis (Yang et al., 1996). Al-Salam and colleagues in 2020 (Al-Salam et al., 2020) observed increased levels of Gal-3 proteins after myocardial infarction and their involvement in anti-apoptotic mechanisms, shaping the response to damage in the cardiac tissue (Al-Salam et al., 2020). These findings support the potential role of this protein in the myocardial injury of AC, causing, if mutated, the destabilization of the intercellular junctions and an uncontrolled apoptotic response. In addition, Gal-3 was demonstrated to be involved in both acute and chronic inflammatory responses and in human samples was found to increase in the acute/inflammatory phase of AC (Cason et al., 2021).

Gal-3 is involved in many processes during the inflammatory response including neutrophil activation and adhesion (Kuwabara and Liu, 1996), chemo-attraction of macrophages (Sano et al., 2000) and activation of mast cells (Frigeri et al., 1993). More specifically, Gal-3 was considered to be a "macrophage activation marker" and is found highly expressed and secreted by mononuclear macrophages (CD68- and CD98- positive) in myocardial tissue of AC patients, as well as being involved in their activation (Liu et al., 1995; Sano et al., 2000; Cason et al., 2021). Therefore, Gal-3 can affect the biological behaviour of macrophages, activating them and causing the release of inflammatory factors, aggravating the inflammatory response (Papaspyridonos et al., 2008; Henderson and Sethi, 2009). Conversely, Gal-3 inhibition markedly decreased the quantity of macrophage-induced inflammatory regulators, including also TNF-α and Il-6 (Silverman et al., 2012; Alturfan et al., 2014; Lu et al., 2020). Gal-3 upregulation was observed also in many different human fibrotic conditions (Henderson and Sethi, 2009), underlining its positive effect on this process, if present. Recently, dysregulated Galectin- 3 protein levels in cardiac tissue have been associated with cardiovascular diseases, often characterized by inflammation and tissue fibrosis substitution (Oz et al., 2017; Blanda et al., 2020). Cason and colleagues in 2021 (Cason et al., 2021) identified *LGALS3* among a pool of genes differently expressed in transgenic mice with a mutation in the Dsg2 gene, which displayed phenotypic signs of AC, finding it dysregulated also in myocardial tissue of patients with AC at early and acute stages of the disease. Therefore, they performed whole exome sequencing in 150 AC patients, revealing the presence of 4% *LGALS3* rare genetic variants. Of note, three patients presenting *LGALS3* mutations carried also pathogenic desmosomal genetic variants. Genomic comparison among species showed that *LGALS3* rare missense variants were highly conserved and predicted to significantly affect protein structure, causing the loss of function (Cason et al., 2021).

1.11. Signalling pathways in AC

Wnt/β-catenin, along with other signalling pathways such as TGFβ and Hippo/YAP-TAZ are fundamental for a correct heart morphogenesis and development, being involved in myocardial differentiation, valves formations as

well as in the making of vessels. These pathways are generally involved in cell proliferation, differentiation and migration and in the cardiac tissue they mediate pro-survival, pro-myocyte and pro-growth stimuli, modulating the tissue remodelling (Brade et al., 2006; Dobaczewski et al., 2011; Lorenzon et al., 2017; Mia and Singh, 2019). If dysregulated, these signals could be involved in adipogenesis and fibrogenesis processes, and their crosstalk and mutual regulation put them in a central position in the study of the pathogenesis and progression of cardiac diseases such as AC. Recent studies on genetically modified cellular and animal models showed a connection between mutation in junctional/desmosomal proteins, like DSP and LGALS3, and the dysregulation of this specific cell signalling pathways (Garcia-Gras et al., 2006; Lombardi et al., 2011; Asimaki et al., 2014; Chen et al., 2014; Chelko et al., 2016; Giuliodori et al., 2018).

1.11.1. Wnt/β-catenin signalling pathway

The canonical Wnt/β-catenin signalling pathway, one of the primary developmental signals, is a highly conserved pathway implied in a wide range of cellular processes during evolution. It acts from the embryonic stage, where it is responsible for development, to the adult stage, where, among other effects, it promotes tissues homeostasis and renewal (Gessert and Kühl, 2010; Clevers and Nusse, 2012; Lorenzon et al., 2017). Its well-known ability to regulate and control cell proliferation and differentiation in many different tissues, among which the cardiac one (Brade et al., 2006), is what gives it such a broad range of activity. The primary signal transducer in the canonical Wnt pathway is the β-catenin protein, an Armadillo protein that, among a variety of functions inside the cell, such as structural protein at cell-cell adhesion junctions, mediates also the Wnt signal transduction (Ben-Ze'ev et al., 2000). In the absence of Wnt ligands, this effector undergoes a quick phosphorylation process in the cytosol, being targeted for proteasome degradation. The scaffold protein (Axin), together with the adenomatous polyposis coli (APC) tumor suppressor protein, the glycogen synthase kinase 3-β (GSK3-β) and the casein kinase 1 (CK1), composes the destruction complex (DC) directly involved in the cytoplasmic phosphorylation of β-catenin N-terminal region specifically by GSK3-β and CK1. When the adaptor protein

disheveled (Dsh) is activated, it recruits and forms a complex with Axin, inhibiting the GSK3-β activity and preventing β-catenin phosphorylation and degradation (**Figure 6**) (Centelles, 2012). As mentioned before, this phosphorylation provokes the ubiquitination and the following proteasome degradation, impeding β-catenin translocation inside the nucleus, not allowing the binding of it to the transcription factors of the T cell factor/lymphoid enhancer-binding factor family (TCF-LEF), stopping the expression of Wnt responsive genes like CyclinD1 and cMyc (Li et al., 2005; Lorenzon et al., 2017). The signalling pathway dysregulation is linked to a wide number of developmental and genetic disorders, including cancer and neuronal and skeletal disorders (MacDonald et al., 2009; Neben and Merrill, 2015; Libro et al., 2016). In the last years, the significance of Wnt/β-catenin signalling in cardiac diseases has become every day more understood, being implicated in cardiac dysfunction, such as hypertrophy, fibrosis, arrhythmias, and infarction (Dawson et al., 2013; Pahnke et al., 2016), and recently being also linked to AC (Garcia-Gras et al., 2006; Calore et al., 2015).

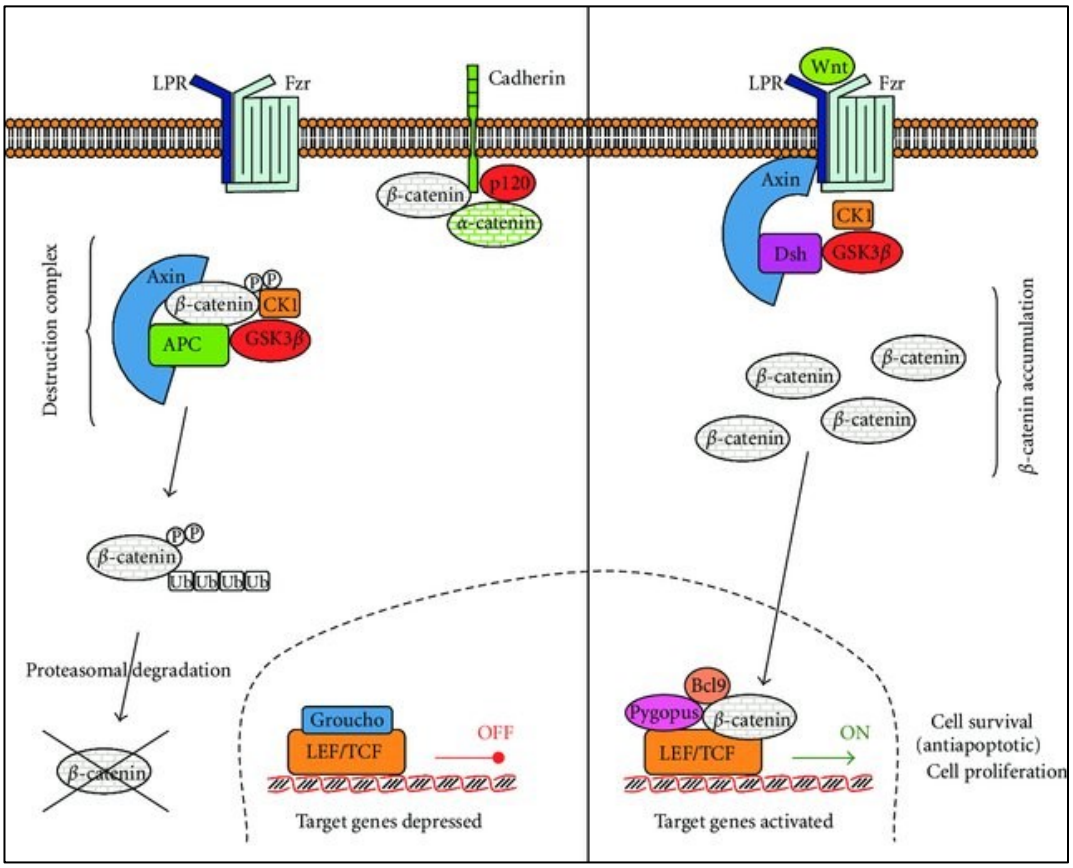

Figure 6: Wnt/β-catenin signalling pathway.

Wnt signalling pathway is shown in the "OFF" (left-hand side) and "ON" (right-hand side) states. In the absence of a Wnt signal, the destruction complex phosphorylates and ubiquitinates β-catenin, being therefore destroyed by the proteasome. In the presence of a Wnt signal, Dsh recruits Axin and inhibits GSK3-β; β-catenin is not phosphorylated and therefore not destroyed. It can translocate to the nucleus and activate transcriptions genes (Modified from Centelles, 2012).

1.11.1.1. Wnt/β-catenin signalling pathway in AC

The Wnt/β-catenin signalling pathway is crucial for both adult cardiac tissue homeostasis and heart development. Although the progressive replacement of cardiomyocytes with fibro-fatty tissue and arrhythmias episodes are primarily related to the destabilization of the intercellular junctions and the subsequent disruption of the myocardial tissue in AC, the alteration of Wnt/β-catenin signalling pathway has recently also linked to this phenotypic condition, as a regulator of myogenesis towards adipogenesis (Lorenzon et al., 2017). This signalling pathway can be dysregulated by the destabilization of the desmosome and the subsequent release of JUP protein in the cytosol, where it competes with β-catenin to go inside the nucleus due to their 70% similarity (Garcia-Gras et al., 2006). JUP commonly referred to as γ-catenin, shares similar protein partners with β-catenin, the effector of the canonical Wnt signalling, and fulfils some of the same activities (**Figure 7**). The interaction between JUP and the TCF-LEF transcription factors induces the expression of pro-adipogenic and pro-fibrogenic target genes (Lorenzon et al., 2017).

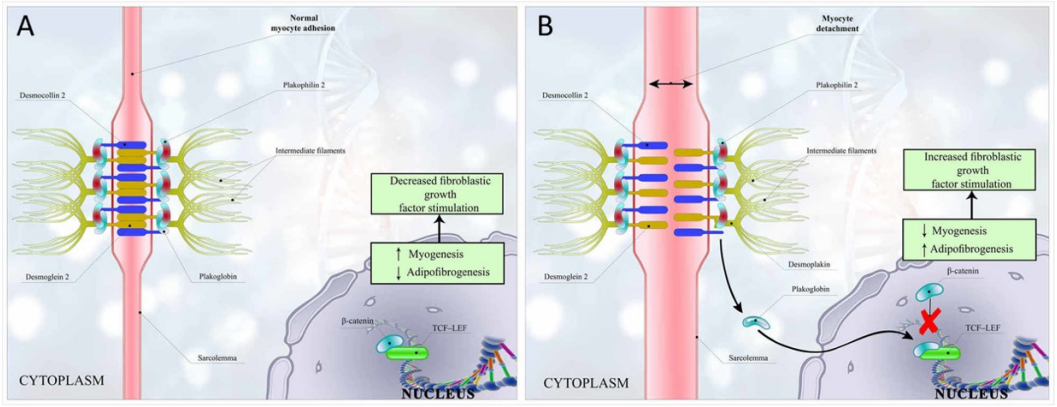

Figure 7: Wnt/β-catenin signalling pathway dysregulation mediated by JUP release. A: Normal attachment of desmosomes components including the connection of DSC-2 and DSG, JUP and PKP-2, connected to each other and to intermediate filaments. β-catenin inhibits fibrogenesis by interacting with TCF-LEF transcription factors. B: Disruption of desmosomes to mutations in desmosomal proteins causes myocyte detachment and release of JUP in the cytosol. JUP causes the separation of β-catenin and TCF-LEF, which, in turn, stimulates fibrogenesis and decreases myogenesis (Modified from Sattar et al., 2019).

Another possible way to dysregulate this pathway is by modulating the activity of GSK3-β, an enzyme directly involved in the phosphorylation of β-catenin and its degradation (Peifer et al., 1994; Yost et al., 1996; Song et al., 2009; Cason et al., 2021). The modulation of this enzyme was found to be controlled also by Gal-3 protein expression levels, leading to the signalling pathway suppression and progression of the disease. More specifically, Gal-3 is an upstream regulator of GSK3-β and it was observed that its downregulation results in reduced amounts of phospho-GSK3-β, which increases its activity. Additionally, decreased phospho-GSK3-β causes β-catenin phosphorylation and degradation, inhibiting the pathway expression (**Figure 8**) (Song et al., 2009; Chelko et al., 2016).

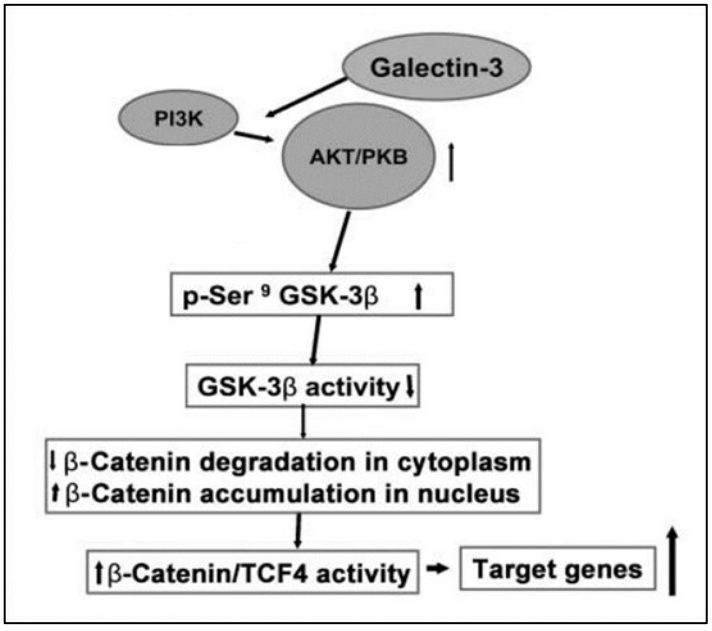

Figure 8: Proposed model by which galectin-3 mediates Wnt/β-catenin signalling pathway dysregulation.

Galectin-3 mediates AKT phosphorylation, thereby increasing the phosphorylation of GSK-3β and decreasing its activity. Inactivation of GSK-3β leads to a reduction in β-catenin degradation and increased cellular β-catenin levels. β-catenin can then translocate to the nucleus, bind to TCF-LEF transcription factors (TCF4), and activate the transcription of its specific target genes (From Song et al., 2009).

1.11.2. Hippo/YAP-TAZ signalling pathway

Like Wnt/β-catenin signalling, also Hippo/YAP-TAZ pathway is an evolutionarily and functionally conserved signal regulator of organ size and tissue growth, very important in the control of stem/progenitor cell fates, cell proliferation, differentiation, and apoptosis (Zhou et al., 2015). In literature, it has also been described to have a central role in cardiac development, survival, and growth, homeostasis, and regeneration but also disease, increasing heart size if downregulated in mice models (Heallen et al., 2011; Chen et al., 2020). It seems that cardiac regeneration is enhanced by inhibiting the Hippo pathway or turning on its downstream effectors, the Yes-associated protein transcription coactivators (YAP and TAZ) (Xie et al., 2022). However, the precise mechanism through which the Hippo pathway controls cardiomyocyte proliferation, apoptosis and regeneration, and contributes to the development of cardiac disease is yet not well understood. The Hippo kinase cascade, which is mainly composed of MST1/2 (Mammalian Ste20-like kinases) and LATS1/2 (Large tumour suppressor) proteins, constitutes the foundation of the pathway. Nuclear response to Hippo signalling is mediated by transcriptional co-activators YAP or TAZ, which are phosphorylated by LATS1/2. This phosphorylation increases the cytoplasmic sequestration of YAP (p-YAP) and TAZ, therefore decreasing their transcriptional activity through the interaction with YAP–TEAD transcription factors (**Figure 9**). Protein kinase C-α (PKC-α), an enzyme that is part of the junctional complex and requires PKP2 to be stable and active (Bass-Zubek et al., 2008), is directly involved in the phosphorylation and inactivation of the Merlin/NF2 tumour suppressor (NF2). Both MST1/2 and LATS1/2 relocate to the sub-membrane space, where their interactions

with NF2 control their activity. Also, YAP phosphorylation is controlled by this protein (Chen et al., 2014). The connection between junctional protein destabilizations and dysregulation of this pathway linked uniquely Hippo/YAP-TAZ perturbations with AC (Hu and Pu, 2014).

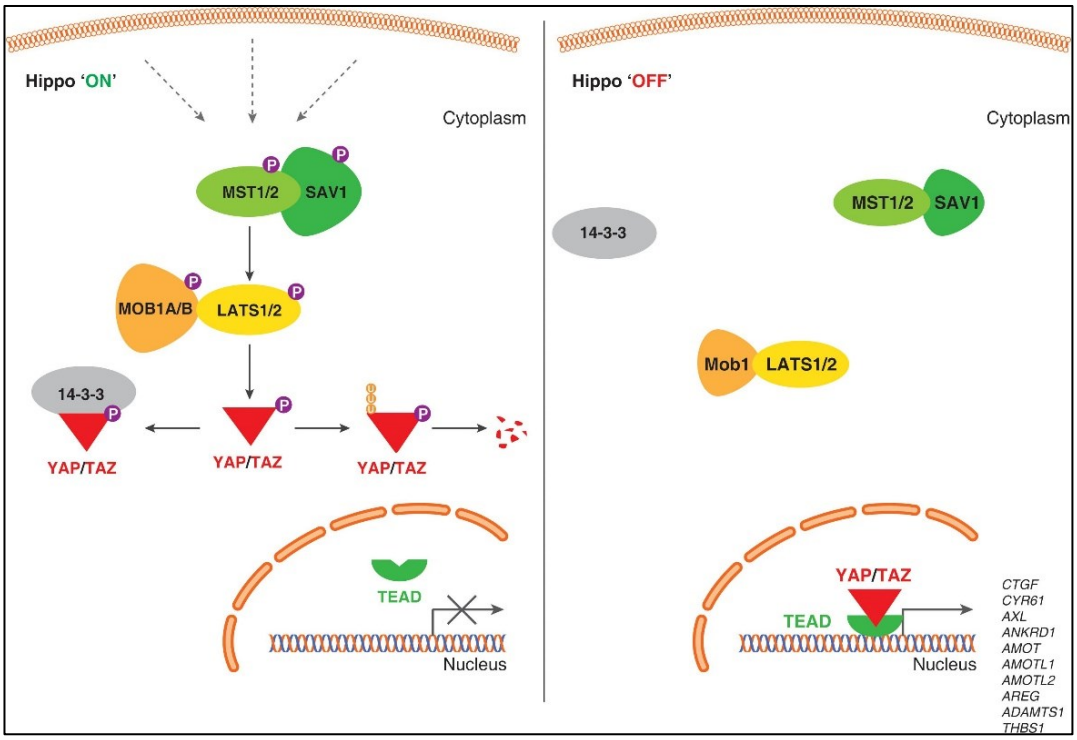

Figure 9: Schematic representation of the Hippo/YAP-TAZ signalling pathway. When the Hippo signalling pathway is "ON" (Left), multiple upstream signals regulate the phosphorylation of MST1/MST2, LATS1/LATS2 kinases, and phosphorylate YAP/TAZ proteins. Phosphorylation of YAP/TAZ leads to cytoplasmic retention or proteolytic degradation. When the Hippo signalling pathway is "off" (Right), YAP/TAZ is not phosphorylated and co-localize to the nucleus, forming a complex with transcription factor TEAD and regulating genes required for proliferation, migration, and survival (From Boopathy and Hong, 2019).

1.11.2.1. Hippo/YAP-TAZ signalling pathway in AC

Pathogenic upregulation of the Hippo/YAP-TAZ pathway was observed in AC patients, resulting from remodelling, impaired assembly, and instability of intercalated disks due to junctional protein mutations. This instability, and specifically the delocalization of the PKP2 protein, reduced the localization of

activated PKC-α at the membrane level. Consequently, the activation of NF2 and Hippo kinases cascade MST1/2 and LATS1/2 increase exponentially the levels of p-YAP, which is not able anymore to translocate into the nucleus and localized in the cytosol or at the membrane. Therefore, p-YAP is not able anymore to interact with the YAP–TEAD transcription factors, stopping the related gene expression and enhancing the expression of genes involved in adipogenesis and apoptosis (Chen et al., 2014). The activation of the Hippo kinases cascade and the subsequent phosphorylation of YAP was identified also as the mechanism for suppression of the canonical Wnt/β-catenin in AC (**Figure 10**) (Austin et al., 2019). The p-YAP, in fact, is observed to be able to bind and sequester β-catenin, forming a complex also with JUP, thus resulting in a reduction of both TCF-LEF and YAP/TEAD transcriptional activities (Chen et al., 2014; Lorenzon et al., 2017).

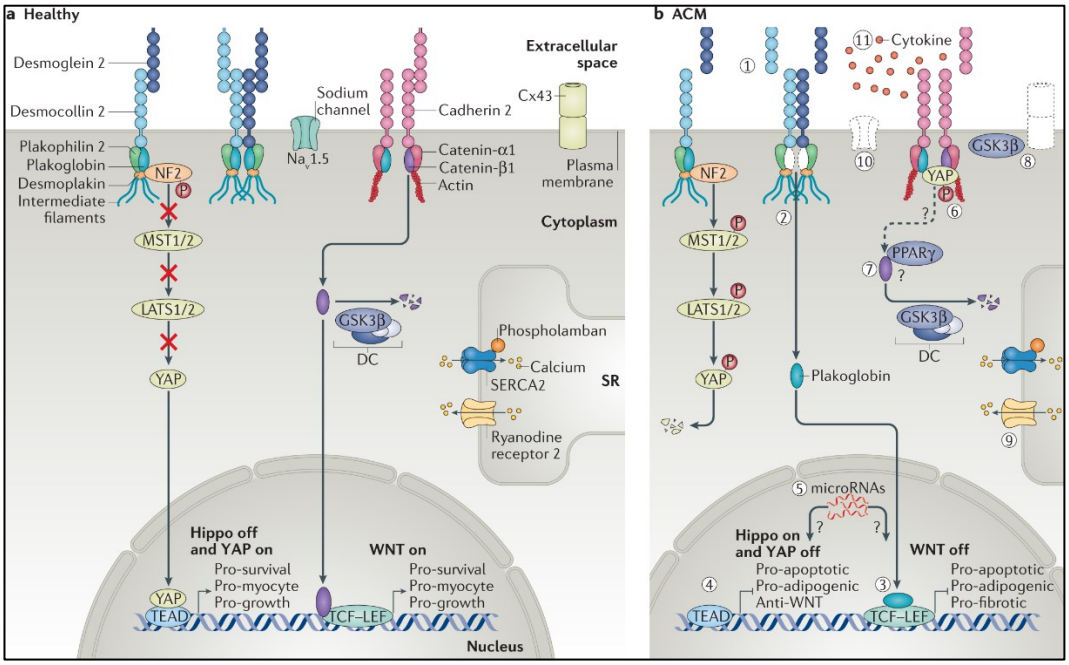

Figure 10: Hippo/YAP-TAZ signalling pathway dysregulation and interplay with Wnt/β-catenin.

A: In healthy cardiomyocytes, both desmosomes and adherens junctions in the area composita form strong intercellular connections with neighbouring cells. β-catenin has a correct localization in both the adherens junctions as well as in the nucleus, activating Wnt/β-catenin. The Hippo pathway is appropriately 'off', allowing YAP/TAZ to go inside the nucleus and promote cardiomyocyte survival and growth. B: In AC cardiomyocyte, disruption of the desmosomes and adherens junctions leads to increased mechanical stress

on the cardiomyocyte. (2) Plakoglobin can dissociate from the desmosome, further destabilizing the intercalated disc, and (3) inhibiting Wnt/β-catenin gene transcription. (4) Activation of the Hippo pathway, potentially through NF2, results in YAP/TAZ phosphorylation and degradation, promoting a pro-apoptotic and adipogenic phenotype. (6) Active Hippo signalling leads to phosphorylation of Yes-associated protein (YAP), which potentially associates with both plakoglobin and β-catenin at the plasma membrane, sequestering β-catenin and further inhibiting Wnt/β-catenin. (11) Increased pro-inflammatory and profibrotic cytokine production, including transforming grown factor-β1 (TGFβ1) and TGFβ3, is thought to contribute to the pathogenesis of AC (Adapted from Austin et al., 2019).

1.11.3. TGF-β SMAD2/3 signalling pathway

TGF-β signalling pathway completes the group of pathways recently associated with AC, together with Wnt/β-catenin and Hippo/YAP-TAZ (Garcia-Gras et al., 2006; Lombardi et al., 2011; Asimaki et al., 2014; Chen et al., 2014; Chelko et al., 2016; Giuliodori et al., 2018). This pathway mediates, at embryonic and adult stages, differentiation, proliferation, and cell- or tissue-specific motility in many different species. TGF-βs family (TGF-β1, -2, -3) is composed of molecules that interact with specific receptors at the membrane level, which are formed by two subunits: TGF-β type I receptor (TGFβRI) and TGF-β type II receptor (TGFβRII) (Heldin and Moustakas, 2016). These two parts of the receptor dimerize after ligand interaction and while the TGFβRII subunit phosphorylates TGFβRI, activating it, the latest one acts directly on proteins of the SMAD family, phosphorylating, in turn, SMAD2 and SMAD3, the major effector molecules of this pathway (Derynck and Budi, 2019). These two phosphorylated molecules interact with a common mediator SMAD4, going inside the nucleus and cooperating with the DNA binding transcription factor controlling the expression of target genes (**Figure 11**) (Tzavlaki and Moustakas, 2020). The TGF-β pathway was observed to be upregulated in myocardial disease, being involved in cardiac repairing, remodelling, and fibrosis. For example, in infarcted myocardium, TGF-β fibrotic activity plays a critical role in healing, but too much or too long-lasting signalling amplifies unfavourable remodelling and causes an aggravation of the heart dysfunction (Frangogiannis, 2022). TGF-β, in fact, promotes myofibroblast trans-differentiation and matrix

formation while inactivating inflammatory macrophages, moving the infarct from the inflammatory phase to the scar forming phase (Dobaczewski et al., 2011).

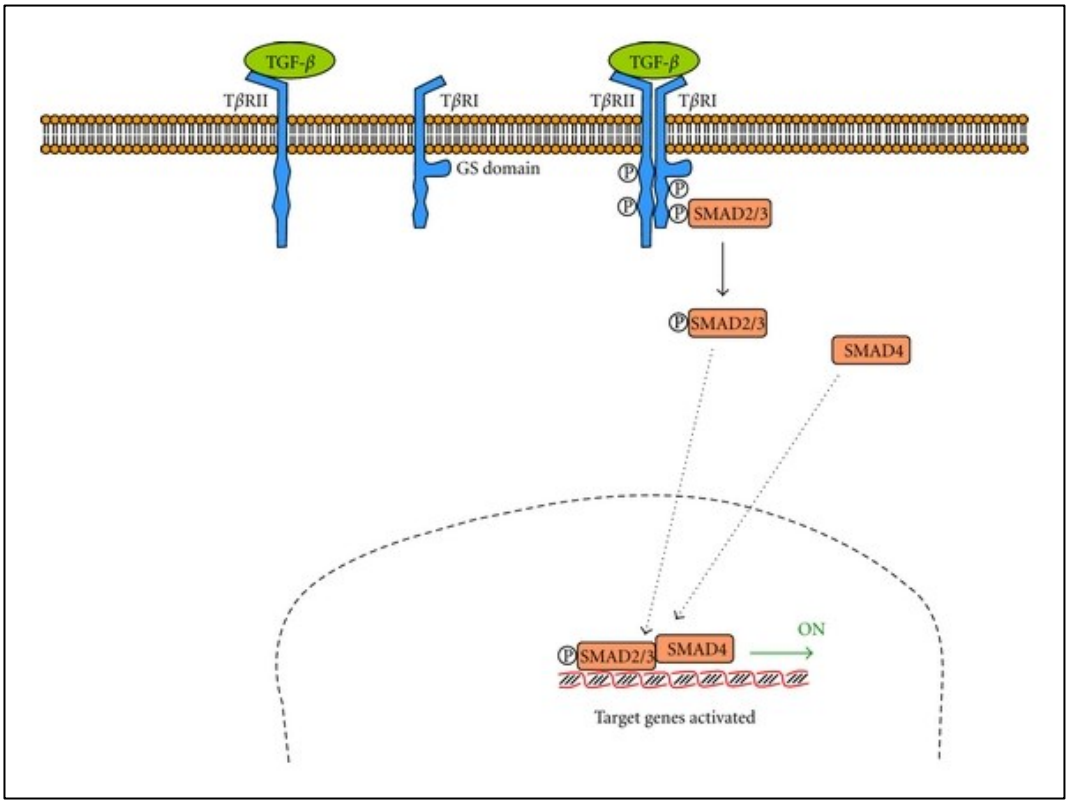

Figure 11: Transforming growth factor-β (TGF-β) pathway.
The TGF-β receptor is a dimer formed by TβRII (with a binding site for TGF-β) and TβRI (with a glycine/serine-rich domain). The complete receptor is autophosphorylated and recruits and phosphorylates gene regulatory proteins called SMADs (From Centelles, 2012).

1.11.3.1. TGF-β SMAD2/3 signalling pathway in AC

The fibrotic hallmark of the pathogenesis of AC was demonstrated to be related to the upregulation of TGF-β signalling pathway in the cardiac tissue of patients with AC, although there is still a lot to understand about this pathogenic step (Maione et al., 2021). Indeed, TGF-β pathway is mainly involved in the regulation of myocyte cell death, including both apoptosis and necrosis, as well as influencing cardiac fibrosis, during the early stages of the disease in AC hearts. Moreover, TGF-β and Wnt/β-catenin pathways are also cross-talking, working together in a synergic

manner stimulating fibrotic processes (Yousefi et al., 2020). Finally, TGF-β pathway can also be inhibited by the Hippo/YAP-TAZ pathway trough interactions between p-YAP and SMADS proteins, preventing their nuclear translocation and transcriptional activity (Ferrigno et al., 2002; Lorenzon et al., 2017). Gal-3 upregulation was observed also in many different human fibrotic conditions (Henderson and Sethi, 2009), underlying its positive effect on this process, if present. It was demonstrated that, in cardiac tissue, Gal-3 and TGF-β interact with each other and, specifically, Gal-3 stimulates the TGF-β pathway, inducing fibrotic processes (Blanda et al., 2020; Xiao et al., 2020).

1.12. Animal models for AC

Animal models are used in research to improve the knowledge of human diseases at cellular and molecular levels, to assess their pathogenesis and progression, to verify the impact of specific environmental factors, and to develop and testing new drug treatments. Due to the great similarity between the murine and human genomes and the many analogies in their morphology, cell biology, and physiology, the mouse is the most used animal model for the study of human disorders. Invertebrates are easier to maintain and manage than vertebrates, and the functional conservation of biological processes between the two groups implies that some disorders can be reproduced in these organisms. However, their use is constrained by the absence of many structures and organs fundamental for the aetiology of several disorders. Despite the progress in identifying the genes responsible for AC, the mechanism that undergoes all these changes and the events that lead to the manifestation of the disease are still not well understood and need an in-depth study. To do so, the use of animal models to study the disease and decode the less clear points of this pathogenesis is probably the only way. Several knock-out (KO) mice models of genes encoding for desmosomal proteins already related to AC, because found in human patients (McKoy et al., 2000; Norgett et al., 2000; Gerull et al., 2004; Pilichou et al., 2006), manifested embryonic lethality due to cardiac abnormalities, connecting undoubtedly these genes with AC but not allowing the study of the disease. Precisely, *Jup*-deficient mice showed a strongly reduced number of cardiac desmosomes and a related embryonic death (Bierkamp et al.,

1996). Moreover, *Dsp*-, *Dsg2*- and *Pkp2*-deficient mice displayed the same phenotype (Gallicano et al., 1998; Eshkind et al., 2002; Grossmann et al., 2004). As said before, despite the promising impacts that the results obtained with these models brought on the understanding of human cardiovascular genetics, the molecular investigations of the pathogenesis responsible for AC were constrained by foetal mortality. Therefore, transgenic knock-in (KI) models, reproducing the mutations found in AC patients, or cardiac-specific KO animal models for AC-related genes have been created to prevent embryonic death, showing a clear AC condition leading to significant discoveries in the field (Garcia-Gras et al., 2006; Pilichou et al., 2006; Rizzo et al., 2012; Zhou et al., 2015; Chelko et al., 2016). However, mice animals do not seem to be as susceptible to heart-related genetic inheritable defects as humans; they frequently require homozygosity (recessive) models for mutations that manifest as heterozygous (dominant) in humans, and hardly develop cardiac fatty tissue. Despite these drawbacks, mice models have helped a lot to understand the pathogenesis and the molecular mechanisms underlying AC.

1.12.1. The zebrafish animal model

The zebrafish (*Danio rerio*), a popular model organism in science, genetics, and developmental biology, is included among the numerous animal models available for AC. Zebrafish is a small tropical teleost fish, belonging to the Cyprinidae family, widespread in fresh waters of Asia, where mostly eats larvae and tiny crustaceans. The name “zebrafish” is derived from the distinctive horizontal blue stripes alternating with white lines, which run across the adult fish's body and the fins (**Figure 12**).

Figure 12: Zebrafish representation.
Image of Zebrafish with the characteristic horizontal blue metallic stripes alternating with white lines, which run along the body and the fins.

The female zebrafish presents a lighter coloration and a bulge at the ventral level, because of the presence of eggs in the ovary. Differently, the male zebrafish is darker, brighter in colour, and more tapered on the ventral side (**Figure 13**) (Dahm and Geisler, 2006). Since experiments with laboratory rodents are very expensive, time-consuming, and limited by ethical considerations, zebrafish can represent an excellent alternative as it offers the combination of invertebrate manipulability and vertebrate biological relevance. About 71% of human proteins have an orthologue in zebrafish and, of these, 82% are known to be implicated in human disease (Dahm and Geisler, 2006; Howe et al., 2013). This strong genetic similarity allows the use of zebrafish to generate various mutant and fluorescent transgenic reporter lines, using several approaches, such as the CRISPR/Cas9 technique, to model specific diseases or pathological conditions. In zebrafish, the breeding is quite simple and requires limited space due to its small size (about 4-5 cm). Several eggs, 100 to 200, are fertilized in every breeding event and the development of zebrafish larvae occurs externally and is extremely rapid. Major organs develop in almost 24 hours and sexual maturity is reached in 3-4 months. Moreover, the reproduction by external fertilization allows the manipulation of the embryos since their first mitotic divisions and, taking advantage of the transparency in the first days of development, it is possible to observe *in vivo* the various stages of the growth or identify any morphological abnormalities in the organs, including the heart (**Figure 13**). The zebrafish model is quite useful to perform drug testing and find new possible therapeutic treatments for humans (Lieschke and Currie, 2007). Drug sensitivity is

high at larval stages and low molecular weight compounds (below about 1 kDa) can be administered directly into the water and easily absorbed.

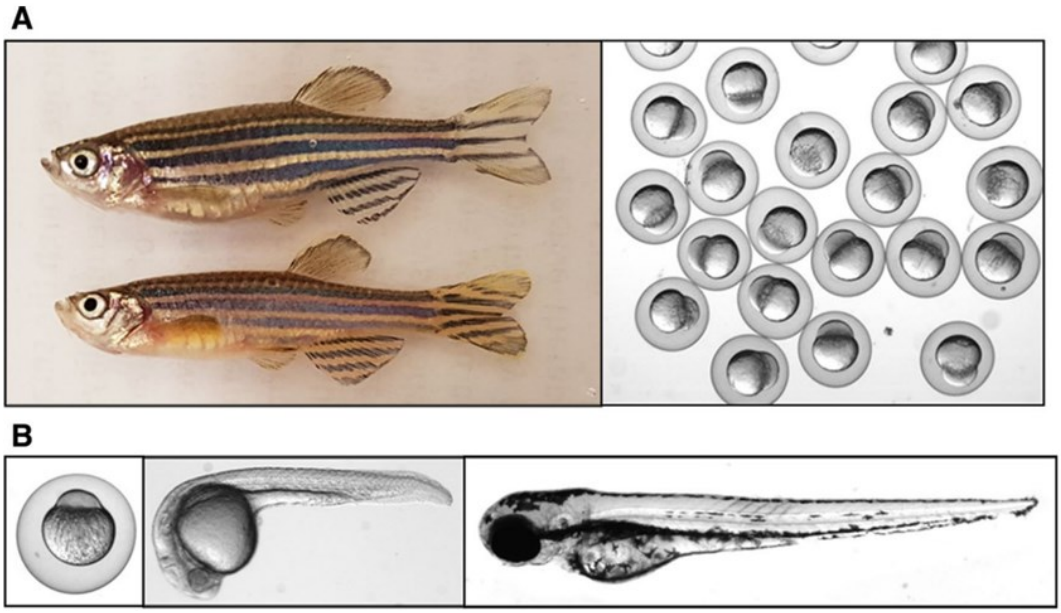

Figure 13: Larve and adult zebrafish.

A: adult female and male zebrafish (left) produces hundreds of eggs (right) weekly. B: Embryos at one-cell stage (left), 24 hpf (middle) and 72 hpf (right) are shown (From Shi et al., 2018)

Approximately 270 million years ago, teleosts had a full genome duplication event and because of functional redundancy, there was a brief secondary loss of some duplicated genes (Postlethwait et al., 1998; Hurley et al., 2007). However, 47% of human genes have just one orthologue in zebrafish, compared to 24% of human genes that have several orthologues. The two orthologues of a human gene may occasionally maintain each all or some functions of the original one (sub-functionalization), or they may occasionally both take on new functions (neo-functionalization) (Howe et al., 2013). This partial genetic duplication that defines also the zebrafish genome is one of its principal drawbacks, increasing a lot the amount of effort work to generate a stable mutant line if the target is duplicated and increasing the factors that should be considered in the process (Dahm and Geisler, 2006).

1.12.1.1. The zebrafish as animal model in AC

Considering that the heart of zebrafish works in a similar way if compared to the human one, *Danio rerio* can be applied to understand the function of specific cardiac genes involved in many human cardiovascular disorders, facilitating the future development of cures (Giardoglou and Beis, 2019). Zebrafish can recapitulate human cardiac pathophysiology due to the conservation of genes and similar structural and electrical features (Genge et al., 2016; Vornanen and Hassinen, 2016). The main difference with the human heart is that the zebrafish one presents only two chambers, the atrium and ventricle, arranged in series and located ventrally in the animal (**Figure 14**) (Bowley et al., 2022). The zebrafish heart is the first functional organ to develop during embryonic growth (Benslimane et al., 2020) and, initially, it is like a "tube" that contracts and move blood trough itself. During development, this primordial heart structure undergoes morphological changes that form the two-chamber conformation (Glickman and Yelon, 2002). A one-way atrioventricular valve allows venous blood to enter the atrium before passing into the ventricle while a one-way outflow valve is used instead by the ventricle to pump blood to the body.

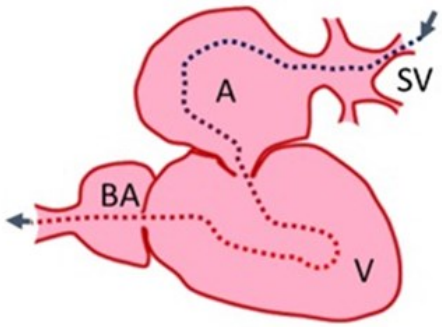

Figure 14: The zebrafish heart structure.
The zebrafish heart consists of two chambers, an atrium (A) where the blood flows into the heart through a sinus venosus (SV), and a ventricle (V) where the blood flows out and they are connected by an atrioventricular valve. The bulbus arteriosus comes after the ventricle and it regulates and maintains the continuous blood flow into the gill arches (Modified from Benslimane et al., 2020).

Yet it still has some essential similarities to the human heart. Despite the simpler morphology, if compared to the four-chambered human heart, the zebrafish heart's physiological and electrical functions, such as heart rate, contractile dynamics, action potential, and overall structure are the same (Genge et al., 2016; Vornanen and Hassinen, 2016). Primary mammalian cardiac development is quite like the zebrafish heart's overall, with genetic processes and signalling pathways conserved between the species. At embryonic stage, this organ is very similar to the heart of a human embryo at 3 weeks gestation (Warren and Fishman, 1998). More precisely, a 12-day old mouse or 35-day old human embryonic heart can be compared morphologically and physiologically to a 2-day post fertilisation (dpf) zebrafish one. Furthermore, prior to septation, the adult zebrafish heart shares morphological characteristics with the embryonic mammalian heart. Several physiological processes are analogous as well. For instance, the zebrafish heart begins to beat as a peristaltic wave 22 hours post fertilization (hpf) and contraction of the atrium and ventricle occurs asynchronously starting at 36 hpf with a heart rate (150 bpm at 72 hpf) that is closer to that of humans (60-100 bpm) than mice (300 bpm). By exploiting the transparency of the embryo, it is possible to observe *in vivo*, non-invasively, the contraction of the atrium and ventricle and the movement of blood in the vessels. Furthermore, during the first days of development, zebrafish embryos are not yet dependent on the cardiovascular system, given the uptake of oxygen by passive diffusion, and can therefore survive even under critical cardiovascular conditions that normally are lethal at embryonic stages in most vertebrates, such as mice (Sehnert and Stainier, 2002). Finally, the possibility to perform intensive physical training on both larvae and adult fishes using different methodologies (Ruparelia et al., 2014; Lucon-Xiccato et al., 2021), allows the study of the involvement and impact of physical exercise in the pathogenesis of several cardiac diseases like AC. However, zebrafish, as mice, difficultly show adipogenic substitution in the cardiac tissue and adult zebrafish cardiomyocytes still can proliferate and regenerate the cardiac tissue after several injuries, a quality that the early postnatal mammalian ventricle has also proved to possess (Poss et al., 2002). Recently, AC zebrafish models, presenting the silencing or the insertion of mutations in AC-related genes, were generated to try to understand better this

disease (Heuser et al., 2006; Martin et al., 2009; Moriarty et al., 2012; Li et al., 2013; Asimaki et al., 2014; Giuliodori et al., 2018). Most of these models, with some exceptions, such as the zebrafish model for AC that presents cardiac myocyte–specific expression of the human 2057del2 mutation in the gene encoding Jup (Asimaki et al., 2014), are transient knock-down (KD) models obtained using morpholinos. These synthetic antisense oligomers present a strong affinity for RNA, working as translation- and/or mRNA splicing-blocking agents, not allowing the expression of the chosen genes until they lose their activity. More in detail, *jup*, *pkp2*, *dsc2,* and *dsp* KD models showed an immediate cardiac phenotype presenting pericardial effusion, structurally deformed hearts, bradycardia, and valvular dysfunction that causes blood reflux between the two cardiac chambers. In addition, desmosome localization and stability appeared affected, with also AC-related signalling pathways dysregulations signs, such as Wnt/β-catenin downregulation (Heuser et al., 2006; Martin et al., 2009; Moriarty et al., 2012; Giuliodori et al., 2018). This temporary silencing of gene expression does not permit the observation of a possible onset and progression of the disease, but make it possible to understand that these desmosomal genes, both in zebrafish neither in human, also in this model are likely involved in the same processes at the cardiac level, validating zebrafish as an excellent animal model to reproduce AC. Therefore, these models should only be considered as preliminary, paving the way for more stable KO or KI ones. As mentioned before, the only KI-stable zebrafish model for AC in literature is Asimaki's which presents the human 2057del2 mutation in the gene encoding Jup, responsible for the Naxos syndrome in humans (Asimaki et al., 2014). Within 48 hours after fertilization, *jup*-mutant zebrafish displayed abnormal cardiac physiology, and after 4 to 6 weeks, completely penetrant cardiomyopathy, which is characterized by cardiomegaly, pericardial effusion, and ultimately death due to arrhythmias episodes, or heart failure. A high-throughput drug screen was performed in this mutant, identifying SB216763, an agonist of the Wnt/β-catenin signaling pathway, as a suppressor of the disease phenotype, preventing heart failure and reducing mortality (Asimaki et al., 2014). This drug molecule was tested later also in the *dsp* knock-down (KD) zebrafish models by my research group (Giuliodori et al., 2018), confirming the positive results obtained before. Regarding the modelling in zebrafish of AC due to non-desmosomal gene mutations, recently

a *lgals3a* KD-zebrafish model was generated with a net effect on embryo development, a reduced number of macrophages, dysregulation of Wnt/β-catenin signalling pathway and cardiomyocyte apoptosis, underling a possible involvement of this gene in the pathogenesis of AC, but also in general in cardiac diseases (Chen et al., 2021).

1.12.1.2. Desmoplakin and Galectin-3 in zebrafish

Both *dsp and lgals3* genes appear duplicated in zebrafish and, specifically, *dsp* is represented by the genes *dspa*, located on chromosome 2, and *dspb*, located on chromosome 20, while *lgals3* duplication generated *lgals3a* on chromosome 13, and *lgals3b* on chromosome 17. The proteins encoded by *dspa and dspb* resembled the DSP human orthologue with a sequence identity of 42% and 45%, and similarity of 67% and 63% respectively with humans. Conserved structure and domain involved in the interaction with DSG and DSC2 in the C-terminal region and with PKP2 and JUP in the N-terminal one are present in the Dsp zebrafish proteins, underlying their well-preserved function and making them suitable for a direct connection, if mutated, with a possible AC phenotype. Both zebrafish orthologous genes are expressed in the skin and in the cardiac tissue as in humans, although *dspa* more markedly than *dspb*, forcing us to consider both for AC model generation (Giuliodori et al., 2018). Regarding the *lgals3a and lgals3b* genes, they also are both present in the cardiac tissue in zebrafish (Ahmed et al., 2004), like the *dsp* genes. The identity with the human *LGALS3,* in this case, is around 47 % for *lgals3a* and 42% for *lgals3b,* with a similarity of 59% and 57% with human respectively. Moreover, also in these proteins the activity and the biological functions are preserved, due to the presence of the conserved CRD domain at the C-terminal region, which allows the interaction with oligosaccharides that contain glycoconjugates and the anti-apoptotic activity. In addition, the N-terminal tail is conserved and involved in nuclear translocation, secretion outside the cells, reduced affinity for its ligands and anti-apoptotic signalling activity for oligomerization.

2. MATERIALS AND METHODS

2.1. Zebrafish handling and maintenance

All experiments were performed in accordance with the Italian and European Legislations (Directive 2010/63/EU) and with permission for animal experimentation from the Ethics Committee of the University of Padua (OPBA) and the Italian Ministry of Health (Authorization number 407/2015-PR). *Danio rerio* (zebrafish) were kept in a temperature-controlled (28.5 °C) environment, with a 12:12 light-dark cycle, staged and maintained following standard procedures (Kimmel et al., 1995). Fish need clean, well-oxygenated water with the constant removing of nitrogenous waste and particles, therefore a water recycling system (continuously operating pumps and filters) is necessary. The water used in this system respects international standards and parameters: Alkalinity 50-150 mg/L CaCO3; pH 6.8-7.5; Temperature 26-28.5°C; Hardness 50-100 mg/L CaCO3. Zebrafish embryos are manually and/or automatically fed with dry food starting on 5 dpf. Until they remain in the facility's nursery, the zebrafish embryos are constantly monitored, with water flux control and weekly tank and filter cleanings. Due to *Danio rerio*'s natural egg-eating tendency, the pairing of adult individuals (from 3 months old) needs to be done in special tanks with a double bottom that allowed the separation of the animals from the freshly laid eggs. The eggs are then collected using a strainer and maintained in Petri dishes where they were cleansed (rotten or unfertilized eggs were removed) and kept at the ideal temperature (27–28.5°C) until 7 dpf. Tricaine (Sigma-Aldrich, St. Louis, Missouri, United States), a chemical compound able to inhibit skeletal muscle activity by blocking the entrance of sodium ions and so the progression of action potentials, was used to anaesthetize or euthanize zebrafish embryos and adult fish (0.16 mg/mL for anaesthesia or 0.3 mg/mL for euthanasia). Wild-type lines used in this work included Tuebingen, Giotto and Umbria strains (Pauls et al., 2007).
The following transgenic lines were used:

- Wnt/β-catenin reporter line *Tg(7xTCF-Xla.Siam:EGFP)*^{ia4}, in which the engineered green fluorescent protein (EGFP) expression is controlled by the Wnt-responsive TCF transcriptional complex (Moro et al., 2013).

- Myocardial reporter line *Tg(tg:EGFP-myl7:EGFP)*^{ia300} in which the EGFP is expressed specifically under the control of the myosin light chain 7 (*myl7*) promoter in the zebrafish heart's myocardium (Porazzi et al., 2012). The line expresses EGFP also under thyroglobulin (*tg*) promoter control.

2.2. Generation of mutant lines

The zebrafish mutant line for desmoplakin a (*dspa*) was obtained from the Zebrafish Mutation Project (ZMP) using the ENU (N-ethyl-N-nitrosourea) mutagenesis, a chemical forward genetic technique that introduces point mutations randomly. The identifying allele *sa13356* carries a nonsense mutation (Chr 2: g.2324300 C>T) on exon 23, leading to the formation of a premature stop codon (p.Gln960Ter). The zebrafish mutant line for desmoplakin b (*dspb*), bearing a 13-nucleotide deletion (Chr 20: g.52912248_52912260del), was produced in our laboratory (allele *ia305*) by using the CRISPR-Cas9 approach. The galectin-3 a (*lgals3a*) and galectin-3 b (*lgals3b*) bear a 4-bp (Chr 13: g. 36578952¬ 36578957del) and a 114-bp (Chr 17: g10832046-10832160del) deletion, respectively, in their exons 3, after CRISPR-Cas9-mediate mutagenesis. To delete the functional protein, single guide RNAs (sgRNAs) (**Table 3**) were designed using the CHOPCHOP software (https://chopchop.cbu.uib.no/), to specifically target an optimal CRISPR sequence within each gene, generated according to Gagnon and colleagues (Gagnon et al., 2014) and transcribed *in vitro* using the MEGAshortscript T7 kit (Life Technologies, Carlsbad, California, United States) (Gagnon et al., 2014). One-cell stage embryos were injected with 2 nL of a solution containing 280 ng/µL of Cas9 protein (New England Biolabs, Ipswich, Massachusetts, United States) and 100 ng/µL of sgRNA; phenol red was used as an injection marker. F0 injected embryos were raised to adulthood and screened, by F1 genotyping, for germline transmission of the mutation. Heterozygous mutants, harboring the mutation of choice, were out-crossed 4 times and then in-crossed to obtain homozygous mutants (F5 generation).

Table 3: List sgRNA oligos for *dspb/lgals3a/lgals3b* mutant lines generation.

Constant oligo	CRISPR/Cas9 DNA oligomer for gRNA	5'-AAAAGCACCGACTCGGTGCCACTTTTTCAAGTT GATAACGGACTAGCCTTATTTTAACTTGCTATTTCTAG CTCTAAAAC-3'
Dspb-specific oligo	gRNA sequence	5'-ATTTAGGTGACACTATA**GGAAGTGCATCTCCA GACTG**GTTTTAGAGCTAGAAATAGCAAG-3'
Lgals3a-specific oligo	gRNA sequence	5'-ATTTAGGTGACACTATA**GGAGGCTTTCCTGCTCA CCCAGG**GTTTTAGAGCTAGAAATAGCAAG-3'
Lgals3b-specific oligo	gRNA sequence	5'-ATTTAGGTGACACTATA**GCAGGCTGACCAGGC CAGACGGG**GTTTTAGAGCTAGAAATAGCAAG-3'

2.3. DNA extraction

The HotSHOT protocol (Meeker et al., 2007) was used to prepare genomic DNA from whole embryos at 24-48 hours post fertilization (hpf). Each embryo was placed in a tube with 0.16 mg/mL Tricaine solution in fish water (0.5 mM NaH2PO4; 0.5 mM Na2PO4; 1.5 g Instant Ocean salts; 2 mg/L Methylene blue). After 2 min, Tricaine was discarded and the tube was filled with 50 µl DNA lysis buffer (NaOH 50 µM). The tubes were heated at 95°C for 20 min and cooled down at 4°C for 5 min; 5 µl of Tris HCl 1 M pH 7.5 were added to neutralize the DNA sample. Genomic DNA from zebrafish adults was prepared likewise after caudal fin biopsy (fin clipping).

2.4. Genotyping of mutant lines

Homozygous and heterozygous nonsense mutations in *dspa* were identified by direct sequencing of *dspa*-specific PCR products. Homozygous and heterozygous deletions in *dspb, lgals3a and lgals3b* were identified by gene-specific PCR followed by agarose gel electrophoresis. The results were then confirmed by direct sequencing analysis.

2.4.1. PCR amplification

The PCR reaction follows the classic proportion between each reagent, with a final reaction mix composed by:

- 2.5 µl of 5xHOT FIREPol® Blend Master Mix (Solis BioDyne, Tartu, Estonia) with 12.5 mM MgCl2
- 0.5 µl of Forward and Reverse primer
- 2 µl genomic DNA (100 ng of DNA)
- Nuclease-Free H2O up to a final volume of 12.5 µl

Negative control samples are always included in the analysis, substituting the 2 µl genomic DNA with Nuclease-Free H2O. The prepared samples were subsequently placed in a QIAamplifier 96 thermocycler (QIAGEN, Hilden, Germany) to proceed with the PCR reaction, which includes 35 cycles of denaturation, annealing, and extension phases:

Phase	Temperature	Time
Taq polymerase activation	95°C	13 min
Denaturation	95°C	20 sec
Annealing	See Table 4	30 sec
Extension	72°C	30 sec
Final extension	72°C	10 min
Sample cooling	8°C 4°C	10 min 15 min

Specific primers are designed to recognize and amplify the genomic regions of interest, in which the mutations were generated (**Table 4**). All primers were designed using the Primer3 software (http://primer3.ut.ee).

Table 4: List of primers for PCR-based genotyping.

Gene name	Forward primer (5'-3')	Reverse primer (5'-3')	Product size (bp)	Ann. T°
dspa	ATCGAGGAGGAAAAGCGCAA	GCCTCATCCTGCAGCTGTAA	194	62°C
dspb	CAAAATGGGCCCGGATGAG	AGCTTCTGGTCTTCGGCTC	114	62°C
lgals3a	AGGAATGTTTCCTCCAGTACCA	CTTACACGTGCAAACCCATTTA	178	60°C
lgals3b	TTGTGAACAGACCATTTTTCTGA	GATTGCAAGCTGTACAAATCCA	422	60°C

2.4.2. Agarose gel preparation and electrophoretic running

The PCR products are loaded into an agarose gel, with a percentage of agarose that depends on the dimension of the deletion that should be observed. The number of grams of Multi-Purpose agarose powder (Thermo Fisher Scientific, Waltham, Massachusetts, United States) was weighed and added to 100 mL of 1X Tris-Borate EDTA (TBE) buffer (45 mM Tris-borate/1 mM EDTA). The suspension was heated in a microwave until the agarose is completely dissolved and a transparent solution is obtained. When the solution cooled down at about 60°C, a GelRed nucleic acid-binding fluorescent dye (Sigma-Aldrich, St. Louis, Missouri, United States), that interacts with DNA and RNA via intercalation between the base pairs, was added under a chemical hood. After that, the agarose solution must be immediately poured into an electrophoretic tray, where the proper comb was inserted, and left to cool until the gel was completely solid. Then, the comb was removed, and the gel was covered with the 1X TBE buffer solution. A 100 bp or 1 kb molecular weight marker (Solis BioDyne, Tartu, Estonia) needs to be loaded into the first well, to determine the fragment size of the PCR products in the adjacent wells, including the negative control to verify the absence of contamination. A voltage generator, set at 70 V, after being connected to the electrophoretic tray, was activated. The DNA is negatively charged thus, depending on the weight, it moves at varying speeds from the negative pole to the positive one. The gel was checked with a UV trans-illuminator and imaged using an Alliance 9 Mini UV Fluorescence Imaging System (Uvitec, Cambridge, UK).

2.4.3. PCR product purification

Before sequencing, primers and dNTPs that were left in PCR products were removed by an Exonucleases 1 (EXO)/Shrimp alkaline phosphatase (SAP) incubation, because they can interfere with the following sequence reaction. Two µl of ExoSAP solution (Illustra ExoProStar 1-Step kit) (GE Healthcare Life Sciences, Chicago, Illinois) were added to 5 µl of PCR product, with SAP enzymes that dephosphorylate dNTPs and EXO enzymes that hydrolyse primers and single-strand DNA filaments. A 15-minute incubation at 37°C is sufficient to complete the reaction, followed by another 15 minutes at 80°C to inactivate the enzymes.

2.4.4. Sanger sequencing analysis

The Sanger method, developed by Sanger in the ’70s (Sanger et al., 1977) needs specific chemically altered bases called di-deoxy nucleoside triphosphates (ddNTPs) that can block the DNA chain elongation. ddNTPs carried four different fluorophores and lack a 3’-hydroxy group that, when incorporated into a newly synthesized DNA fragment due to the presence also of normal dNTPs, terminates the DNA strand elongation at specific bases (A, C, T, or G). Using capillary electrophoresis, this procedure generates DNA fragments of various sizes that can be separated and identified using laser-induced fluorescence. The reaction and the analysis itself were carried out at the Department of Cardio-Thoraco-Vascular Sciences and Public Health, through the collaboration with the Cardiovascular Genetics Laboratory of the Cardiovascular Pathology Unit (COU).

2.5. Body length measurements and morphological analysis

Fish lengths and morphological observations were analyzed using a bright field microscope (Leica M165FC, Leica Microsystems, Wetzlar, Germany) equipped with a digital camera (Leica DFC7000T, Leica Microsystems, Wetzlar, Germany), connected to a computer with Leica Software (LAS V4.8, Leica Microsystems, Wetzlar, Germany) for image acquisition and processing. The zebrafish were

anesthetized with 0.16 mg/mL Tricaine solution in fish water, placed in microscope slides with 2% methylcellulose in 1X PBS, and oriented laterally to facilitate the measurement and observation. Hearts were extracted from adult fish (1-year-old) using tweezers and other dissection tools and then acquired using the same aforementioned experimental settings. A morphological comparison of the hearts was also conducted. For the image analysis, ImageJ software was used.

2.6. Heart rate analysis

The zebrafish larvae were anesthetized with 0.16 mg/mL Tricaine solution in fish water and placed in microscope slides with 2% methylcellulose in 1X PBS and oriented laterally to facilitate heart rate counting. A bright field microscope (Leica M165FC, Leica Microsystems, Wetzlar, Germany) was used to perform the experiments. Heart rates were determined by counting the number of atrial contractions during 60 seconds in embryos from 2 to 7 dpf. The number of heartbeats per unit of time was expressed as beats per minute (bpm).

2.7. Quantitative Real-Time Reverse Transcription PCR

2.7.1. RNA extraction, isolation and quantification

For RNA extraction, TRIzol reagent (500 µL) (Thermo Fisher Scientific, Waltham, Massachusetts, United States) was added to pools of 30 zebrafish embryos at 3 dpf or to hearts of 12-month-old zebrafish that were homogenized with glass/stainless steel beads for 3 minutes in a tissue-lyser machine (Tissue Lyser II, QIAGEN, Hilden, Germany). After incubation for 5 minutes at RT to allow complete dissociation of the nucleoprotein complexes, total RNA was isolated inside the solution adding chloroform (100 µL in 500 µL of TRIzol). The sample was immediately vortexed for 15 seconds and incubated again for 5 minutes at RT. To separate the superior aqueous phase that contains RNA, from the underlying protein and DNA phase, centrifugation at 16,000 g for 15 minutes at 4°C was needed. The aqueous phase with the RNA was then transferred into a

new 1.5 mL tube and 250 µL of Isopropanol were added and mixed to the solution, which was left at -20°C overnight (O/N) to allow the precipitation of the RNA pellet. The following day, after 10 minutes of incubation at RT, Isopropanol has pulled away from the 1.5 mL tube and EtOH 75% was added and removed 3 times, alternated by centrifugation at 16,000 g for 15 minutes to wash the RNA pellet. In the end, it was suspended one last time in 21 µL of Nuclease-Free H2O, heated for 5 minutes at 55°C, and conserved at -80°C. The NanoDrop (Thermo Fisher Scientific, Waltham, Massachusetts, United States) spectrophotometer allowed the analysis of the nucleic acid concentration (ng/µL) and the check of possible protein/solvent contamination (260/280 and 260/230 ratios).

2.7.2. Reverse Transcription

The Applied Biosystems™ High-Capacity cDNA Reverse Transcription Kit (Applied Biosystems, Waltham, United States) contains all the reagents needed for reverse transcription (RT) starting from 1 µg of isolated total RNA that is converted into a single-stranded cDNA, suitable for qPCR. The random primer method is used for initiating cDNA synthesis, and ensuring that the first strand synthesis occurs efficiently with all species of RNA molecules present, including mRNA. A 10 X RT buffer, 25 X dNTP (100 mM), 10 X RT Random primers mix, Nuclease-free H20, MultiScribe™ Reverse Transcriptase, and an RNase Inhibitor to prevent RNA degradation, compose the reaction mix (10 µL final volume).

Component	Volume (µL)
10X RT Buffer	2
25X dNTP Mix (100 mM)	0,8
10X RT Random Primers	2
MultiScribe™ Reverse Transcriptase	1
RNase Inhibitor	1
Nuclease-free H2O	3,2
Total per reaction	10

In parallel, the RNA solution was prepared to dilute 1 µg of total RNA in 10 µL of Nuclease-free H20 and is mixed with the reaction mix, for a final volume of 20 µL.

The thermocycler, programmed as follow, will perform the retro-transcription reaction:

Steps	Temperature (°C)	Time (minutes)
Step 1	25	10
Step 2	37	120
Step 3	85	5
Step 4	4	Hold

2.7.3. Quantitative Real-Time PCR

The steps of the Quantitative Real-Time PCR (qPCR) are the same as for the standard PCR described before, with the only difference that this specific reaction can determine the actual amount of PCR product present at a given cycle by adding fluorescent intercalated agents (SYBR Green). SYBR Green binds to all newly synthesized extended filaments and emits fluorescence. The fluorescence accumulates during the cycle of PCR and is measured at the end of it. As a result, the fluorescence given off by the fluorophore, above the set background level (the Cq value), will be proportional to the amount of initial template. Given the cycle a threshold (Ct), the latter will be attained sooner the more starting cDNA there is. qPCR was performed in triplicate by using the 5X HOT FIREPol EvaGreen qPCR Mix Plus (Solis BioDyne, Tartu, Estonia) and Light Cycler 480 II (Roche, Basel, Switzerland) following the below protocol:

Phase	Temperature	Time
Taq polymerase activation	95°C	14 min
Denaturation	95°C	15 sec
Annealing	60°C	35 sec
Extension	72°C	25 sec
Final extension	72°C	10 min

The denaturation/ Annealing/ Extension phases were repeated 40 times each. All primers were designed using the software Primer3 (http://primer3.ut.ee), with an optimal annealing temperature of 60°C (**Table 5**). Quality control was assessed by introducing in each run a sample with no template and/or no-reverse transcriptase. Housekeeping gene *gapdh* was selected based on stable transcript abundances across sequenced samples.

Table 5: List of primers for genotyping and gene expression analysis by quantitative Real-Time RT-PCR.

Gene name	Signalling Pathway	Forward primer (5'-3')	Reverse primer (5'-3')	Product size (bp)
dspa		ACATTCGCAACTCCATCACG	TCCAGAGCATGTAGTCCAGC	156
dspb		ATGCTGAACGAACTCAACGC	TATCTCTGCACTTCCTCCGG	148
lgals3a		ACGGGACCTGGTACTTCTCA	AGCTGATGGATTGGTGTGCT	118
lgals3b		TCCCGTTTGTCCCAGGAAAG	CTGGTTGAGCTCGAAGACCC	122
tnfa		CCGTCTGCTTCACGCTCC	GTCTTTGATTCAGAGTTGTATCC	148
il6		GTGAAGACACTCAGAGACG	GTTAGACATCTTTCCGTGCTG	149
gapdh	House keeping	GTGGAGTCTACTGGTGTCTTC	GTGCAGGAGGCATTGCTTAA	173
ccnd1	Wnt/ β-catenin	CCAACTTCCTCTCGCAAGTC	TGGTCTCTGTGGAGATGTGC	123
myca	Wnt/ β-catenin	AGAAAGCTGGAGTCCTCGAC	CTGCTGCAGTGTGTTCAGC	118
smad2	TGFβ	TCATGTCATCTACTGCCGCC	GTCTTGGCACGAGAACAGGA	176
smad3	TGFβ	CTATCAGCGGGTCGAGACAC	AGTTGCTCTGGGGTTCGATG	149
ccn2a	Hippo/ YAP-TAZ	CTCCCCAAGTAACCGTCGTA	CTACAGCACCGTCCAGACAC	140
ccn2b	Hippo/ YAP-TAZ	CCCACAAGAAGACACCTTCC	ATTCGCTCCATTCAGTGGTC	119

2.8. Protein extraction

Pools of ten embryos were treated with 1 mL of deyolking buffer (1/2 Ginzburg Fish Ringer without Calcium: 55 mM NaCl, 1.8 mM KCl, 1.25 mM $NaHCO_3$), shaken for 5 minutes at 1100 rpm to dissolve the yolk sac and centrifuged at 300 g for 30 seconds to pellet the cells. Optionally, two additional wash steps were done by adding 1 mL of wash buffer (110 mM NaCl, 3.5 mM KCl, 2.7 mM $CaCl_2$, 10 mM Tris/Cl pH 8.5), shaking 2 min at 1100 rpm and pelleting as before. Finally, pellets were dissolved in LDS-sample buffer 4X (Invitrogen, Waltham, Massachusetts, United States) and incubated for 5 min at 95°C. Extracted proteins were frozen and conserved at -20°C or directly loaded on a gel (Link et al., 2006).

2.9. Western blot analysis

The protein samples were loaded and separated on NuPAGE™ 3-8% Tris-Acetate Protein Gels, 1.5 mm, 10-well (Invitrogen, Waltham, Massachusetts, United States). The Spectra Multicolor Broad Range Protein Ladder (Thermo Fisher Scientific, Waltham, Massachusetts, United States) was used as a molecular weight marker for protein samples in the 10-260 kDa range. After the electrophoretic run in Tris-acetate SDS Running buffer (Invitrogen, Waltham, Massachusetts, United Statesi) at 100V for 2 hours, proteins were transferred from the gel to a PVDF (polyvinylidene difluoride) Immobilon-FL transfer membrane (Merck, Darmstadt, Germany) by Trans-Blot Turbo Transfer System (BIO-RAD, Hercules, California, United States), following the manufacturer's instructions (25V/1A/30 minutes program). The membrane was incubated for 1 h at 4°C in 10% non-fat dry milk (AppliChem GmbH, Darmstadt, Germany) in TBS-T (0.1% Tween-20) to saturate, block, and avoid non-specific binding of the antibody. Then, it was incubated overnight at 4°C with primary antibody diluted in 5% non-fat dry milk TBS-T. Four washes for 5 minutes in 5% non-fat dry milk in TBS-T preceded secondary antibodies incubation for 1 hour in 5% non-fat dry milk TBS-T at RT. The signal was detected using an Alliance 9 Mini Chemiluminescence Imaging System (Uvitec, Cambridge, UK), after incubation with Pierce™ ECL Western Blotting Substrate (Thermo Fisher Scientific, Waltham, Massachusetts, United States). Band intensities were normalized against Tubulin protein expression.
Primary antibodies used for Western blot were:

- α-Tubulin (mouse, A11126, Invitrogen, Waltham, Massachusetts, United States) diluted 1:1000 in 5% non-fat dry milk TBST;
- Desmoplakin 1/2 (mouse, 651155, Progen, Heidelberg, Germany) diluted 1:200 in 5% non-fat dry milk TBST.

Secondary antibodies used for Western Blot were:

- Anti-mouse IgG (goat) (H+L)-HRP Conjugate (Bio-Rad, Hercules, CA, USA) diluted 1:2000 in 5% non-fat dry milk TBST

2.10. Fluorescent expression analysis

The Wnt/β-catenin *Tg(7xTCF-Xla.Siam:EGFP)*^{ia4} (Moro et al., 2013) and Myocardial *Tg(tg:EGFP-myl7:EGFP)* (Porazzi et al., 2012) reporter lines fluorescence, with and without mutated genetic background, were outcrossed with wild-type fish, to obtain a heterozygous fluorescent signal in all the embryos analysed. Anesthetized embryos with fish water plus 0.16 mg/mL Tricaine solution were placed on microscope slides with 2% methylcellulose in PBS 1X, oriented laterally. The emitted signals and the fluorescent tissues were quantified under the fluorescence microscope (Leica M165FC, Leica Microsystems, Wetzlar**,** Germany) equipped with a digital camera (Leica DFC7000T, Leica Microsystems, Wetzlar**,** Germany) and connected to a computer with Leica Software (LAS V4.8) for image acquisition and processing. The pixel intensity was analyzed with the ImageJ software.

2.11. Immunofluorescence analysis

Embryos at 3 dpf were fixed in 4% PFA/PBS overnight at 4°C and stored at -20°C in 100% MetOH. Samples were rehydrated in a MetOH/PBS series (75%, 50%, 25%), 5 minutes each, depigmented using 3% H_2O_2 and 1% KOH in PBS 1X, and washed 2 times in PBS 1X + 0.5% Triton X. Samples were washed in distilled water 5 minutes and frozen in acetone at -20°C, 7 minutes, for tissue permeabilization. After an additional wash for 5 minutes in distilled water and another one for 5 minutes in PBS 1X + 0.5% Triton X, embryos were blocked for 30 minutes in PBDT (PBS 1X + 1% BSA + 1% DMSO + 0.5% Triton X) plus 2% goat serum at RT, and then incubated for 2 days at 4°C in PBDT + 2% Goat serum + Rabbit Anti-Plastin L antibody (Abcam, Cambridge, UK) 1:5000. After four washes for 15 minutes in PBDT, embryos were incubated in PBDT + Goat-anti-Rabbit AP (alkaline phosphatase) conjugated antibody (12-448, Merk, Darmstadt, Germany) at 1:1000 overnight at 4°C in the dark. The day after, samples were washed four times for 15 minutes in PBDT and stained with 0.25 mg/mL Fast Blue BB (Sigma-Aldrich, St. Louis, Missouri, United States) + 0.25 mg/mL Naphthol-AS-MX-phosphate (Sigma-Aldrich, St. Louis, Missouri, United States) in staining

buffer solution (100 mM Tris HCl pH 8.2, 50 mM $MgCl_2$, 100 mM NaCl, 0.1% Tween 20). Finally, samples were stored in 4% PFA at 4°C in the dark or embedded in 1.5% low melting agarose on a glass dish for acquisition with the confocal microscope (Leica SP5, Leica Microsystems, Wetzlar**,** Germany), exploiting the far-red emission from Fast Blue. The images were analysed using Volocity 6.0 software (Perkin Elmer, Milan, Italy).

2.12. Acridine Orange staining

After removing the chorion manually *in vivo* with needle tools, the 3-dpf embryos were incubated in the staining solution for 30 minutes at RT.

Staining solution:

- 5 µg (1 dpf) /mL in fish water with Acridine Orange (AO) (A6014, Sigma-Aldrich, St. Louis, Missouri, United States) (e.g. 3 dpf embryos = 15 µg/mL)

Three 5-minutes washes in Fish water at RT required to remove the excess staining, with the last one performed, if necessary, in fish water plus 0.16 mg/mL Tricaine solution, to anesthetize them and allow an easier acquisition. Immediately place the embryos in microscope slides with 2% methylcellulose and orient them laterally to acquire the signals under the fluorescent microscope (Leica M165FC) equipped with a digital camera (Leica DFC7000T, Leica Microsystems, Wetzlar**,** Germany), connected to a computer with Leica Software (LAS V4.8, Leica Microsystems, Wetzlar**,** Germany) for image acquisition and processing. The pixel intensity was then analyzed with the ImageJ software.

2.13. Trasmission Electron Microscopy analysis

Small pieces of heart tissue (about 2-3 mm^3) were fixed with 2.5% glutaraldehyde (EMS, Hatfield, PA, USA) plus 2% paraformaldehyde (Sigma-Aldrich, St. Louis, Missouri, United States) in 0.1 M sodium cacodylate buffer pH 7.4 overnight at 4°C. Subsequently, the samples were post-fixed with 1% PFA in 0.1 M sodium cacodylate buffer for 1 hour at 4°. After three water washes, samples were

dehydrated in graded ethanol series and embedded in epoxy resin (Sigma-Aldrich, St. Louis, Missouri, United States). Ultrathin sections (60-70 nm) were obtained with a Leica Ultracut EM UC7 ultramicrotome, counterstained with uranyl acetate and lead citrate, and viewed with a Tecnai G2 transmission electron microscope (FEI, Hillsboro, OR, USA) operating at 100 kV. Images were captured with a Veleta digital camera (Olympus Soft Imaging System, Olympus, Segrate, Italy).

2.14. Histological analysis

2.14.1. Dehydration and paraffin embedding

Three, six and twelve months old adult zebrafish were euthanized and fixed in Bouin solution (75% picric acid in milliQ water/ 25% formalin/ 2mL glacial acetic acid) for a minimum of 24 up to a maximum of 72 hours at RT, depending on the dimension of the fish. To allow a better fixation, the abdomen was opened along the ventral midline starting from the anal pore. The fixed samples were washed in ethanol 70% plus few droplets of ammonia solution 32% until the fish appeared with normal color and the washing solution was clean. After dehydration washes in a series of graded EtOH (80%/95/100%) 2 times each for 1 hour, the fixed fish were left in EtOH 100% O/N and then cleaned by xylene 3 times for 1 hour, until the fish become translucent. After that, the samples were gradually washed in a xylene/paraffin (Paraplast Plus, Leica, Wetzlar**,** Germany) (50%/50%) solution 2 times for 1 hour at 60°C ,then in 100% paraffin O/N at 60° and the day after other two times for 1 hour, to allow the evaporation of all the xylene. Each fish was placed in an embedding block and allowed to solidify at RT after lateral orientation with the head on the right, to place the heart in the first half of the fish that will be cut. At this point, included fish can be conserved at 4°C. Paraffin sectioning (7-8 µm) was put in glass slides at 30/40 °C until they perfectly adhered to them.

2.14.2. Hematoxylin & Eosin staining

Hematoxylin & eosin staining (Abcam, Cambridge, UK) was conducted based on standard procedures: the glass slides containing the paraffin sections were washed initially for 5 minutes in 100% xylene to remove the paraffin, then 3 minutes each in EtOH 100%/80%/50% and in the end with ddH2O. Hematoxylin staining was performed at a time depending on the age and condition of the staining solution and then washed under running water for 5 minutes. Five quick washes in Acetic acid 2% in H2O, a 30-second one in Scott solution (20 gr $MgSO_4$ and 3,5 gr $NaHCO_3$ in 1L of ddH2O) and other 5 quick in running water removed the excess of staining solution. Also, the eosin staining timing of incubation depends on the age and condition of the starting solution and is followed by 10 quick washes in EtOH 80% and 100%, to end with 5 minutes one in xylene. The cover slide placed above the colored sections was mounted with a specific mounting medium (Eukitt® Quick-hardening mounting medium (Sigma-Aldrich, St. Louis, Missouri, United States)), an adhesive and specimen preservative able to protect the sections and ameliorate the staining. After an O/N heating step at 37°C, to allow the xylene to evaporate, the slides were ready to be photographed under a light microscope (Leica DFC7000T, Leica Microsystems, Wetzlar**,** Germany), connected to a computer with Leica Software (LAS V4.8, Leica Microsystems, Wetzlar**,** Germany) for image acquisition and processing.

2.15. Birefringence analysis

Anesthetized embryos were placed in 2% methylcellulose PBS 1X solution and subsequently positioned on a glass slide. The sample was then inserted between two polarizing-rotating filters and subsequently analyzed under a Leica M165FC microscope (Leica Microsystems, Wetzlar**,** Germany). Skeletal muscle fluorescence was recorded in a bright field with a DFC7000T digital camera (Leica Microsystems, Wetzlar**,** Germany), rotating the upper polarizing filter until the light refracted by the skeletal muscles was uniform and homogeneous all along the larval body. The pixel intensity was then analyzed with the ImageJ software.

2.16. Locomotion analysis

Behavioural experiments were performed using the DanioVision tracking system (Noldus Information Technology, Wageningen, The Netherlands). Zebrafish larvae at 5 dpf were placed in 48-well plates, with one larva per well in 1 mL of fish water. After 20 min of acclimation, movements of larvae were recorded repeating three cycles of 10 min of light and 10 min of dark, as previously described (Risato et al., 2022).

2.17. Physical exercise of zebrafish larvae and adults

Wild type and mutated zebrafish larvae were let grow for 10 days, from 3 dpf to 13 dpf, in a 1% Methylcellulose solution dissolved in fish water. This solution, due to its high density, increased the force needed to reach food and move normally, simulating a physical training protocol (Ruparelia et al., 2014). For mechanical stress induction in adults, groups of 3-month-old mutated and WT fish were put inside a homemade swim tunnel. The water flow was created using an electric pump with different power levels (**Figure 15**) (Brushless DC Pump AD20P-1230D; Qmax = 67 cm^3/s equal to 85 cm/s).

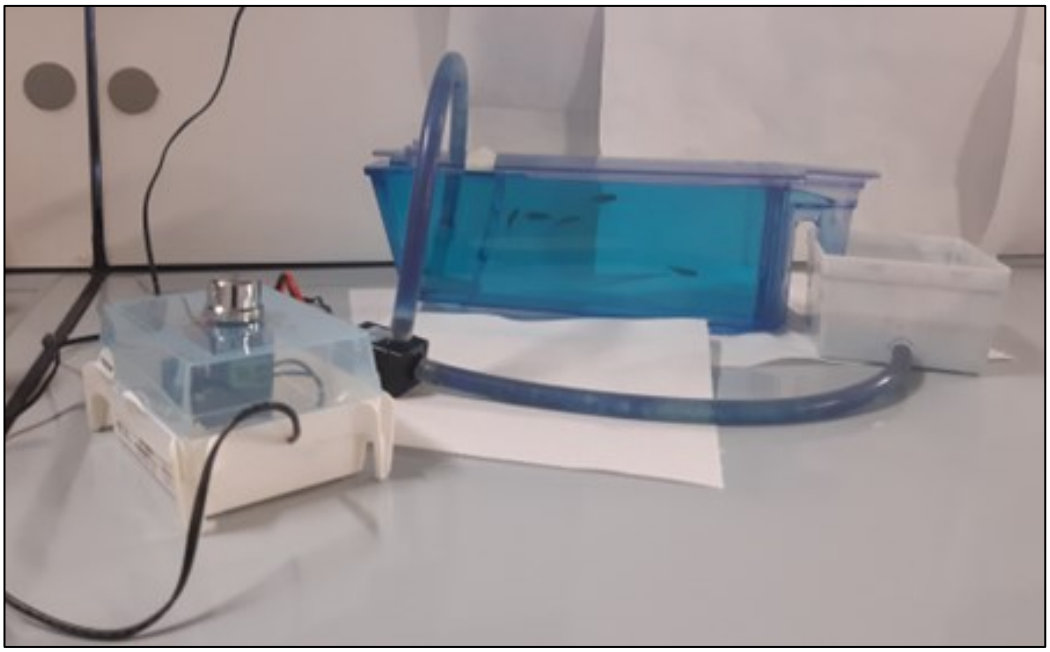

Figure 15: Homemade swim tunnel for adult zebrafish training.
A zebrafish tank was connected to an electric pump with different power levels (Brushless DC Pump AD20P-1230D; Qmax = 67 cm^3/s equal to 85 cm/s), to create the water flow.

In a natural environment, zebrafish swim with a speed between 3.5-13.9 cm/s (Arunachalam et al., 2013). We divided the power of the electric pump into three different levels (1/2/3) where 1 corresponds to 11 cm/s, 2 to 12 cm/sec, and 3 to 13 cm/sec. We set a training protocol characterized by a 1-hour workout, including 5 minutes at power levels 1 and 2 (acclimation), 50 minutes at level 3, representing the real intense workout, and 5 minutes at levels 2 and 1, returning to rest (**Figure 16**). The training was repeated 5 days per week for 3 months; this protocol allowed recovery from manipulation stress and exercise during the two rest days of the weekend.

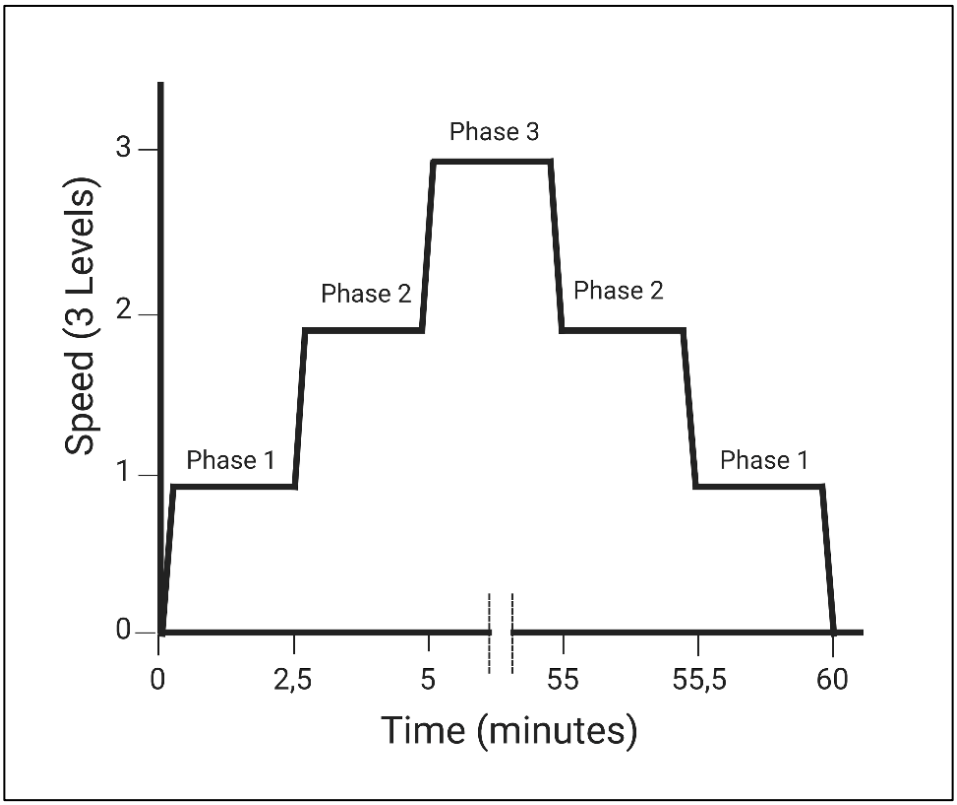

Figure 16: Scheme of the adult training protocol.

The power of the electric pump in the swim tunnel was divided into three different levels (1/2/3 speed) where 1 corresponds to 11 cm/s, 2 to 12 cm/s and 3 to 13 cm/s output. The training protocol is 1-hour long, including 5 minutes at power level 1 and 2 (acclimation), 50 minutes at level 3 (real intense workout), and 5 minutes at level 2 and 1, returning to rest. The training was repeated 5 days per week for 3 months. (Created by Biorender.com)

2.18. Pharmacological modulation of the Wnt/β-catenin signaling pathway

Zebrafish embryos were treated for 48 hours with 40 µM SB216763 or 5 µM XAV939 (S3442 and X3004, Sigma-Aldrich, St. Louis, Missouri, United States), directly dissolved in fish water, to activate (SB216763) or inhibit (XAV939) Wnt/β-catenin signaling. More specifically, SB216763 is a potent and selective cell permeable inhibitor of both glycogen synthase kinase 3 α and β (GSK-3α/ 3β). This enzyme is directly involved in the phosphorylation and subsequent ubiquitination of β-catenin and therefore its inhibition induces an accumulation of this protein, a key downstream effector in the Wnt signaling pathway. Regarding

the antagonist of the Wnt/β-catenin signaling pathway, XAV939, by inhibiting the tankyrase (TNKS) activity, increases the protein levels of the axin-GSK-3β complex and promotes the degradation of β-catenin, thereby inhibiting the pathway's downstream actions.

2.19. Signal quantification and statistical analysis

Signal quantification and morphological analysis were performed using the Measurements option of Volocity 6.0 (Perkin Elmer, Milan, Italy) and ImageJ software. Pairwise analysis was carried out by unpaired t-test while multiple comparisons were performed by one-way ANOVA followed by Tukey's test; survival analysis was made instead using Log-rank (Mantel-Cox) test (Graph Pad Prism V7.0 software, San Diego, CA, U.S.A.). In the charts, error bars display standard errors of the mean. Asterisks indicate significant differences from controls. Correspondence between asterisks and significance levels is indicated in the figure legends. Sample final sizes were obtained from multiple mating events.

3. AIM OF THE THESIS

To date, Arrhythmogenic Cardiomyopathy (AC) patients are treated primarily through lifestyle changes like abstention from intensive physical activity, with AADs (anti-arrhythmic drugs) such as β-blockers, ICD (implantable cardioverter-defibrillator), catheter ablation and, in severe cases, HTX (heart transplantation). Apart from HTX, these are palliative approaches of symptomatic therapy that do not address the onset and progression of the disease, being mainly focused on the prevention of SCD (sudden cardiac death). The first goal of my PhD was to complete the generation, phenotypic characterization and validation of zebrafish stable mutants for *dsp* (Desmoplakin) genes as models for AC. These models were used to understand how alterations in desmosomes can cause replacement of cardiomyocytes by fibro-adipose tissue and to observe whether exercise (training) could cause phenotypic worsening, looking for possible correlations with the human condition. Analyses were also designed to investigate the role of signalling pathways such as Wnt/β-catenin, Hippo/YAP-TAZ and TGFβ, recently identified by several authors as possible pathogenic pathways involved in this pathology. The deciphering of the signalling pathways involvement in the pathogenesis and progression of this disease and the suitability of zebrafish as a model for large-scale drug screening may lead to the identification of new molecular targets for targeted therapy and to understand the pathogenesis of this disease, which to date is still unknown. Furthermore, the generation of zebrafish stable mutants for *lglas3a* (Galectin-3) gene was another topic of my PhD. This gene was recently correlated with AC condition, being found mutated in human patients, and is known to be involved in stabilization of intercellular junctions, inflammation and apoptotic responses in the cardiac tissue. Therefore, understanding its potential role in cardiac disease pathogenesis, finding a stronger connection with AC, is very important to have a deeper knowledge of how this gene could be involved in the disease course and if it could be in the future a possible therapeutic target to mitigate the progression of AC.

4. RESULTS

4.1. Stable *dsp*-KO zebrafish lines

The characterization of the *dsp* mutant lines, generated in this project, was divided into two main phases linked to the age of the animal model, the larval and the adult phase, both divided into sub-phases.

4.1.1. Larval phase

4.1.1.1. Generation of zebrafish lines mutated in the *dsp* genes

In zebrafish, the desmoplakin gene is present in two copies: desmoplakin a (*dspa*) (ZDB-GENE-030131-2743) on chromosome 2, and desmoplakin b (*dspb*) (ZDB-GENE-030131-1662) on chromosome 20. Two different strains were used to generate fish with mutations in both desmoplakin genes:
- *dspa* line *sa13356*, obtained from the Sanger Institute as part of the Zebrafish Mutation Project (ZMP), a consortium that produced a collection of KO alleles for several genes in the zebrafish genome. In this case, the gene encoding the "desmoplakin a" member carries a non-sense C>T point mutation in exon 23 (Chr 2: g.2324300 C>T), leading to the production of a truncated protein (p.Gln960Ter), consisting of 960 amino acids, out of 2244 total, and lacking the C-terminal domain;
- *dspb* Δ13 line (allele *ia303*), produced in our laboratory by Crispr/Cas9 approach. A deletion of 13 bp in exon 3 was obtained in the "desmoplakin b" gene (Chr 20: g.52912248¬52912260del), which leads to the shift of the reading frame and the production of a truncated protein of 129 amino acids, out of 2207 total, thus lacking most of the sequence, which is likely to undergo degradation.

4.1.1.2. Genotyping of *dspa* and *dspb* zebrafish mutants

The genotyping of the mutant zebrafish lines was obtained with two different techniques. Regarding the *sa13356* point mutation in the *dspa* gene, the PCR reaction specific for this gene was followed by direct sequencing. The results obtained are shown in **Figure 17** (**A-C**), where the nucleotide involved in the mutation is indicated with an arrow: the wild-type (**A**) sample presents a single peak corresponding to a C (by convention in blue); the homozygous mutant (**C**) presents a single peak corresponding to a T (by convention in red); finally, the heterozygote (**B**) presents two overlapping peaks, corresponding to a C and a T. To identify the deletion in the *dspb* gene, a PCR was performed and then the final products were run on a 3.5% TBE agarose gel. After electrophoresis, the PCR products were observed by UV trans-illuminator. Three different profiles can be detected according to the genotype of the analysed animal: the WT sample, represented by a single band corresponding to a length of 114 bp; the homozygous mutated sample, represented by a single band of lower molecular weight, corresponding to 101 bp, due to the deletion of 13 nucleotides; the heterozygous sample represented by two bands, corresponding to the two different alleles (**Figure 17 D**). The presence of 13-bp deletion in the *dspb* gene was confirmed by sequencing (**Figure 17 E-F**).

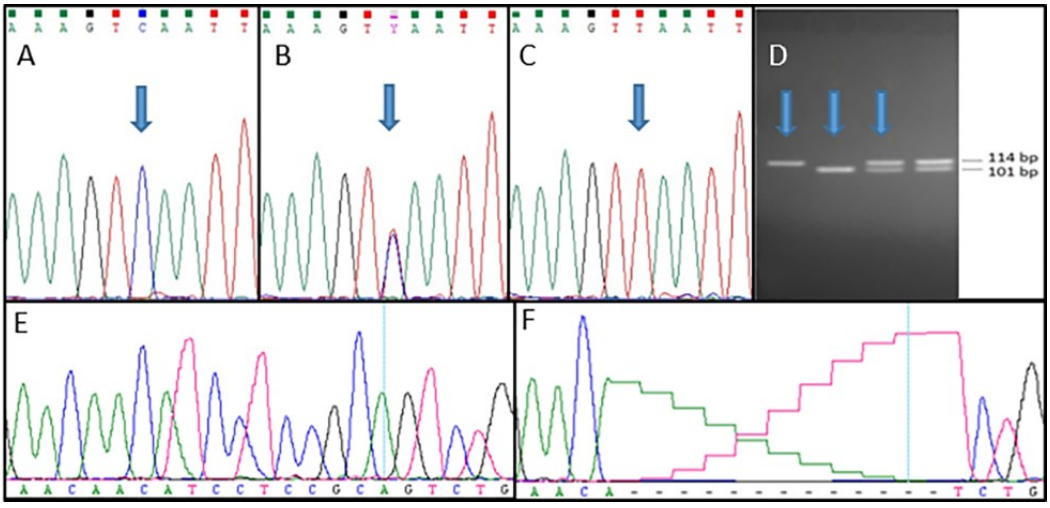

Figure 17: Genotyping of *dspa* and *dspb* zebrafish mutants.

A-C: sequence-based identification of the *dspa* sa13356 point mutation (arrow) in case of homozygous control (A), heterozygous (B), and homozygous mutant (C). D: gel-based identification of the three *dspb* genotypes (arrows); from left to right: undeleted control,

homozygous deletion, and heterozygous condition. E-F: sequence-based identification of the *dspb* 13-bp deletion in the homozygous mutant (F), compared to control (E).

4.1.1.3. Generation of zebrafish with mutations in both *dspa* and *dspb* genes

Inter-breeding heterozygous *dspa* fish generated WT, heterozygous (*dspa* +/-) and homozygous (*dspa* -/-) individuals; similarly, inter-breeding also heterozygous *dspb* fish produces WT, heterozygous (*dspb* +/-) and homozygous (*dspb* -/-) fish.

dspa+/- x dspa+/- = ¼ dspa+/+, ½ dspa+/- and ¼ dspa-/-

dspb+/- x dspb+/- = ¼ dspb+/+, ½ dspb+/- and ¼ dspb-/-

Inter-crossing fish homozygous for only *dspa* or dspb mutations produced double heterozygous fish (i.e., heterozygous for both the *dspa* and *dspb* mutations).

(dspa-/-; dspb+/+) x (dspa+/+; dspb-/-) = (dspa+/- dspb+/-)

4.1.1.4. Segregation analysis according to Mendel's independent assortment

For each developmental stage, larvae from inter-crossed double heterozygous lines were genotyped and their frequencies were normalized to the total population. All genotype frequencies follow Mendel's law prediction; however, a survival reduction of borderline significance is observed for the double homozygous (**Table 6**).

Table 6: Analysis of genotype frequencies from *dspa/dspb* inter-cross.

Counting of the larvae, obtained from the inter-cross of double heterozygous (-ab) fish, at 3 and 14 dpf. The number of individuals observed for each of the 4 pools of genotypes (columns "N.") and the relative frequency in percent (columns "%") are reported. In the right column, the expected frequency and percentage are reported, based on Mendelian inheritance ("expected values "). Below the Chi-square statistical analysis shows that all genotype frequencies follow Mendel's law prediction; a reduction of the survival (p-value 0.0645) is observed for the aabb (double homozygous) individuals.

	3 dpf (n=187)		14 dpf (n= 160)		Expected values	
Genotype	N.	%	N.	%	Frequency	%
A/-B/-	100	53.47	95	59.37	9/16	56.25
A/-bb	32	17.11	34	21.25	3/16	18.75
aaB/-	40	21.3	29	18.12	3/16	18.75
aabb	15	8	2	1.25	1/16	6.25
Chi-square		2.766		7.244		
p-value		0.4292		0.0645		

4.1.1.5. Selection of the most characteristic genotypes

Due to the results obtained so far, we decided to focus our attention only on 4 main genotypic conditions. Specifically, we selected the WT condition, as standard for comparison, and the mutated forms *dspa* -/- and *dspb* -/-, as they represent a halving of the global expression of the Desmoplakin protein. As last, it was chosen to keep the double heterozygous mutant, with the balanced reduction of protein expression from both *dsp* genes. The latter mutant, from an allelic perspective, might more closely mirror the human condition of heterozygosity. Double homozygous fish could also have been a very interesting model to analyse, but the low fertility and developmental rates, associated with sudden death events, make this line very difficult to be maintained and used for larval production and experiments, so we decided not to include it in the subsequent analyses. However, double homozygous line might be used in the future, in targeted experiments or to validate results obtained in double heterozygous model. From now on, WT samples will be identified with the word "WT", *dspa* -/- and *dspb* -/- mutants with a "-aa" and "-bb" respectively, double heterozygous mutant with a "-ab" and double homozygous with -aa/-bb.

4.1.1.6. qPCR analysis of Dsp mRNAs and analysis of Dsp protein expression on 3-dpf mutated larvae

First thing, we decided to test whether the mutations caused alterations in the amount of *dspa* and *dspb* mRNA and subsequently also in the protein expression. A qPCR analysis was then performed showing statistically significant changes for

mRNA produced at this developmental stage only in -aa and -bb mutants (**Figure 18 A**). We then performed a Western blot analysis using a monoclonal antibody developed in mice and specific for the region between amino acid residues 2115 and 2132, in the C-terminal portion of human Desmoplakin (Desmoplakin 1/2 (PROGEN 651155, mouse). The antibody was shown to be specific for the two zebrafish isoforms Dspa and Dspb. The truncated forms are not recognized by the antibody because it binds the C-terminal portion of it. WT larvae showed three bands with a molecular weight of about 240 kDa, as expected, corresponding to two isoforms of Dspb and one isoform of Dspa, while larvae lacking only one of the two isoforms showed only the band corresponding to the non-mutated one: both mutations in *dspa* and *dspb* lead to the formation of a truncated protein, lacking the C-terminal portion, to which antibodies consequently cannot bind. Specifically, in -aa mutant line only the two isoforms of Dspb are present, whereas in -bb mutant larvae, only the Dspa isoform is present. In -ab larvae, all three bands observed in the wild-type larvae are present, as expected, but with reduced intensity, confirming that all Dsp isoforms are less expressed. To compare the amounts of Desmoplakin protein produced by the different genotypes, the ubiquitous protein α-Tubulin was detected with a specific antibody and the intensities of the various bands corresponding to α-Tubulin and Dsp proteins were compared. In -ab larvae, there was approximately half expression (45%) of both Desmoplakin proteins isoforms. In the –aa and –bb larvae, that completely lack the Dspa and Dspb isoforms, the normal ones appeared anyway affected, with Dspa showing a 70% reduction in –bb, and Dspb a 30% reduction in -aa (**Figure 18 B**). Therefore it is possible to state that mutations in the *dspa* and *dspb* genes in our stable zebrafish mutant lines alter the production of protein-coding mRNA and, because of the mRNA translation process, truncated proteins will be produced and likely degraded or no longer functional. Furthermore, the 50% global reduction of protein in –ab larvae confirmed our hypothesis that a balanced model potentially better represents the condition of heterozygosity in humans. The presence in control samples of two bands of different molecular weights for the Dspb protein had never been described before and could depend on the presence of two isoforms resulting from alternative splicing or post-translational modifications that could change a portion of the

protein (e.g. by phosphorylation), as reported for humans (Stappenbeck et al., 1994).

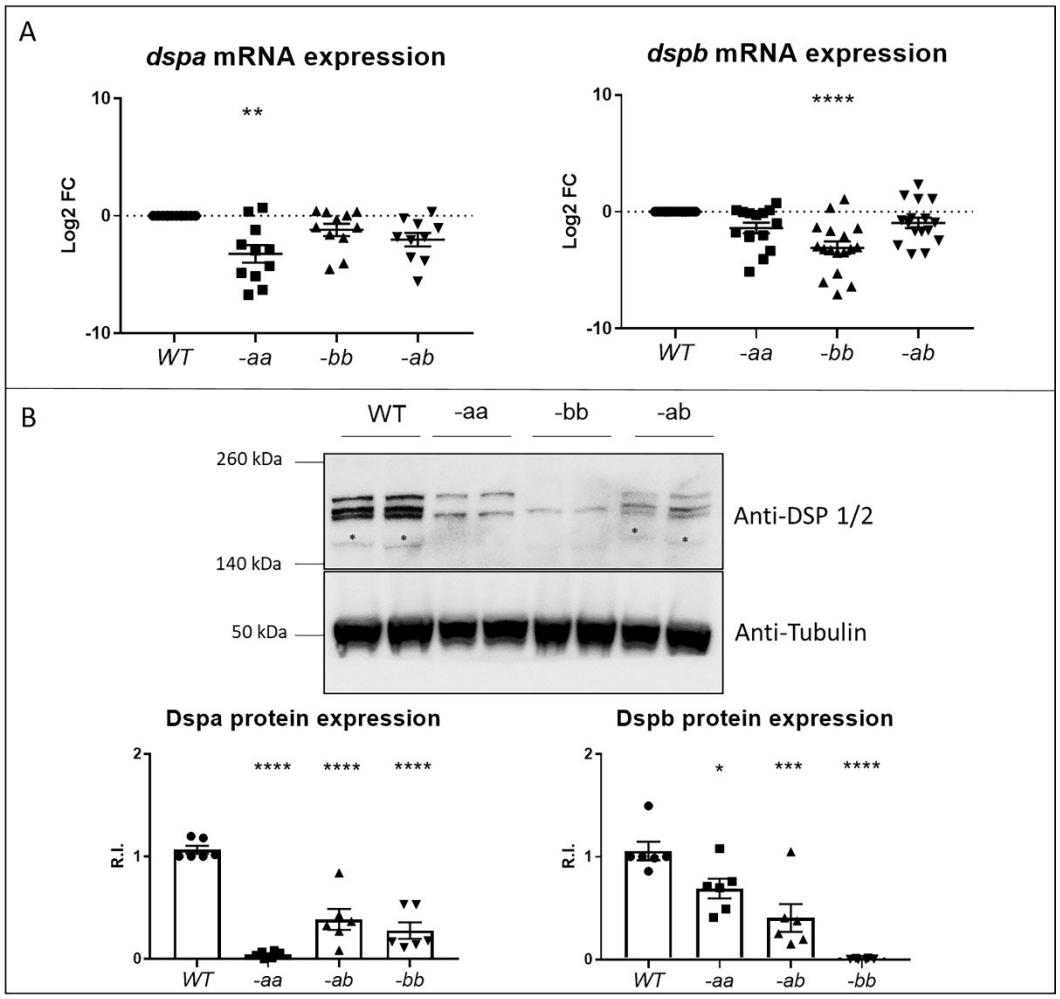

Figure 18: **Reduced Dsp mRNA and protein levels in zebrafish Dsp mutants.**
A: qPCR analysis of *dspa* and *dspb* mRNAs expression in 3 dpf embryos of four different genotypes (WT: *dspa+/+; dspb+/+*; -aa: *dspa-/-; dspb+/+*; -bb: *dspa+/+; dspb-/-*; -ab: *dspa+/-; dspb +/-*). The *dspa* and *dspb* mRNA expression decreases significantly in -aa and -bb, respectively. Each point on the graph corresponds to a pool of 30 embryos of the same genotype. Sample size: n=11±5. Log2 FC: Log2 Fold Change. **=p<0.01; ****=p<0.0001. Test: One-way ANOVA followed by Tukey's test. B: Western blot analysis on 3 dpf embryos detected alterations in Dspa and Dspb protein expression. The WT sample presents 3 bands of nearly 240 kDa (A), one for Dspa and two for the Dspb isoforms. The -aa and -bb homozygous samples exhibit only the not mutated isoforms. In the -ab sample, all isoforms are present, with a reduced amount. Each point corresponds to a pool of 10 embryos of the same genotype. Asterisks in images indicate not specific

signals. Sample size: n=6. R.I: Relative Intensity. *=p<0.05; ***=p<0.001; ****=p<0.0001. Test: One-way ANOVA followed by Tukey's test.

4.1.1.7. Morphological analysis of the cardiac region on 3-dpf mutated larvae

After this initial characterization of our *dsp* zebrafish lines, we decided to better investigate possible alterations in the cardiac region and heart structure. We observed that mutant larvae exhibited several cardiac morphological abnormalities when compared with WT larvae. Specifically, we noticed that -ab and -aa mutants showed a disease penetrance close to 30%, very similar to that observed in human patients (Pilichou et al., 2017) (**Figure 19 F**). More specifically, for –aa (**Figure 19 A-A''**) and -bb (**Figure 19 B-B''**) the heart is structurally dilated, with pericardial effusion and hemopericardium in the cardiac region. In some cases, it was also possible to observe the total absence of blood inside the heart (**Figure 19 B'-B''**), suggesting the presence of possible problems of the circulatory system, which in embryos at this stage of development can be compensated by the ability to absorb oxygen by diffusion but, in later stages of development, could cause premature death. In -ab embryos (**Figure 19 C-C''**), the situation is much more critical: a more severe hemopericardium, pericardial effusion, and cardiac malformations are present. In -aabb larvae (**Figure 19 D**) the cardiac phenotype shows from the beginning a condition too severe to allow the survival of the individuals (**Figure 19 E**). Moreover, in all mutant lines, the cardiac region was significantly dilated if compared with WT controls. Further, mutated larvae displayed a significant reduction in the developmental rate, as indicated by the reduced body length and eye area, both important quantitative parameters for determining the developmental stage of 24–72 hpf zebrafish embryos. More specifically, it was possible to observe a significant reduction of the body length in -aa and -ab lines, while the -bb line did not show differences if compared with controls. The eye area was significant reduced only in -ab line (**Figure 19 G**).

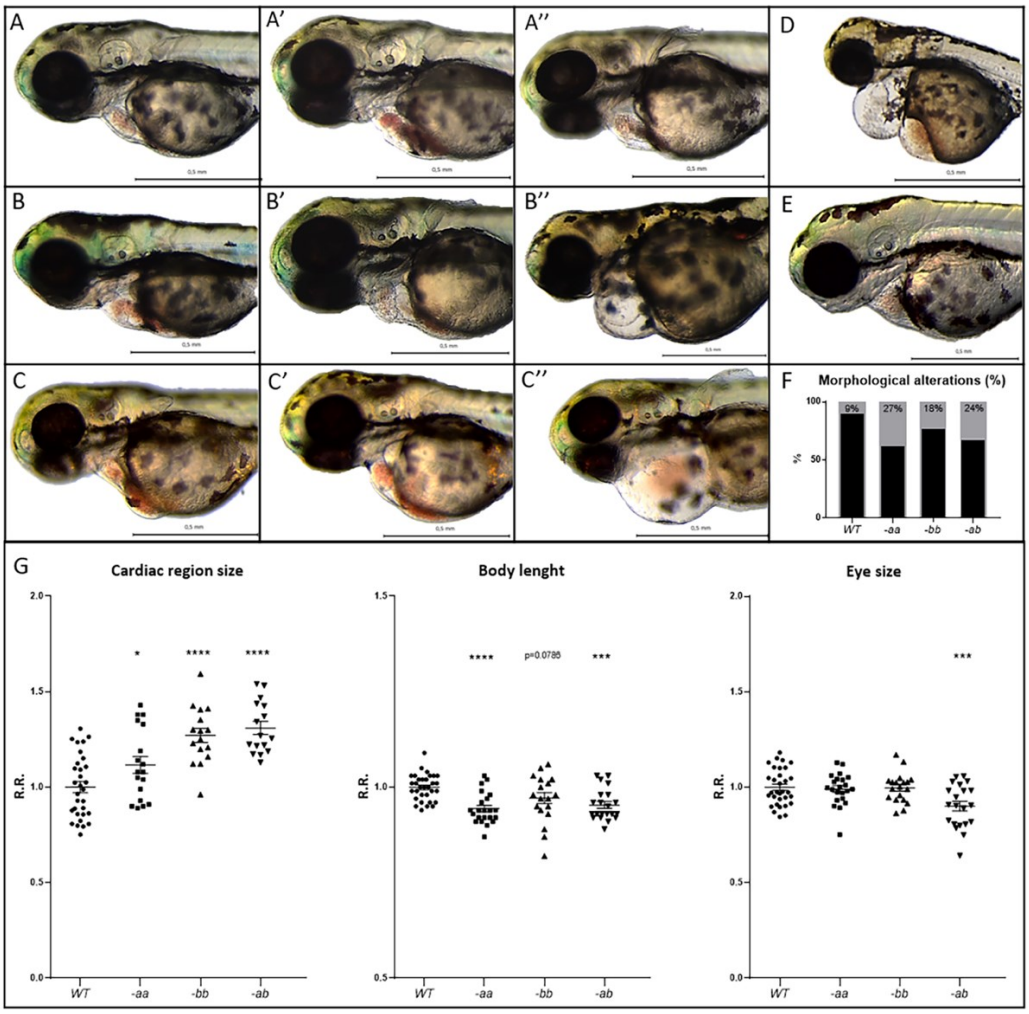

Figure 19: Cardiac alterations and developmental delay in Dsp mutant lines.

A-F: Mutant embryos (A-C", D) display cardiac alterations, compared to WT (E). Homozygous -aa (A-A") and -bb (B-B") mutant hearts appear dilated and/or structurally altered, with cardiac pericardial effusion and/or hemopericardium in the cardiac region. Double heterozygotes -ab (C-C") show a more serious phenotype than -aa and -bb lines. Double homozygotes -aa/-bb display the most severe phenotype (D). F: Percentage of heart alteration in different genotypes. Sample size: n=100. G: Cardiac size analysis shows that all mutants present heart dilation. Body length and eye size measurements indicate a developmental delay in mutants, especially in the -ab condition. All embryos are at 3 dpf in lateral view, anterior to the left. Sample size for cardiac region size: WT n=31; -aa n=18; -bb n=16; -ab n=16. Sample size for body length: WT n=32; -aa n=22; -bb n=19; -ab n=21. Sample size for eye size: WT n=32; -aa n=22; -bb n=19; -ab n=21. R.R.: Relative Ratio. *=p<0.05; **=p<0.01; ***=p<0.001; ****=p<0.0001. Test: One-way ANOVA followed by Tukey's test

4.1.1.8. Heart rate alterations on 2-3-5- and 7-dpf mutated larvae

Heart rate (beats per minute, bpm) at 2 dpf was calculated before the appearance of the first signs of heart malformations, detected for the first time at 3 dpf in our model, by analysing a random group of 60 embryos for each condition. Indeed, at 2 dpf no evident alterations of heart rate were yet visible, but some signs of the disease started already to manifest themselves. At 3, 5, and 7 dpf heart rate alterations were detected only in mutants showing cardiac morphological changes. The mean heart rate in tricaine-anesthetized larvae showed an increase as the developmental stages progressed. In WT larvae at 2-3 dpf, the mean beats-per-minute rate was around 135/140 bpm, and then increased and stabilized at 5-7 dpf around 170/200 bpm. More in detail, as mentioned above, at 2 dpf the average beats per minute of WT larvae was precisely 136 bpm, while in -ab mutants was 131 bpm; in -aa and -bb mutants it was 144 and 124 bpm, respectively. At this first developmental stage analysed, all mutant conditions showed statistically significant differences when compared with controls. At 3 dpf the mean beats-per-minute frequency in WT controls was 142 bpm, while in -ab mutants it was 114 bpm. It is interesting to observe how in only one day of development the differences between mutant and control larvae increased so drastically. In addition, also -aa mutants showed a significant difference from WT, with a mean beats-per-minute rate of 152 bpm, confirming the tachycardia alteration already observed at 2 dpf. The -bb mutants, like –ab mutant larvae, showed a significant reduction of heartbeats with an average of 125 bpm. At 5 dpf, -aa larvae started to present a significant bradycardia phenotype (130 bpm), like -ab (139 bpm) and -bb (130 bpm) mutants, compared to WT controls (166 bpm). Finally, at 7 dpf the heart rate per minute was 210 bpm in controls, in -ab 177 bpm, and in -aa and -bb mutants 182 bpm and 193 bpm, respectively. Also in the latter analysis, all three mutated genotypes showed statistically significant alteration compared to WT larvae. -ab lines showed the most dramatic alterations, enduring always below the mean WT rate and showing a 16% reduction in rate (**Figure 20**).

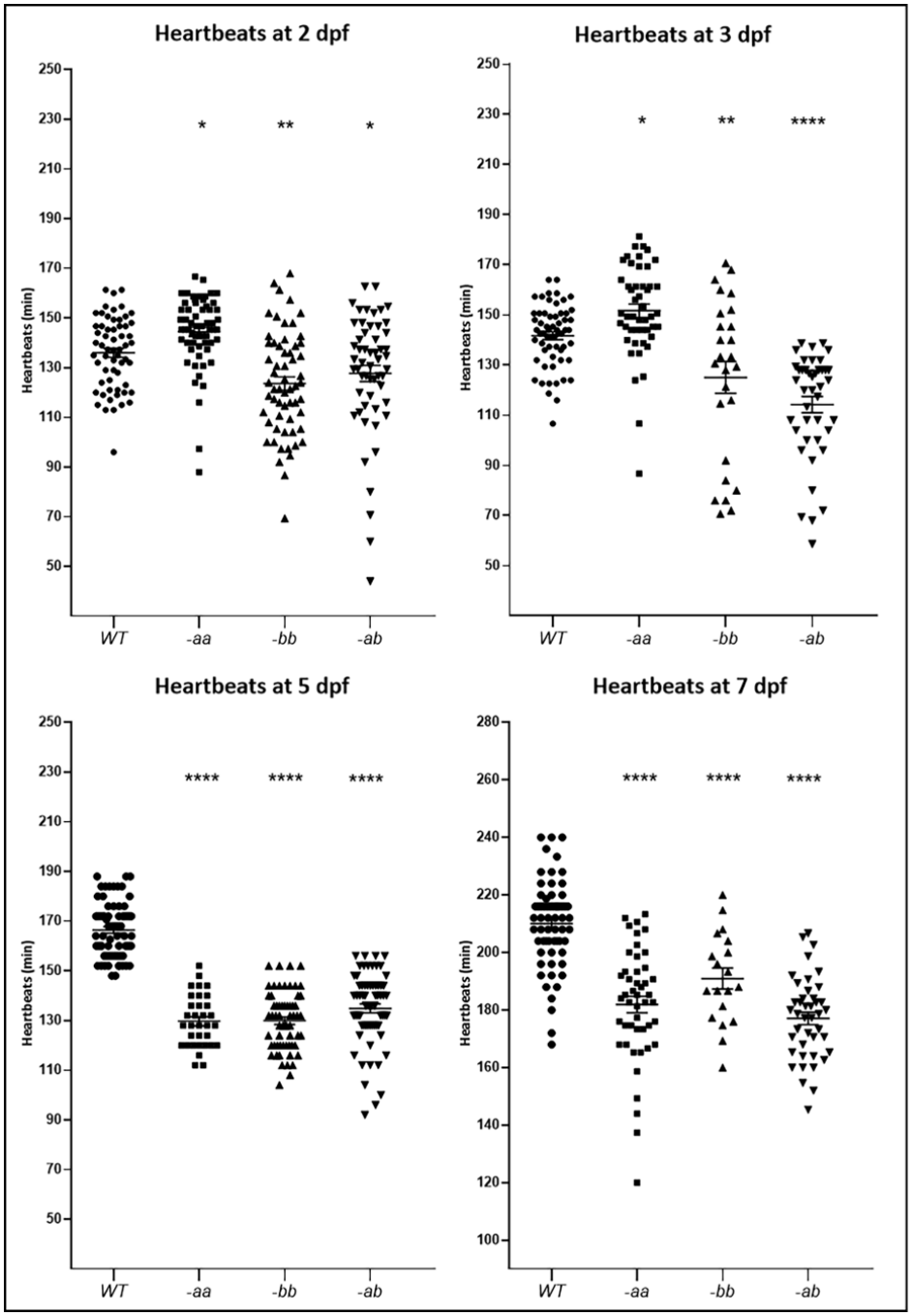

Figure 20: Heart rate alterations in Dsp mutant embryos and larvae.

At 2 dpf, the heart rate frequency in WT was 136 beats per minute (bpm), while in -ab was 127 bpm; in -aa and -bb was 144 bpm and 123, respectively. At 3 dpf, heartbeat was 142 bpm in WT and 114 bpm in -ab; -aa and -bb presented 125 and 152 bpm, respectively. At 5 dpf, the heartbeat changes appeared more evident; -aa larvae display a significant bradycardia phenotype (130 bpm), like -ab (139 bpm) and -bb (130 bpm), compared to WT (166 bpm). At 7 dpf, the heart rate of mutant larvae was significantly reduced for all genotypes. Sample size 2 dpf: WT n=60; -aa n=60; -bb n=60; -ab n=55. Sample size 3 dpf: WT n=60; -aa n=48; -bb n=26; -ab n=42. Sample size 5 dpf: WT n=70; -aa n=33; -bb n=60;

-ab n=66. Sample size 7 dpf: WT n=63; -aa n=47; -bb n=19; -ab n=42 *=p<0.05; **=p<0.01; ****=p<0.0001. Test: One-way ANOVA followed by Tukey's test.

4.1.1.9. Survival analysis of mutant lines at juvenile stages

Starting with the same number of fish per tank (100 larvae) for each of the four mutant lines chosen, we grew them under the same conditions for one month, recording the number of death events every day. We observed that all mutant lines showed significantly lower survival rates than controls. Specifically, the -ab line showed the highest percentage of mortality, around 80%, emphasizing that this genotype seems to be the most severe and prone to sudden death events (**Figure 21**). The -aabb survival curve is not displayed due to the very low fitness and fertility of these individuals.

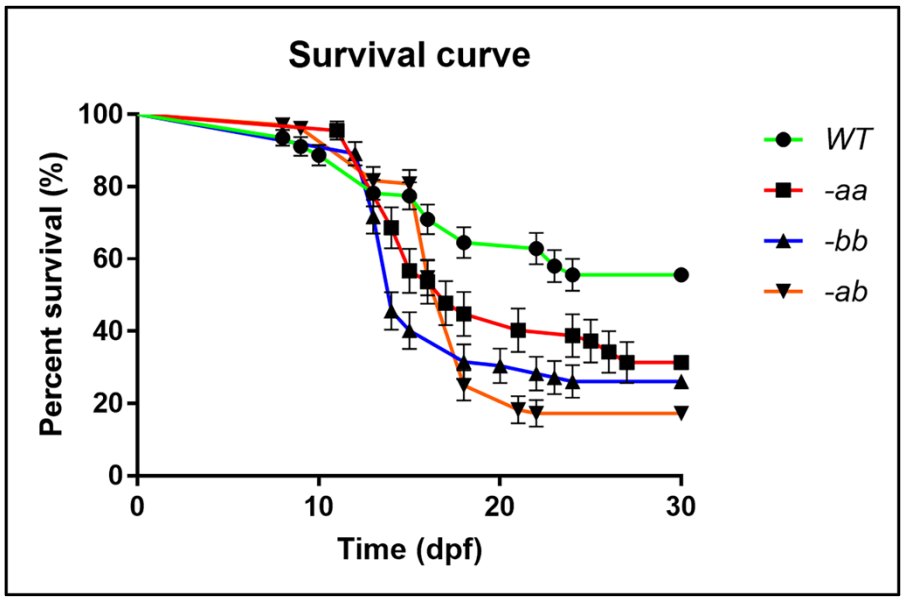

Figure 21: Decreased survival of zebrafish Dsp mutants at juvenile stages.
One-month survival analysis of mutant lines showed a significant decrease in the survival rate of mutated larvae (-aa ($p<0.01$), -bb ($p< 0.0001$), -ab ($p< 0.0001$)) in comparison with WT. Sample size: n=100. Test: Log-rank (Mantel-Cox) test.

4.1.1.10. Signalling pathways analysis on 3-dpf mutated larvae

As already discussed in the introduction, the dysregulation of specific cell signalling pathways, such as Wnt/β-catenin, Hippo/YAP-TAZ, and TGF-β, was recently connected with mutation in junctional/desmosomal proteins (Garcia-Gras et al., 2006; Asimaki et al., 2014; Giuliodori et al., 2018). qPCR analysis was performed to confirm the dysregulation of these pathways also in our models at the larval stage. Specifically, we examined the mRNAs levels of two target genes involved in the Wnt/β-catenin signaling pathway, *ccnd1,* and *myca*, demonstrating a global down-regulation trend of this signal, although not always consistent for both markers in each genotype. We also checked the expression level of target genes related to the Hippo/YAP-TAZ signalling pathway and TGF-β pathway, *ccn2a*, *ccn2b*, *smad2,* and *smad3*, confirming a dysregulation. In particular, we observed a global up-regulation of YAP-TAZ signalling and a down-regulation trend of TGF-β pathway (**Figure 22**).

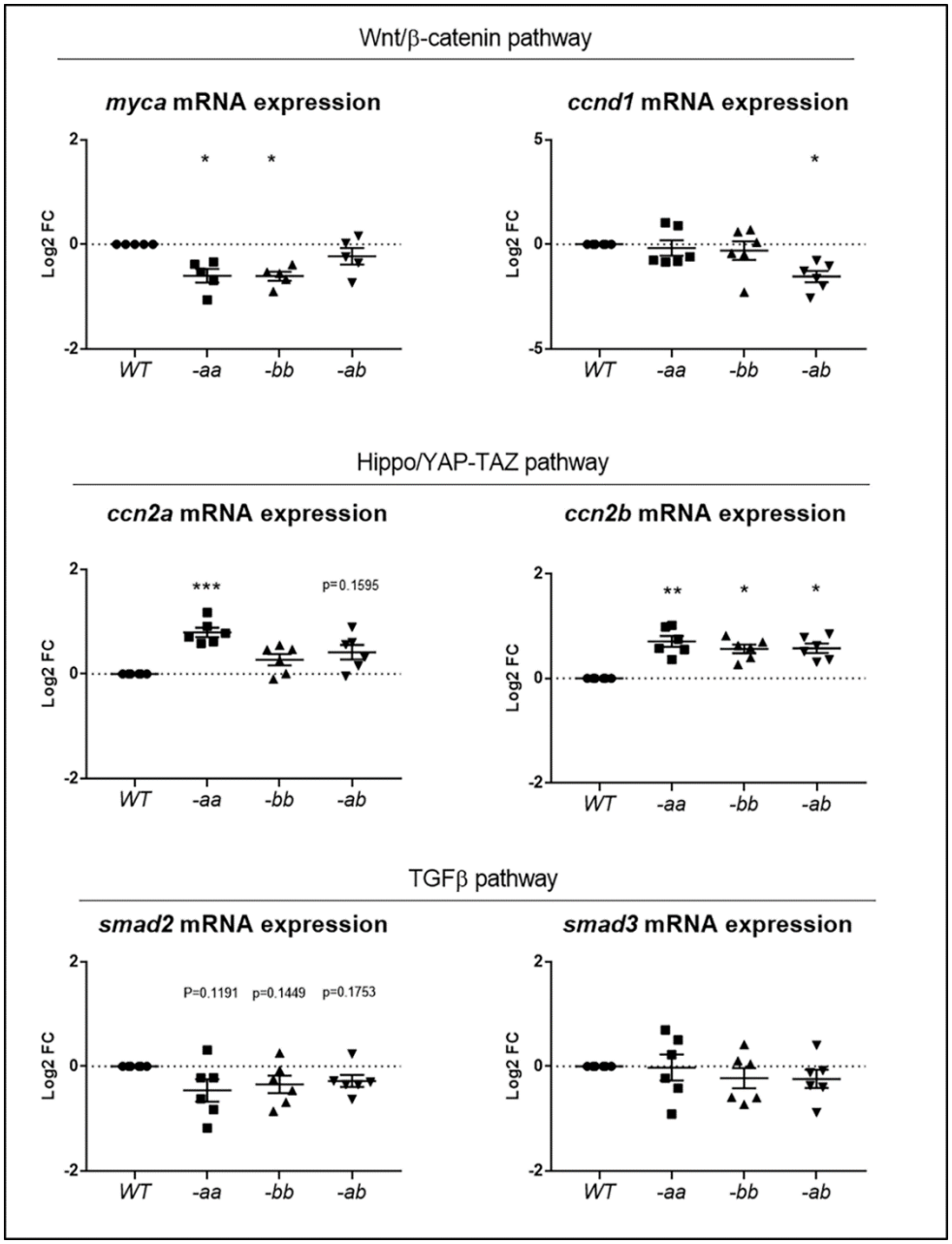

Figure 22: Signalling pathways dysregulation in Dsp mutant larvae.

qPCR analysis detected Wnt/β-catenin, YAP-TAZ, and TGF-β signaling dysregulation in Dsp mutants, significant for the first two pathways and as a trend for TGF-β. Each point on the graph corresponds to a pool of 30 embryos of the same genotype. Sample size: n=6±1. Log2 FC: Log2 Fold Change. *=p<0.05; **=p<0.01; ***=p<0.001. Test: One-way ANOVA followed by Tukey's test.

4.1.1.11. Choice of the -ab mutant line as a model for AC

Based on the results obtained from the above-described experiments, we decided to focus our attention only on the -ab mutant line, as a suitable system to model the human genetic and phenotypic AC condition. This mutant line displayed a balanced reduction of both Dspa and Dspb protein expression, and showed a consistently severe phenotype in terms of cardiac morpho-function and signalling pathway expression. Thus, from now on, all reported experiments will refer to the -ab line and their WT controls.

4.1.1.12. Detection of cardiac dilation and inflammation on 3-dpf -ab mutated larvae

A myocardial-specific *Tg(tg:EGFP-myl7:EGFP)ia300 dsp*-mutated transgenic line (Porazzi et al., 2012) was used to detect possible alterations in the heart chambers structure. Fluorescent mutated -ab larvae showed a statistically significant increase in the total area of both the heart's chambers (atrium and ventricle), indicating the presence of a prominent cardiac dilation (**Figure 23 A-A'-A''**). To verify whether ongoing inflammatory processes, recently associated with the pathogenesis of AC (Lin et al., 2021), could coincide and be associated with the alterations observed in mutants, we used an anti-L-plastin antibody as a leukocyte marker for the detection of inflammatory cells. This immunostaining revealed a two-fold significant increase of L-plastin-positive cells in mutant hearts compared to controls (**Figure 23 B-B'-B''**).

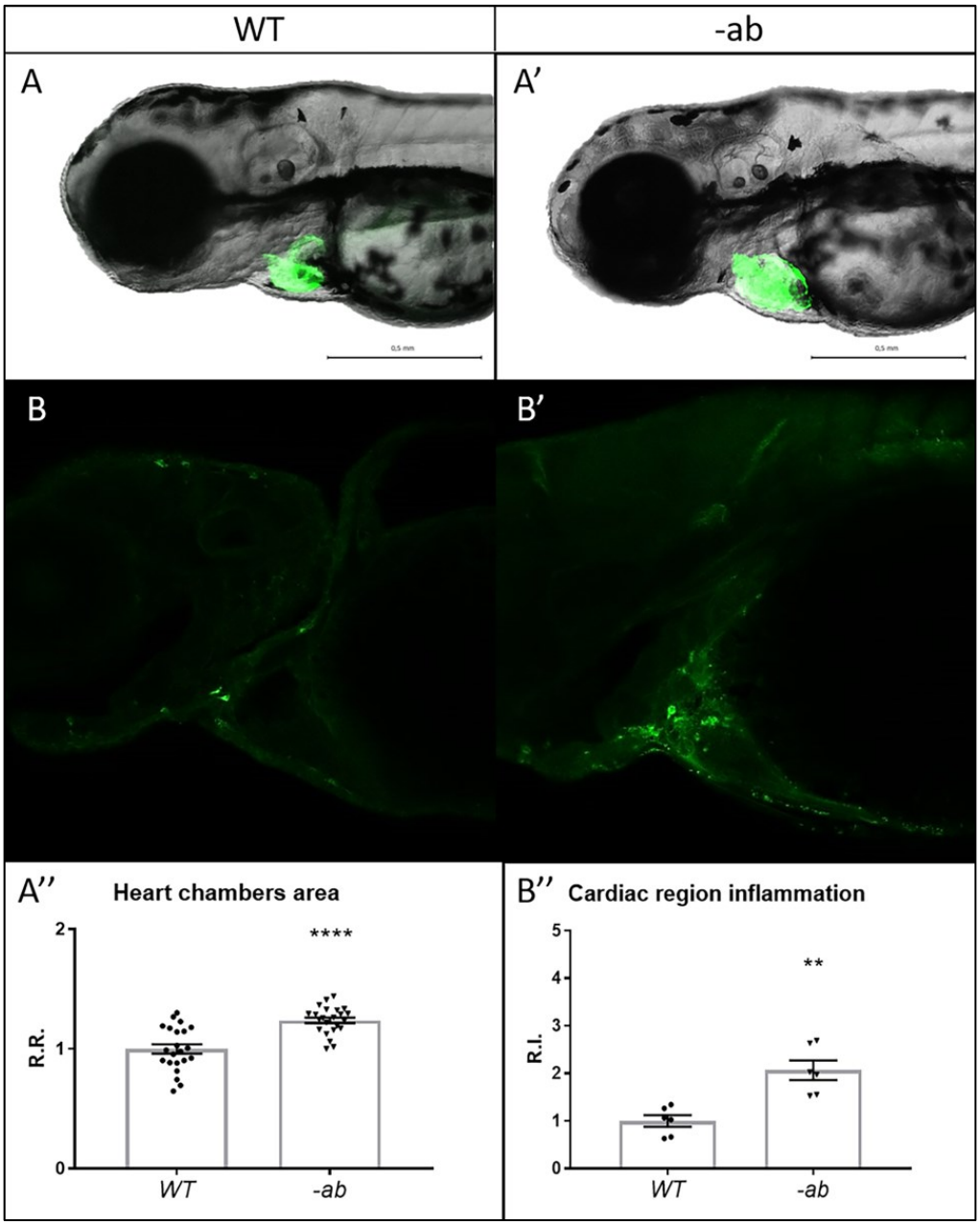

Figure 23: Detection of cardiac dilation and inflammation in zebrafish Dsp mutants. A-A'-A'': Heart morphology analysis of the wild-type and -ab mutant zebrafish embryos using a myocardial-specific transgene *Tg(tg:EGFP-myl7:EGFP)ia300* identified a global dilation of both chambers in -ab mutants. All embryos are at 3 dpf, in lateral view. Sample size: n=2022±1. R.R: Relative Ratio. ****=p<0.0001. Test: Unpaired t-test. B-B'-B'': Cells expressing the inflammatory marker L-plastin are more abundant in -ab mutants, compared to WT. All embryos are at 3 dpf, in lateral view, anterior to the left. Sample size: n=6. R.I.: Relative Intensity. **=p<0.01. Test: Unpaired t-test.

4.1.1.13. Motor behaviour analysis and effects of physical exercise on -ab mutated larvae

To investigate possible alterations in the motor behavior of -ab mutated zebrafish larvae, locomotion tests were performed at 5 dpf. However, before that, to be sure that possible detected abnormalities were due only to cardiac problems, we preliminarily checked the state of the skeletal musculature using birefringence, known to be brighter in highly organized skeletal muscle fibers. In **Figure 24**, it is possible to observe the results of the analysis, performed on two pools of larvae, WT (**Figure 24 A**) and -ab (**Figure 24 A'**), both represented as the mean of birefringence intensity normalized on the fish length. According to our results, there was no evidence of significant differences between the two pools (**Figure 24 A''**), indicating preserved organization of the skeletal muscle structure in -ab mutant larvae. Continuing the analysis, the motor behavioral assay showed that mutations in *dsp* genes do not affect the ability to respond to light stimuli (dark/light periods), but reduce the normal physical response to them in mutated larvae if compared to the WT ones (**Figure 24 B**). A statistical significant reduction in the total distance swum compared to controls confirmed the preserved sensory perception associated with impaired motor performance (**Figure 24 B'**). It is well known that physical activity can cause early onset and acceleration in the progression of this disease, provoking also in some cases SCD (Nava et al., 1988; Thiene et al., 1988; Basso et al., 1996, 2009, 2011). We tried to recreate this condition also in our -ab zebrafish larvae. Wild type and mutated zebrafish larvae were let to grow in 1% methylcellulose solution dissolved in fish water for 10 days from 3 to 13 dpf. This solution, due to its high density, increased the force needed to reach food and move normally, simulating a physical training protocol (Ruparelia et al., 2014). Specifically, we observed increased mortality in both WT and mutated trained pools, statistically significant in trained mutants when compared with their controls. Of note, Dsp mutants under physical exercise showed the highest mortality rate when compared with the other conditions (**Figure 24 C**).

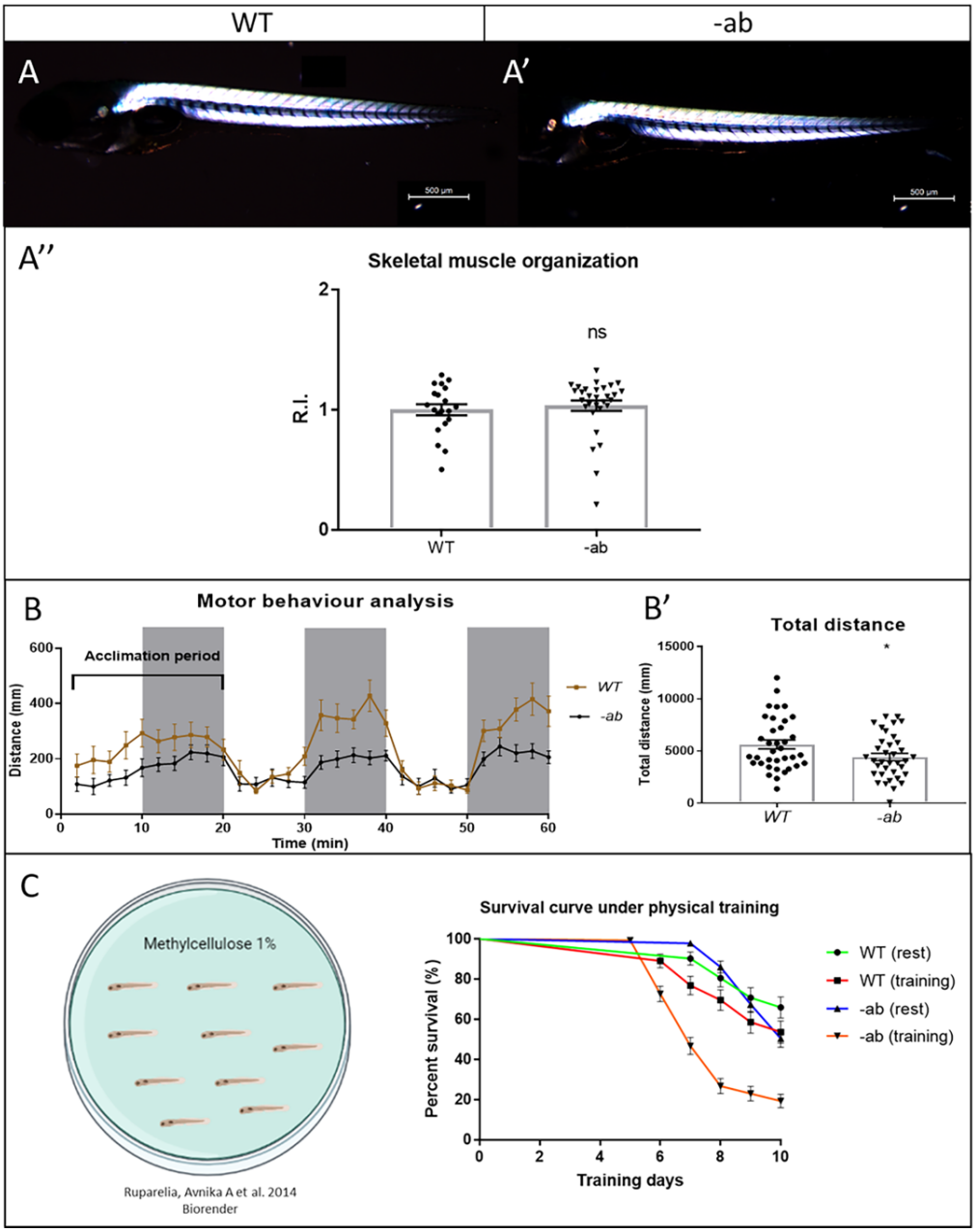

Figure 24: Impaired motor behaviour and exercise-induced mortality in zebrafish Dsp mutant larvae.

A-A'-A'': Birefringence analysis on WT and mutant larvae at 5 dpf does not detect any significant difference in the skeletal muscle structure. All embryos are at 5 dpf, in lateral view, anterior to the left. Sample size: WT n=20; -ab n=30. R.I.: Relative Intensity. ns =not significant. Test: Unpaired t-test. B-B': WT and -ab larvae at 5 dpf display normal response to light (white areas) and dark (grey areas) stimuli, but with reduced motor performances if mutated, evaluated as total distance swum (B). Sample size: n=36. *=p<0.05. Test: Unpaired t-test. C: A mild training protocol was applied for 10 days on larvae from 3 to 13 dpf. A statistically significant increase in mortality was observed in trained mutants when

compared with resting controls ($p<0.0001$). Sample size: n=50. Test: Log-rank (Mantel-Cox) test.

4.1.2. Adult phase

Since AC is a late-onset and progressive disease, adult fish were analysed to evaluate long-term pathological alterations.

4.1.2.1. Signalling pathways analysis on adult -ab mutant heart

Also at the adult stage, we investigated the possible dysregulation of Wnt/β-catenin, Hippo/YAP-TAZ, and TGF-β signalling pathways in the hearts of 1-year-old adult fish, to confirm the signs of alterations observed at the embryonic-larval stage. We examined in -ab and WT samples the tissue-specific cardiac expression of mRNAs encoding *ccnd1* and *myca* target genes, involved in the Wnt/β-catenin signalling pathway, demonstrating a statistically significant down-regulation in the mutant samples. We also checked if the expression levels of components of the Hippo/YAP-TAZ and TGF-β pathways (*ccn2a*, *ccn2b*, *smad2,* and *smad3*) were dysregulated. We observed, unlike the analysis at the larval stage, a statistically significant down-regulation of the YAP-TAZ signalling pathway, while the TGF-β pathway remained down-regulated (**Figure 25**).

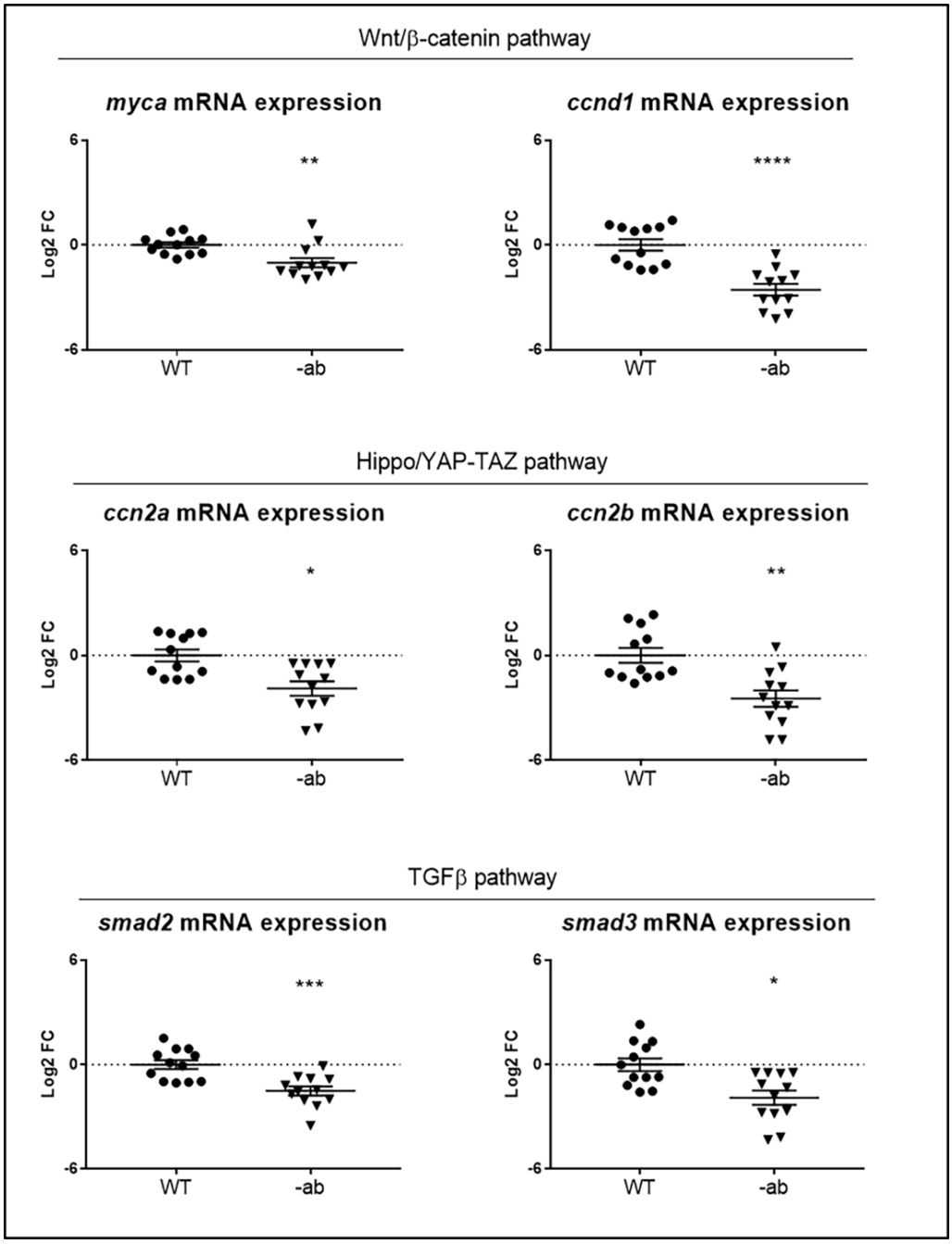

Figure 25: Signalling pathways dysregulation in adult Dsp mutant hearts.

qPCR analysis of the expression of Wnt/β-catenin, YAP-TAZ, and TGF-β signaling members showed a down-regulation of all pathways in Dsp mutant hearts. Each point on the graph corresponds to a pool of 3 hearts of the same genotype. Sample size: n=12. Log2 FC: Log2 Fold Change. *=$p<0.05$; **=$p<0.01$; ***=$p<0.001$; ****=$p<0.0001$. Test: Unpaired t-test.

4.1.2.2. Ventricular dilation and disorganized desmosomes in -ab mutant heart

AC is characterized by a progressive replacement of cardiomyocytes with fibro-fatty tissue and ventricular dilation is very common in patients carrying mutations in *DSP*. We performed the analysis of the ventricle area in heart of -ab mutated adult fish normalized to their body size, demonstrating that hearts showed a statistically significant dilatation in comparison with WT controls, as previously observed in mutant larvae (**Figure 26 A-A'-A''**). Moreover, a deeper analysis of the organization of desmosomes of 3- and 6-month old -ab zebrafish heart by TEM analysis revealed "pale", disorganized, and delocalized desmosomes (**Figure 26 B'-C'**) when compared with WT ones (**Figure 26 B-C**) at both stages. In addition, the extracellular space distance was significantly increased in 6-month-old -ab samples (**Figure 26 B''-C''**).

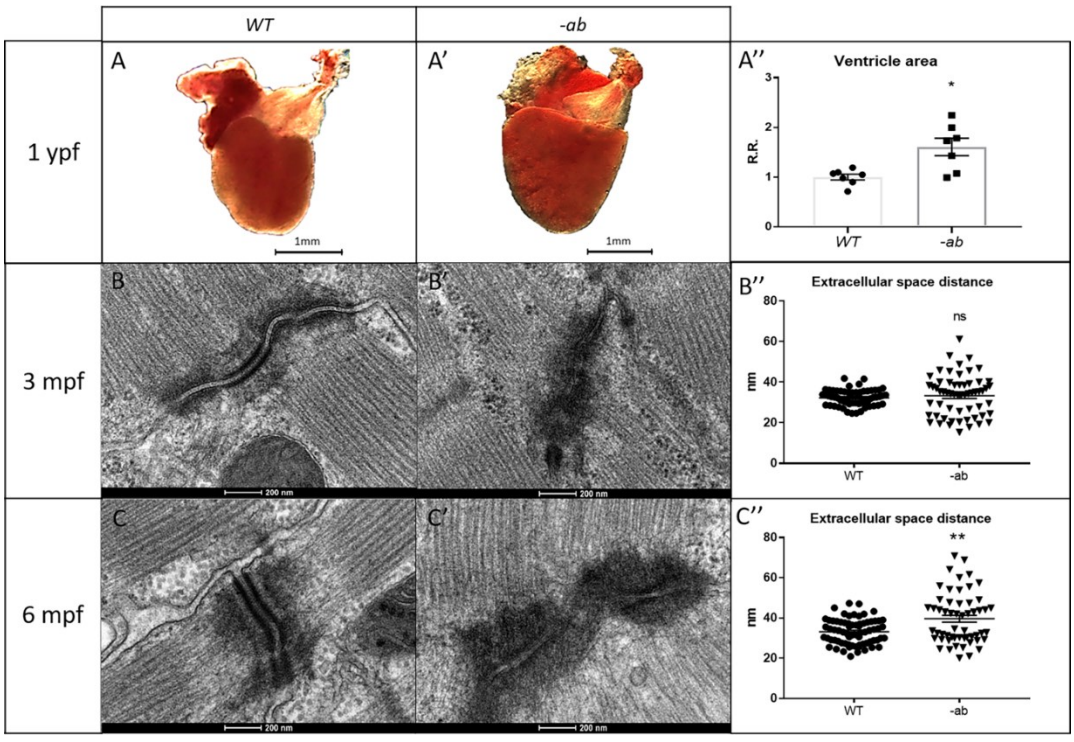

Figure 26: Cardiac dilation and disorganized desmosomes in Dsp mutant zebrafish hearts.

A-A'-A'': 1-year-old -ab mutant ventricles showed a statistically significantly dilation ($p<0.05$) in comparison with WT controls. Sample size: n= 7. R.R: Relative Ratio. *=$p<0.05$. Test: Unpaired t-test. B-B'-B''-C-C'-C'': TEM analysis of 3- and 6-month old

mutated zebrafish heart revealed “pale”, disorganized, and delocalized desmosomes. 6-month-old -ab hearts showed a significantly increased distance in the extracellular space. Sample size: n= 60±10. ns=not significant; **=p<0.01. Test: Unpaired t-test.

4.1.2.3. Structural changes in -ab mutant heart are exacerbated by exercise

Heart sections of 3-, 6- and 9-month-old mutant fish were analysed using Haematoxylin and Eosin staining. At 3 months of age, no differences were seen between WT and mutated heart, so we deduced that it was too early to observe structural changes (data not shown), although, through TEM analysis, we know that desmosomes are already severely damaged at this age. Instead, 6- month old mutated zebrafish hearts showed mild rarefaction of cardiomyocytes, thinning of the myocardial layer, age-related alterations in the distribution and organization of the trabeculae network, and abnormal shape of the ventricle. Moreover, this analysis underlined the presence of vessels dilation and accumulation of adipose cells inside the myocardial layer (**Figure 27, 6 mpf Resting**). After an intensive training protocol from 3 to 6 mpf, the WT adult zebrafish hearts did not show any changes in tissue structure and organization, while the mutants showed increased disorganization of the trabeculae, vessels dilations, and adipose tissue accumulation in the myocardial layer (**Figure 27, 6 mpf Training**). After doubling the duration of the training, no worsening of the condition was observed compared to the WT controls (data not shown). In 9-month-old mutated fish hearts, the phenotypic condition observed in 6-month-old heart was getting worse, the shape of the ventricle was more altered and dilated, and a clear trabeculae network disorganization was observable. The myocardial layer appeared thicker, suggesting a possible compensatory process due to the poor contractility of the heart tissue. Moreover, in the myocardial layer, we observed more dilated vessels and a more intrusive presence of adipose cells (**Figure 27, 9 mpf Resting**), strengthening the idea that this disease gets worse over time both in zebrafish and in humans. Interestingly, the 6-month-old trained phenotypic condition resembles the 9-month-old resting one, confirming again that in zebrafish, as in human, intensive physical training accelerates the progression of the disease.

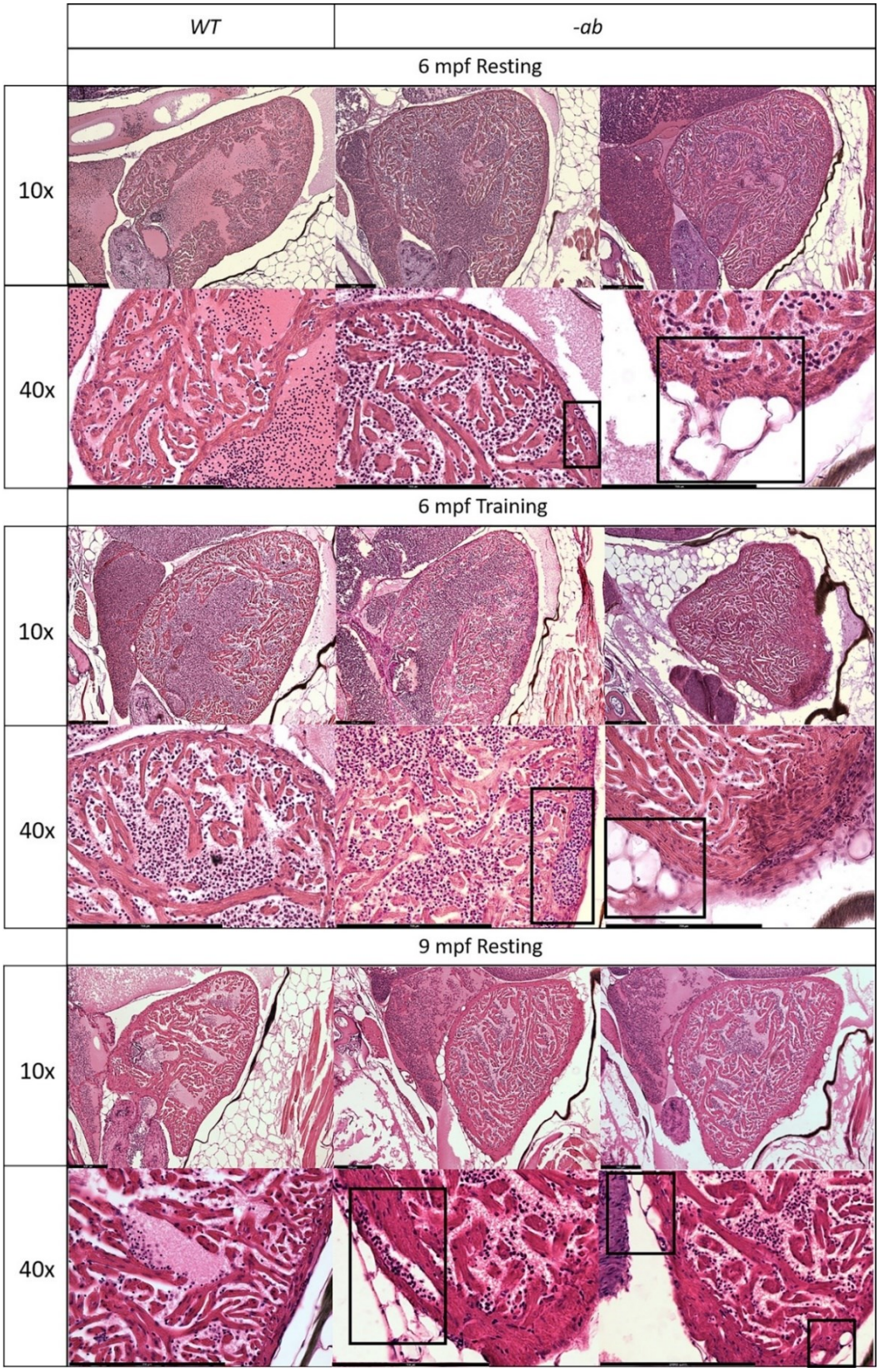

Figure 27: Cardiac dilation and structural changes in Dsp mutant hearts.

Histological analysis of 6-month-old -ab mutant zebrafish showed mild rarefaction of cardiomyocytes, thinning of the myocardial layer, age-related alterations in the distribution

and organization of the trabeculae network, an abnormal shape of the ventricle, the presence of possible vessels dilation (rectangular box) and accumulation of adipose cells inside the myocardial layer (square boxes). Histological analysis of 6-month-old mutated zebrafish confirmed the worsening of the condition after intensive physical training, like vessel dilation (rectangular box) and a more intrusive presence of adipose cells (square boxes), showing similarities with 9-month-old mutant hearts at rest. 9-month-old -ab mutant zebrafish showed worsening of the cardiac phenotype compared to 6-month-old mutant hearts, with a thickness of the myocardial layer, vessels dilation (rectangular box), and the more intrusive presence of adipose cells (square boxes). Sample size: n=3 for each condition and age. Scale bar: 200 m.

4.1.3. Rescue of AC phenotype by Wnt/β-catenin activation in -ab mutant larvae

Wnt/β-catenin signalling down-regulation has been demonstrated to be central in the pathogenesis of AC and in our –ab mutant line showed the same dysregulation observed in humans. Therefore, we decided to treat the zebrafish larvae with the Wnt agonist SB216763 and the Wnt inhibitor XAV939, from 1 to 3 dpf, to check for possible recovery or worsening of the pathway expression. Mutant transgenic Wnt/β-catenin GFP reporter zebrafish larvae treated with SB216763 at 40 μM revealed a statistically significant recovery of pathway expression, while the treatment with XAV939 at 5 μM caused a strong reduction of Wnt activation in a statistically significant way when compared with the WT control and with the untreated -ab pool (**Figure 28 A**). Interestingly, we observed a significant reduction of cardiac abnormalities in mutant larvae after SB216763 treatment (**Figure 28 B**), associated also with a recovery of developmental parameters analysed, body length and eye size, as well as the reduction of the dilation of the cardiac region, originally due to pericardial effusion and hemopericardium (**Figure 28 C**). We also tried to rescue the bradycardic phenotype through the Wnt/β-catenin modulation with the treatment carried out in this case from 3 to 5 dpf. The 2-day treatment with 5 μm XAV939 did not alter significantly the heart rate rhythm, while on the other hand, after the 40 μm SB216763 treatment, the mutated larvae partially recovered the bradycardic pathological condition, when compared with untreated mutants and controls (**Figure 28 D**). Moreover, we repeated the survival rate analysis for WT

and mutant larvae with and without SB216763 treatment. Therefore, starting with the same number of fish per tank, we made them grow in the same environment for a month, counting every day the number of deaths. We observed that untreated WT and -ab mutants showed mortality ratios like those seen in previous analyses with all the other genotypes, validating the obtained result. On the other hand, Dsp mutants treated with 40 μM SB216763 for 4 days presented a statistically significant decrease in mortality, becoming similar to the WT condition (**Figure 28 E**). Finally, after these encouraging results on SB-induced rescue of several mutant phenotypes, we decided to evaluate the SB effects also on mutant larvae after forced physical exercise in a 1% methylcellulose viscous medium in fish water for 5 days, from 3 to 8 dpf. The survival curves in **Figure 28 F** confirm a net difference between resting and training conditions, with untrained pools that ended the analysis without experiencing any fatality (100% of survivors). The comparison among trained pools showed similar death trends, starting at 6 dpf (the third day of training), increasing the slope in the following days but ending up with a significant difference in the number of survivors. Interestingly, the trained WT pool (green line) displayed a survival rate constantly placed in between the mutants' curves. This is a noteworthy fact since it implies that the trained SB-treated mutant pool, which ended up with the highest number of survivors (53%) – manifested an overall resistance to the physical training even better than the reference trained WT. Looking instead at the differences between trained mutants with or without treatment, we can see that the pairwise comparison was statistically relevant, with a final number of survivors that was more than two times higher in SB-treated mutants compared to the untreated ones.

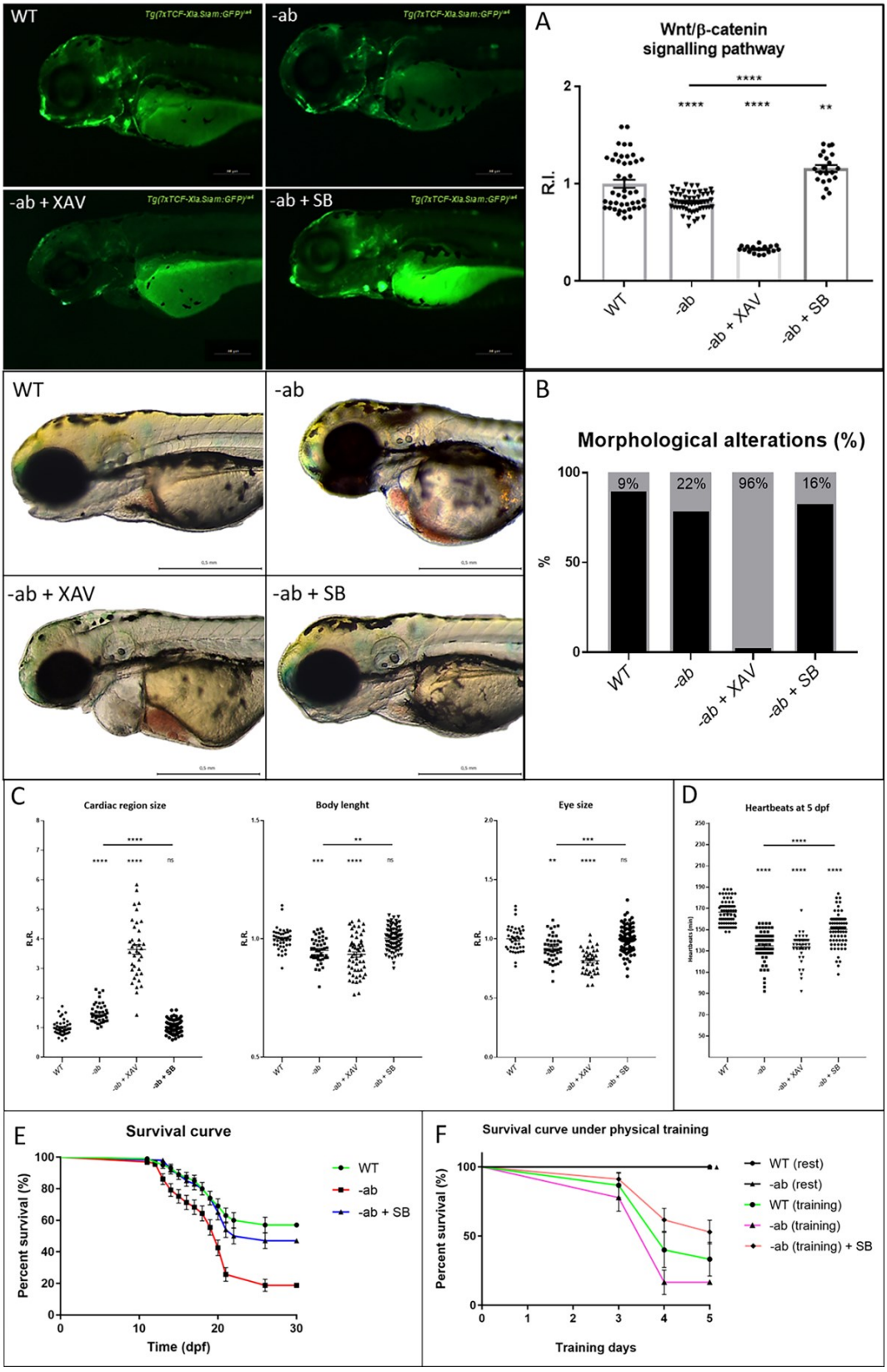

Figure 28: Wnt/β-catenin activation rescues AC phenotypes in Dsp zebrafish mutants. A: Zebrafish -ab mutants treated for 2 days with 5 µM XAV939 (XAV, Wnt inhibitor) or 40 µM SB216763 (SB, Wnt agonist) showed a down-regulation or a full recovery of the

pathway activity (GFP reporter) when compared to WT controls or untreated mutants. All embryos are at 3 dpf and displayed in lateral view, anterior to the left. Sample size: WT n=45; -ab n=55; -ab + XAV n=17; -ab + SB n=21. R.I.: Relative Intensity. **=p<0.01; ****=p<0.0001. Test: One-way ANOVA followed by Tukey's test. B: The -ab larvae treated with 40 µM SB showed a significant reduction of cardiac dysmorphisms, while 5 µM XAV induced a worsening of the condition when compared to WT controls or untreated mutants. All embryos are at 3 dpf and displayed in lateral view, anterior to the left. Sample size: n=100. C: The -ab larvae treated for 2 days with 40 µM SB216763 showed a significant rescue of the main morphological alterations. The treatment with 5 µM XAV939 induced a worsening of the condition. Sample size for cardiac region size: WT n=41; -ab n=41; -ab + XAV n=37; -ab + SB n=82. Sample size for body length: WT n=41; -ab n=46; -ab + XAV n=54; -ab + SB n=82. Sample size for eye size: WT n=41; -ab n=46; -ab + XAV n=36; -ab + SB n=81. R.R.: Relative Ratio. ns= not significant; **=p<0.01; ***=p<0.001; ****=p<0.0001. Test: One-way ANOVA followed by Tukey's test. D: At 5 dpf, treated -ab larvae showed a statistically significant recovery of the bradycardia phenotype. Sample size: WT n=70; -ab n=66; -ab + XAV n=40; -ab + SB n=77. ****=p<0.0001. Test: One-way ANOVA followed by Tukey's test. E: One-month survival rate of WT and -ab larvae untreated or treated with 40 µM SB216763 for 4 days; a statistically significant decreased mortality in mutants is observed after treatment, compared to untreated mutants (p<0.0001). Sample size: n=100. Test: Log-rank (Mantel-Cox) test. F: 5-day survival analysis, from 3 to 8 dpf, of untrained or trained WT and -ab, as well as -ab simultaneously SB-treated and trained (training induced in 1% methylcellulose). Trained -ab, treated with SB, showed a statistically significant decrease in mortality when compared with -ab subjected to training in the absence of SB (p<0.01). Sample size: n=50. Test: Test: Log-rank (Mantel-Cox) test.

4.2. Stable *lgals3a*-KO zebrafish line

4.2.1. Generation of zebrafish with mutations in the *lgals3* genes

In zebrafish, the *lgals3* gene presents in two copies: galectin-3a (*lgals3a*) (ZDB-GENE-030131-7667) on chromosome 13, and galectin-3b (*lgals3b*) (ZDB-GENE-030131-4324) on chromosome 17. Both *lgals3*-KO zebrafish lines were produced in our laboratory by Crispr/Cas9 approach. A deletion of 4 bp in exon 3 was obtained in the *lgals3a* gene (Chr 13: g. 36578952¬ 36578957del), which leads to

the shift of the reading frame and the production of a truncated protein of 218 amino acids, out of 332 total, thus lacking the C-terminal domain. The synthesis of a non-functional protein, without the carbohydrate recognition domain (CRD) of the protein, placed at the C-term as in humans, causes its premature degradation. For the *lgals3b* gene, deletion of 114 bp in exon 3 (Chr 17: g10832046-10832160del) leads to the removal of almost all the exon 3 sequences. This region of the gene encodes for the collagen-alpha domain, nearly 110 amino acids long, a region of the protein that participates in the oligomerization of Gal-3 molecules and in its interactions with other proteins (Mehul et al., 1995; Ippel et al., 2016). The ablation of 38 amino acids out of 110 in this domain is expected to induce a loss of function of the protein, impeding its normal activity.

4.2.2. Genotyping of *lgals3a* and *lgals3b* zebrafish mutants

The genotyping of both mutant zebrafish lines was obtained by PCR product analysis, followed by sequencing to confirm the results. The amplicons obtained from *lgals3a* PCR analysis were loaded in a 3.5% TBE 1X agarose gel, showing the WT single band (on the left) of 178 bp, while the mutant sample on the right showed a reduced length (174-bp lower band), due to presence of the 4-nucleotide deletion (**Figure 29 C**). The confirmation of the result was obtained by sequencing analysis: the homozygous (**Figure 29 A**) mutant sample presents a deletion of 4 nucleotides (red box), while the WT sequence does not show any changes in the sequence (blue box) (**Figure 29 B**). To identify the mutation in the *lgals3b* gene, a PCR was performed and then analysed on a 2% TBE 1X agarose gel. We can observe that the WT PCR product on the left, with a total length of 288 bp, presents a difference of about 100 bp, considering the marker loaded next to it, if compared with the homozygous mutant sample loaded on the right, confirming the presence of an evident deletion in exon 3 (**Figure 29 F**). We validated the results also in this case by sequencing analysis, observing a deletion of precisely 114 bp in the homozygous mutant sample (red box) (**Figure 29 E**), if compared with the WT sequence without any change (blue box) (**Figure 29 D**).

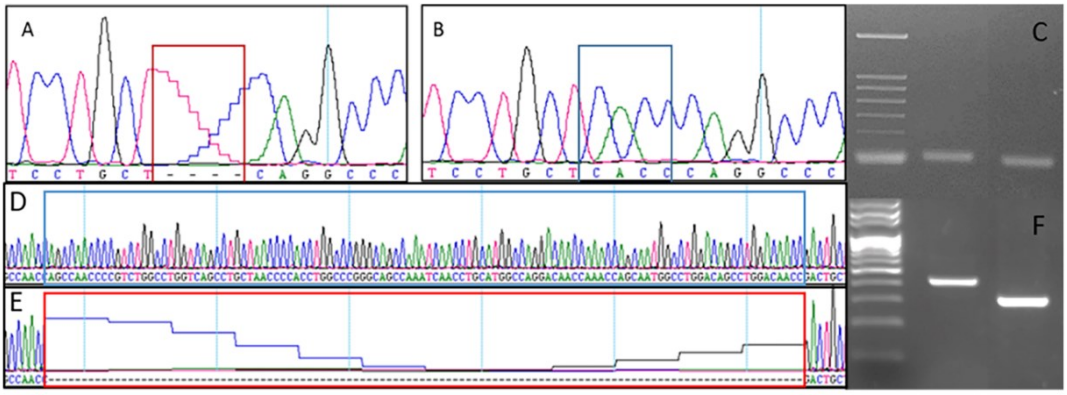

Figure 29: Genotyping of *lgals3a* and *lgals3*b zebrafish mutants.

A-B-D-E: sequence-based identification of the *lgals3a* 4-nt and *lgals3b* 114-nt deletions (red boxes) in case of homozygous control (B-D) and homozygous mutant (A-E). C- F: gel-based identification of the *lgals3a* (C) and *lgals3*b (F) genotypes; from left to right: size marker, WT control, and homozygous mutant.

4.2.3. Fertility analysis of *lgals3b* mutated fish

During the generation of the *lgals3a* and *lgals3b* KO stable zebrafish lines, we observed a strong decrease in the fertility in *lgals3b* homozygous mutants. Therefore, a fertility analysis was conducted outcrossing male and female *lgals3b* with *wild-type* counterparts. The eggs were collected after every single mating and transferred in a Petri dish in Fish water. The check of the fertilization was performed after few hours at 28.5° C. The results underlined that *lgals3b* homozygous male fish have regular spermatogenesis; in fact, they are able to fertilize 72% of the total eggs, in line with the percentages obtained by crossing two WT fish. *Lgals3b* homozygous female fish exhibited instead an abnormal ovulation, as they tend to release already degrading eggs, with 67% of the remaining eggs unfertilized (**Figure 30**).

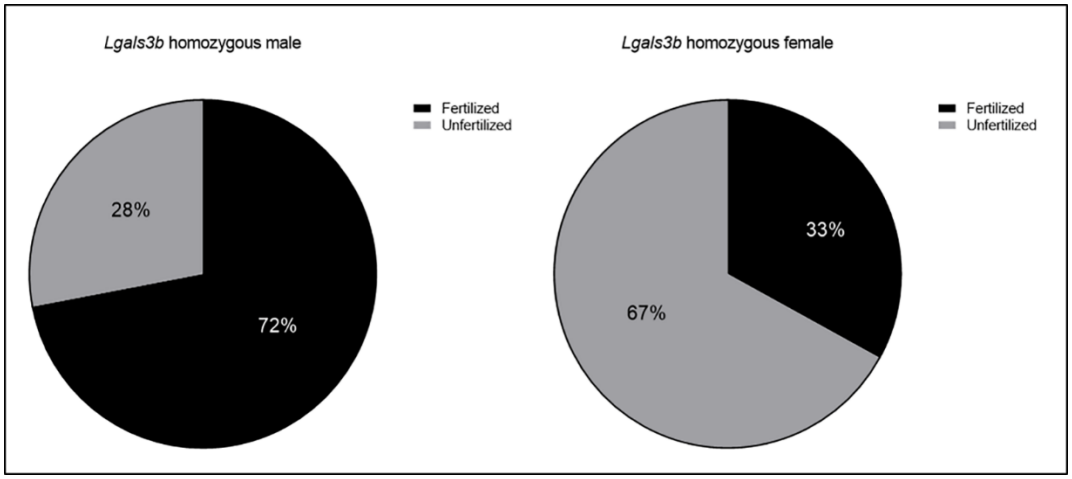

Figure 30: Graphical representation of fertility analysis of *Lgals3b* homozygous male and female adult zebrafish.

Left: *lgals3b* homozygous male fish fertilize 72% of the total eggs. Right: *lgals3b* homozygous female fish may exhibit abnormal ovulation, releasing already degrading eggs; 67% of the obtained eggs resulted unfertilized.

4.2.4. Choice of the homozygous *lgals3a* mutant line

These fertility issues made it very difficult to maintain a stable mutant line and generate all possible genetic combinations with the other *lgals3a* gene member. Based on these findings, we made the decision to focus our attention only on the *lgals3a* zebrafish mutant line (-aa) as a suitable system to mimic the genetic and cardiac phenotypic condition observed in AC human patients. In addition, *lgals3a* gene was already identified in the literature as the counterpart of the human *LGALS3* (Chen et al., 2021), validating our partially forced choice. Thus, from now on, all reported experiments will be referred only to the -aa line and their WT controls.

4.2.5. qPCR analysis of Lgals3 mRNAs and analysis of Dsp protein expression on -aa mutated larvae

We decided to investigate if the mutation in the *lgals3a* gene affected the own and the *lgals3b* mRNA expression. A qPCR study was carried out, revealing that the -aa mutant had statistically significant downregulation of the quantity of *lgals3a* mRNA at the embryonic stage. We confirmed also that the mRNA expression of

lgals3b gene was not affected by changes in the *lgals3a* one (**Figure 31 A**). Due to the absence of Lgals3 antibodies that work in zebrafish, we decided to check by Western Blot analysis the effect of the *lgals3a* mutation on the expression and possible degradation of desmosomal proteins. Using a monoclonal antibody made in mice that is specific for the C-terminal region of human Desmoplakin (Desmoplakin 1/2) (PROGEN 651155, mouse), we observed that the two Dspa and Dspb isoforms in zebrafish were affected by the *lgals3a* mutation. As expected, WT larvae displayed three bands (two for Dspb and one for Dspa) with a molecular weight of about 240 kDa, whereas in *dsp -ab* mutant larvae the expression was less intense, with a reduction of about 65%, confirming the results obtained in the *dsp*-KO zebrafish line characterization. Interestingly, also in the *lgals3 –aa* sample the Dsp protein expression was reduced at 9 dpf (29%), not as strongly as in *dsp –ab* pools, but still significantly. The ubiquitous protein α-Tubulin was identified with a specific antibody, and the intensities of the various bands corresponding to α-Tubulin and Dsp proteins were examined to compare the quantities of Desmoplakin protein in the different genotypes (**Figure 31 B**).

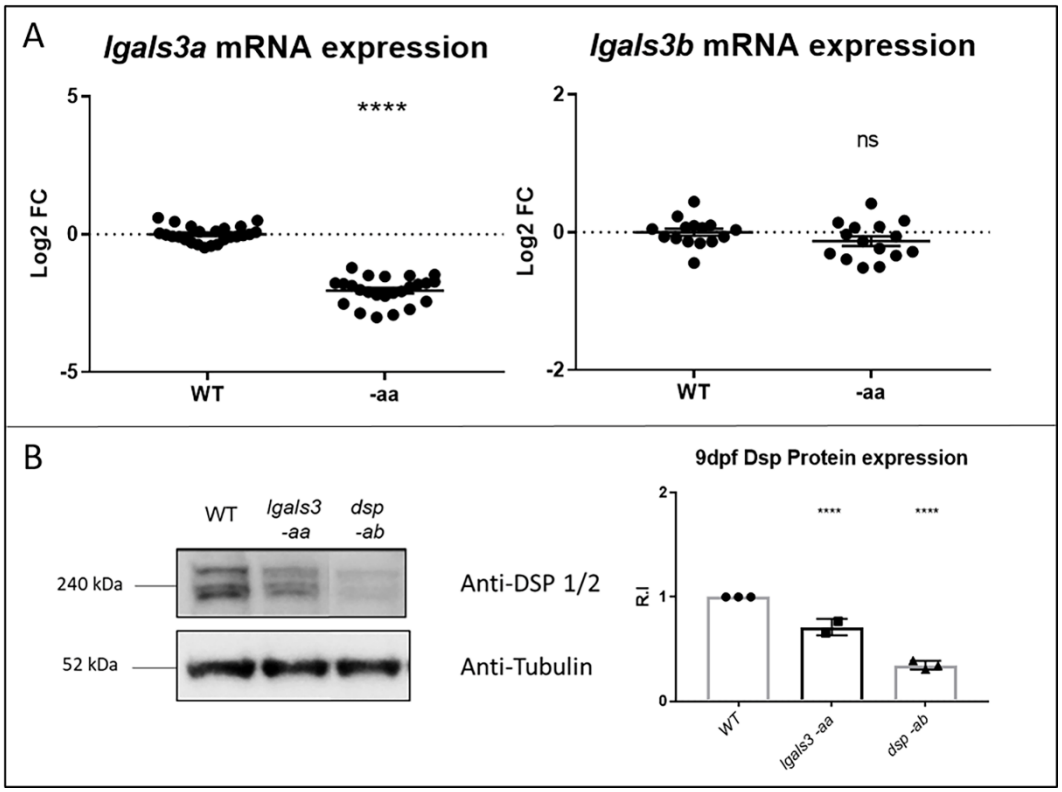

Figure 31: **Reduced *lgals3a/b* mRNAs and Dsp protein levels in zebrafish *lgals3a* (-aa) mutant larvae.**

A: qPCR analysis of *lgals3a* and *lgasl3b* mRNAs expression in WT and –aa embryos at 3 dpf. The *lgals3a* mRNA expression decreases significantly in -aa sample, while the expression of *lgals3b* does not change. Each point on the graph corresponds to a pool of 30 embryos of the same genotype. Sample size: n= 15. Log2 FC: Log2 Fold Change. ****=p<0.0001; ns= not significant. Test: Unpaired t-test. B: Western blot analysis on 9 dpf embryos detected alterations in Dspa and Dspb protein expression. The WT sample presents 3 bands of nearly 240 kDa, one for Dspa and two for the Dspb isoforms. The *lgasl3* -aa samples exhibit a reduced Dsp protein expression (29%). In the *dsp* -ab sample, all isoforms are present, with a reduced amount (65%). Each point corresponds to a pool of 10 embryos of the same genotype. Sample size: n=3. R.I: Relative Intensity. ****=p<0.0001. Test: One-way ANOVA followed by Tukey's test.

4.2.6. Morphological analysis of the cardiac region on 3-dpf -aa mutated larvae

Knowing the involvement of Lgals3 protein in the stabilization of cell-cell interactions and the demonstrated destabilization of Dsp protein expression by Western Blot analysis, made us look also at potential changes in the cardiac region and heart structure in our *lgals3a* zebrafish line. When compared to WT larvae, -aa mutants showed heart morphological defects with a disease penetrance close to 35%, which is extremely comparable to that seen in our *dsp*-KO zebrafish line and in patients with AC (**Figure 32 C**) (Pilichou et al., 2017). For -aa, the heart was structurally dilated presenting hemopericardium and/or pericardial effusion in the cardiac region (**Figure 32 B-B'**). More specifically, when compared to WT controls, the cardiac area was significantly dilated in the mutant line, confirming the morphological observations described before. Additionally, mutant larvae showed a statistically significant slowdown in their growth, as seen by their smaller bodies' length and eye area, two key quantitative indicators of the developmental stage in 24-72 hpf zebrafish embryos (**Figure 32 D**).

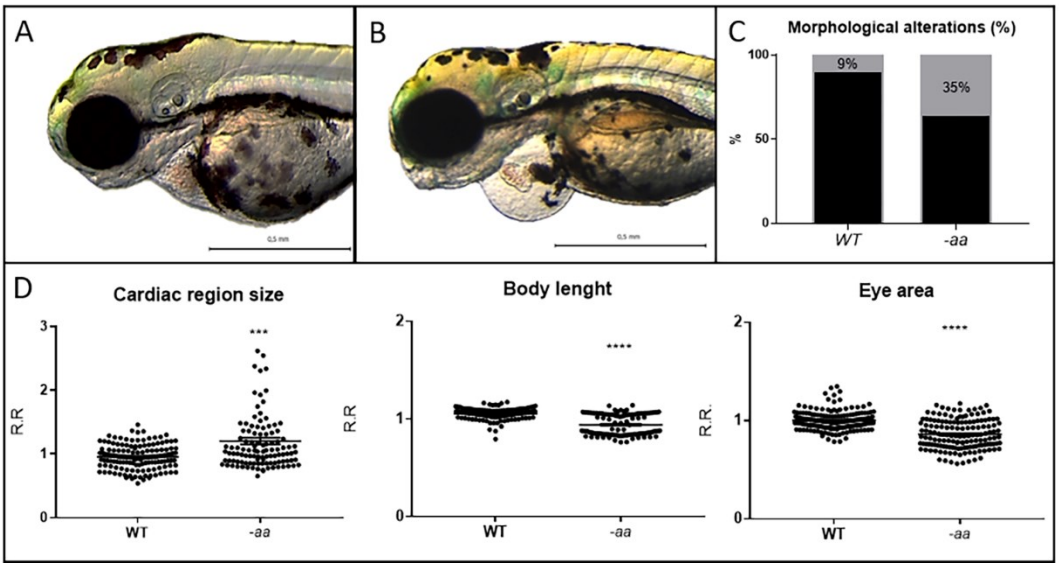

Figure 32: Cardiac alterations and developmental delay in *lgals3a* (-aa) mutants.
A-C: Mutant embryos (B) display cardiac alterations, compared to WT (A). Homozygous -aa (B) mutant hearts appear dilated and/or structurally altered, with pericardial effusion and/or hemopericardium in the cardiac region. C: Percentage of heart alterations in different genotypes. Sample size: n=100. D: Cardiac size analysis shows that mutants present cardiac area dilation. Body length and eye size measurements indicate a developmental delay in the mutant, if compared to WT. Embryos are displayed at 3 dpf in lateral view, anterior to the left. Sample size for cardiac region size: WT n=148; -aa n=104. Sample size for body length: WT n=152; -aa n=122. Sample size for eye size: WT n=171; -aa n=156. R.R.: Relative Ratio. ***=p<0.001; ****=p<0.0001. Test: Unpaired t-test.

4.2.7. Heart rate alterations on 2-3- and 5-dpf -aa mutated larvae

Heart rate frequency (beats per minute, bpm) was calculated at 2-3 and 5 dpf, before and after the appearance of the first signs of cardiac malformations and abnormalities, usually at 3 dpf. Normally, the mean heart rate in larvae showed an increase as the developmental stages progressed but at 2 and 3 dpf some signs of cardiac problems start already to manifest themselves in the tricaine-anesthetized mutant ones, with a significant reduction of heart rate at both developmental stages. More in detail, WT larvae presented a mean cardiac frequency of 138 bpm and 143 bpm at 2 and 3 dpf respectively, while mutant ones presented a bradycardia phenotype with a mean rate of 117 bpm at 2 dpf and 126 at 3 dpf. At 5 dpf, while the WT embryos increased their mean heart rate due to development, reaching 165 bpm, the mutant ones remained at the same mean rate already observed at 3 dpf,

around 123 bpm. Thus, the bradycardic phenotype was more dramatically evident in 5 dpf larvae, when compared with the control pools (**Figure 33**).

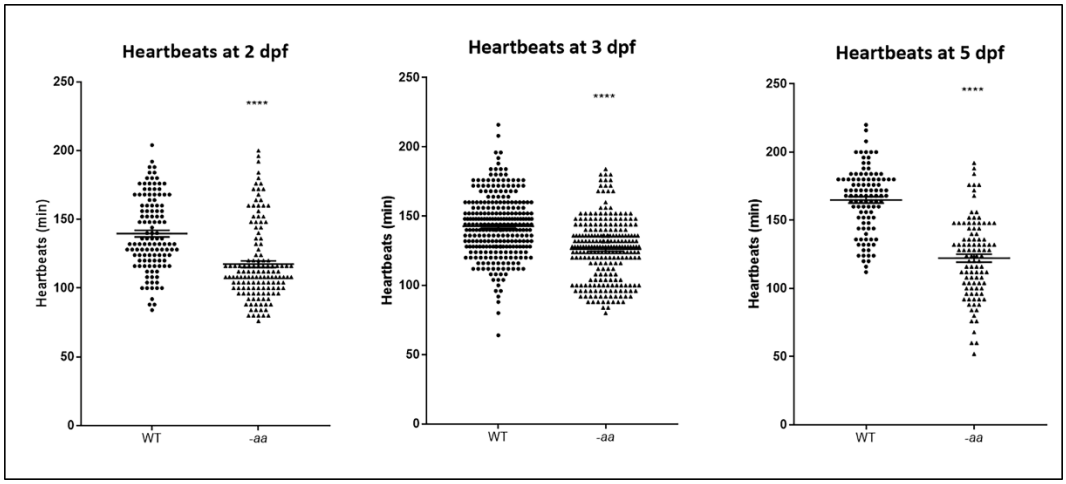

Figure 33: Heart rate alterations in *lgals3a* mutant larvae.

At 2 dpf, the heart rate frequency in WT was 138 beats per minute (bpm), while in -aa was 117 bpm; at 3 dpf, heartbeat was 143 bpm in WT and 126 bpm in -aa; at 5 dpf, the heartbeat changes appeared more evident; -aa larvae display a more significant bradycardia phenotype (123 bpm), compared to WT (165 bpm). Sample size at 2 dpf: WT n=120; -aa n=135. Sample size at 3 dpf: WT n=276; -aa n=243. Sample size at 5 dpf: WT n=103; -aa n=99. ****=p<0.0001. Test: Unpaired t-test

4.2.8. Survival analysis of mutant lines at juvenile stages

We raised the same number (100) of both WT and mutant larvae under identical conditions for a month while counting the number of deaths that occurred each day. We noticed that the mutant line's survival rate was statistically much lower (65%) than controls (90%) (**Figure 34**).

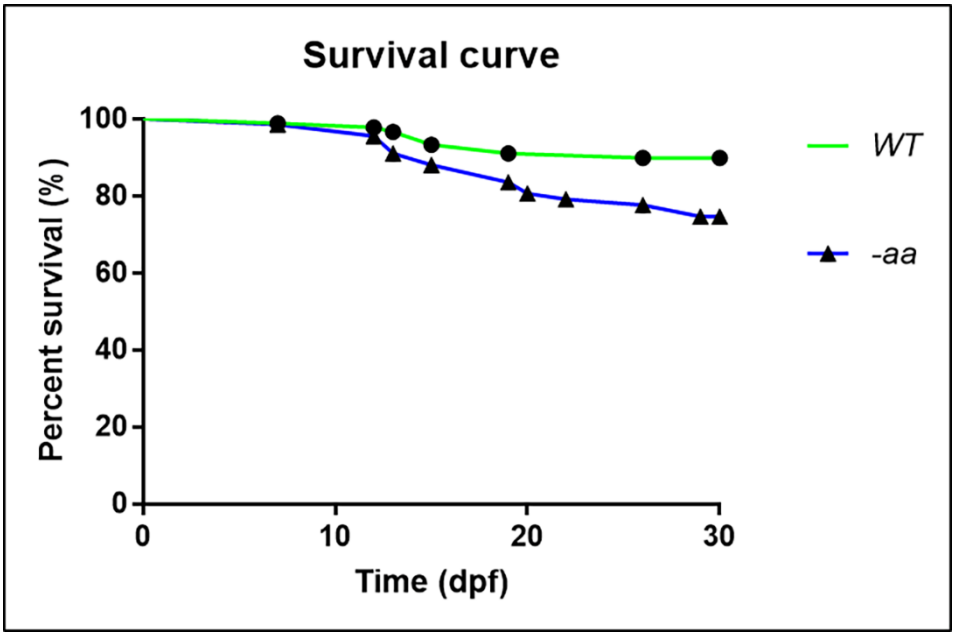

Figure 34: Decreased survival of zebrafish *lgals3a* mutants at juvenile stages.
One-month survival analysis of mutant lines showed a significant decrease in the survival rate of mutant larvae ($P<0.01$), in comparison with WT. Sample size: n=100. Test: Log-rank (Mantel-Cox) test.

4.2.9. Cardiac dilation on -aa mutated larvae and adult hearts

To look for potential changes in the anatomy of the heart chambers, the transgene *Tg(tg:EGFP-myl7:EGFP)ia300* (Porazzi et al., 2012) was used, specifically designed for myocardial observations. The overall area of the atrium and ventricle in fluorescent transgenic mutant -aa larvae increased significantly, demonstrating the presence of cardiac dilatation. (**Figure 35 A-A'-A''**). We reconfirmed the dilation of mutant hearts also in 1- year- old fish, reinforcing the idea that this gene is involved in the instability of cell-cell junctions and desmosome structures, causing structural fragility of the myocardial tissue and the subsequent dilation of the ventricle chamber (**Figure 35 B-B'-B''**).

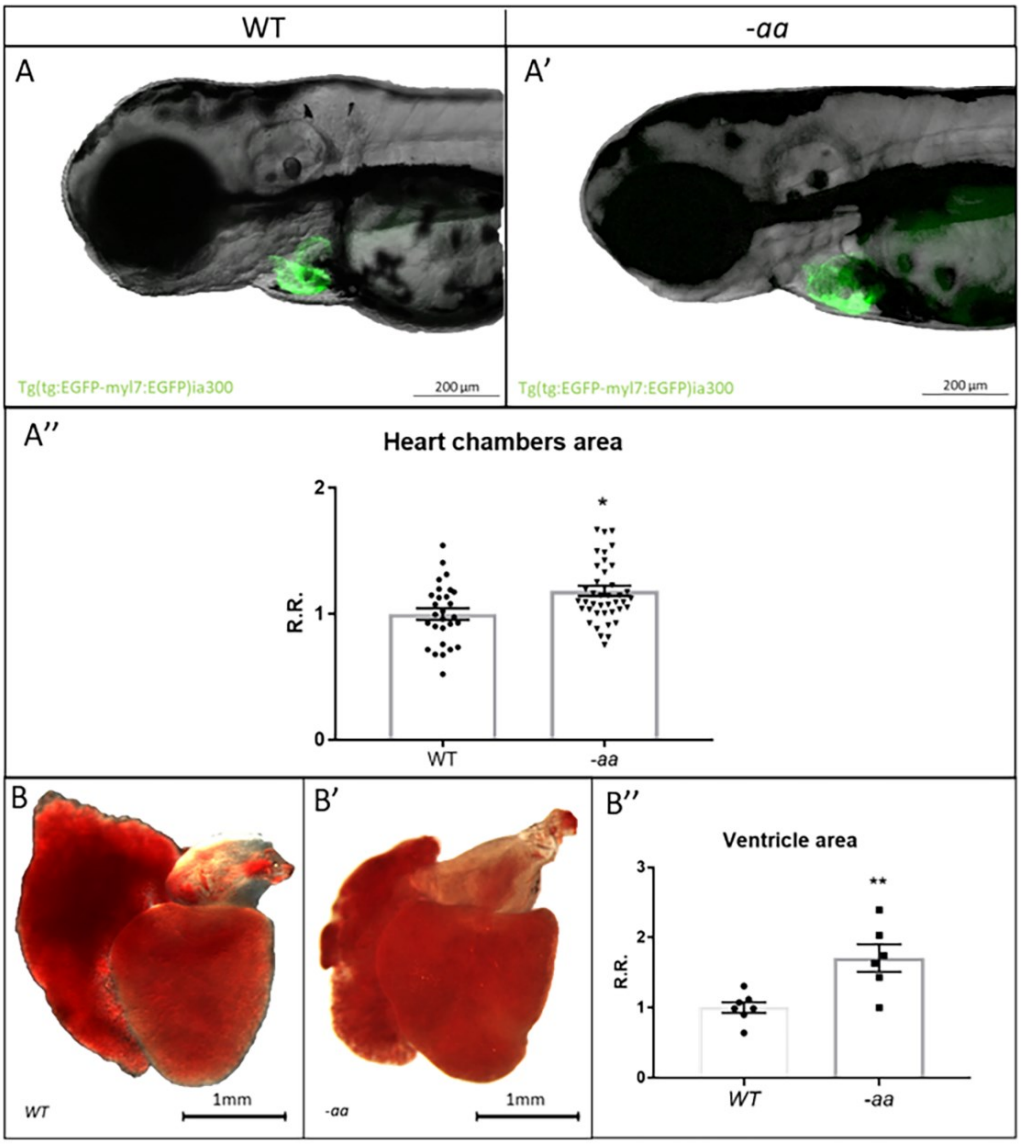

Figure 35: Cardiac dilation in zebrafish *lgasl3a* fluorescent mutant lines.

A-A'-A'': Using a myocardial-specific transgene *Tg(tg:EGFP-myl7:EGFP)ia300*, heart morphology analysis of wild-type and -aa mutant zebrafish embryos revealed dilation of both chambers in -aa mutants. Embryos are displayed at 3 dpf, in lateral view. Sample size: WT n=28; -aa n=42. R.R: Relative Ratio. *=p<0.05. Test: Unpaired t-test. B-B'-B'': 1-year old -aa mutant ventricles showed a significant dilation in comparison with WT controls. Sample size: n= 6±1. R.R: Relative Ratio. **=p<0.01. Test: Unpaired t-test.

4.2.10. Motor behaviour analysis on -aa mutated larvae

Locomotion experiments were carried out at 5 dpf to look at changes in the motor behavior of -aa mutant zebrafish larvae. Prior to that, however, we used birefringence, which is known to be brighter in well-organized skeletal muscle

fibers, to examine the condition of the musculature to make sure that any potential issues and modifications were exclusively caused by cardiac problems. The results of this analysis, based on two pools of larvae, WT (**Figure 36 A**) and -aa (**Figure 36 A'**), are shown as means of birefringence intensity adjusted on fish length. No substantial variations were found between the two pools (**Figure 36 A"**), indicating that the skeletal muscle structure in *lgals3a* mutant larvae was intact. Motor behavior analysis, instead, underlined that while *lgals3a* gene mutations do not affect the larva's ability to respond to light stimuli (dark/light intervals), they do diminish the larva's normal motor response to those stimuli in comparison to WT ones (**Figure 36 B**). In addition, it is possible to notice that in the dark phases the ability to swim is only slightly reduced in the mutant pool, while the most evident difference is in the second part of the light phases when the larvae recover from the stress and start to move again. In this specific part of the motor analysis, the *–aa* larvae showed more difficulty in starting to move again than WT controls, underlining a condition characterized by greater fatigue. A statistical significant reduction in the total distance swum compared to controls confirmed the preserved sensory perception associated with impaired motor performance (**Figure 36 B'**).

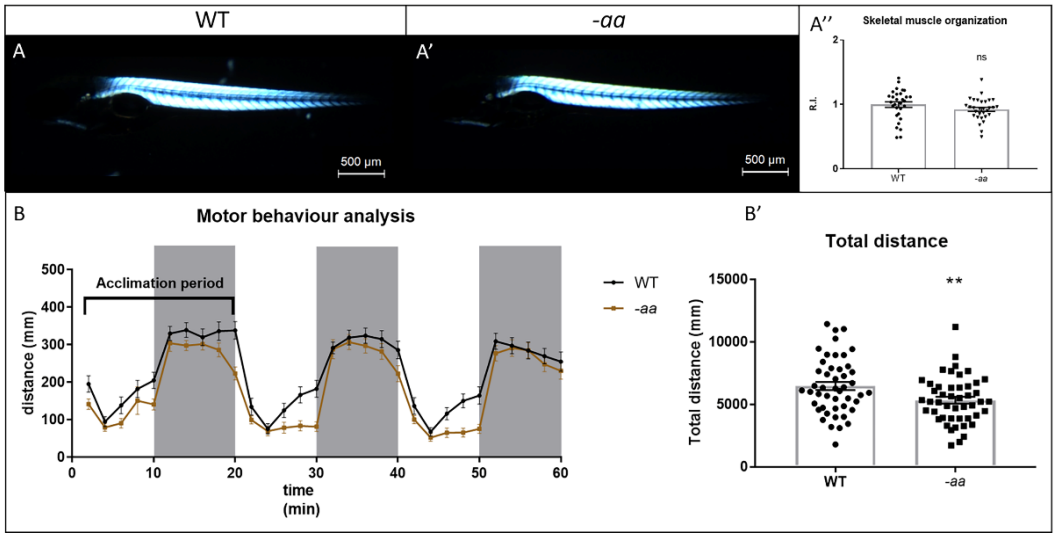

Figure 36: Impaired motor behaviour and exercise-induced mortality in zebrafish *lgals3a* mutant larvae.

A-A'-A'': Birefringence analysis on WT and mutant larvae at 5 dpf fails to detect any significant difference in the skeletal muscle structure. Embryos are displayed at 5 dpf, in lateral view, anterior to the left. Sample size: n=30. R.I.: Relative Intensity. ns =not

significant. Test: Unpaired t-test. B-B': WT and -aa larvae at 5 dpf display normal response to light (white areas) and dark (grey areas) stimuli, but with reduced motor performances if mutated, evaluated as total distance swum (B). Sample size: n=47. **=p<0.01. Test: Unpaired t-test.

4.2.11. Signalling pathways analysis on 3-dpf –aa mutated larvae

In this *lgasl3a* zebrafish model, as done in Desmoplakin mutants, we checked the possible dysregulation of Wnt/β-catenin and Hippo/YAP-TAZ signalling pathways, recently associated with AC and cardiac diseases, as previously mentioned, and known to be dysregulated by *lgasl3* and desmosomes instability, respectively. We examined the mRNA levels of two target genes involved in the Wnt/β-catenin signalling pathway (*ccnd1* and *myca*), demonstrating a global down-regulation of it. We also performed qPCR to check if the expression level of target genes related to the Hippo/YAP-TAZ pathway, *ccn2a,* and *ccn2b,* were dysregulated, confirming a downregulation of YAP-TAZ expression. These results resemble the human AC patients' conditions, in which the Hippo cascade is activated and YAP is phosphorylated and not able anymore to enter the nucleus and activate the transcription of its target genes (Chen et al., 2014) (**Figure 37**).

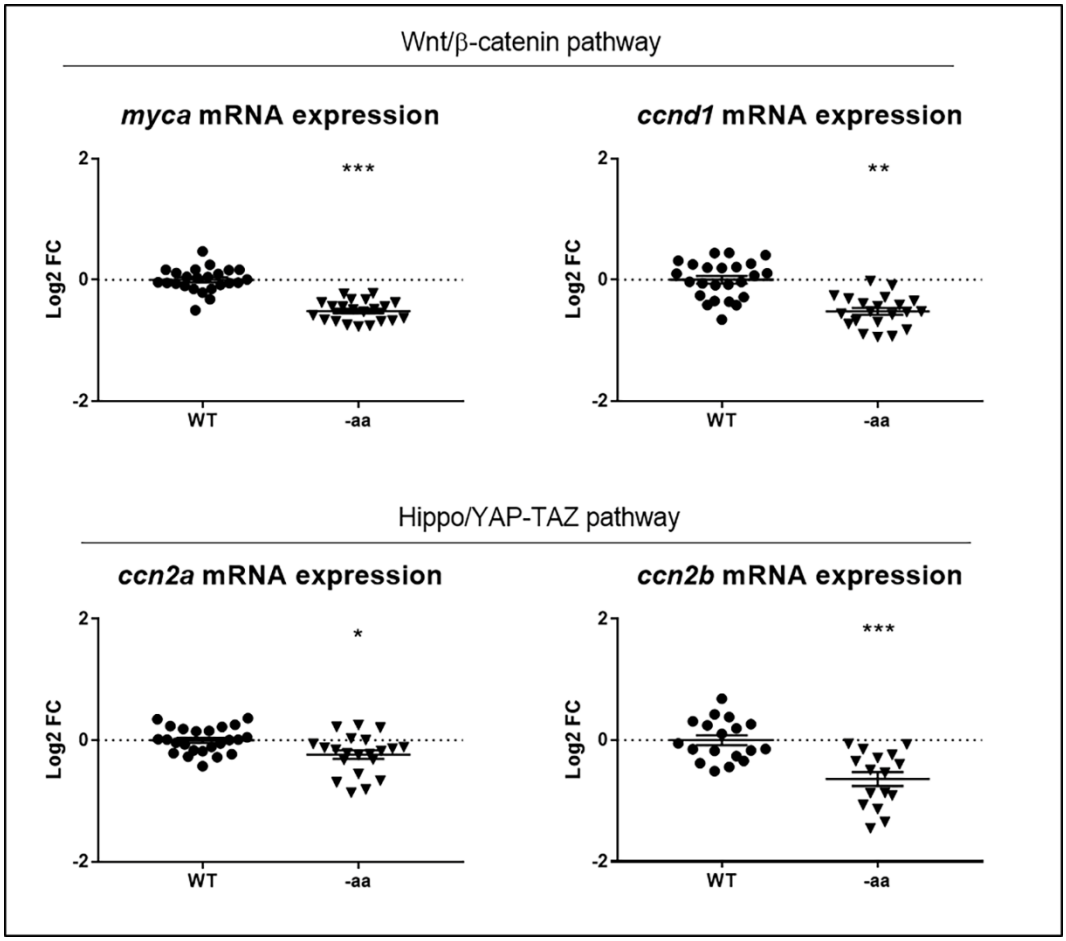

Figure 37: Signalling pathways dysregulation in *lgals3a* mutant larvae.
qPCR analysis detected Wnt/β-catenin and YAP-TAZ signaling dysregulation in *lgals3a* mutants, significant for both pathways, but with different effects. Each point on the graph corresponds to a pool of 30 embryos of the same genotype. Sample size: n=15. Log2 FC: Log2 Fold Change. *=p<0.05; **=p<0.01; ***=p<0.001. Test: Unpaired t-test.

In our *dsp*-KO zebrafish line, the downregulation of Wnt/β-catenin signalling has been shown to be crucial in the pathophysiology of AC. Its pharmacological rescue caused a mitigation of the pathological phenotype, putting this signalling pathway in a central position as a candidate therapeutic target to treat AC patients. As we demonstrated by qPCR analysis, this pathway is dysregulated also in our *lgals3a* zebrafish model at the larval stage, so we decided to confirm this result using a Wnt/β-catenin reporter line *Tg(7xTCF-Xla.Siam:EGFP)ia4* (Moro et al., 2013). Outcrossing our *lgals3a* mutant line with this transgenic background, we obtained an *lgals3a* mutant line harbouring a Wnt/β-catenin reporter transgene. Mutant fluorescent larvae showed a statistically significant reduction of pathway

expression, both in the head region, where the pathway is normally expressed at this developmental stage, and specifically in the cardiac region, at low levels in the epicardium and at high levels in the valves, being involved in their formations (**Figure 38**).

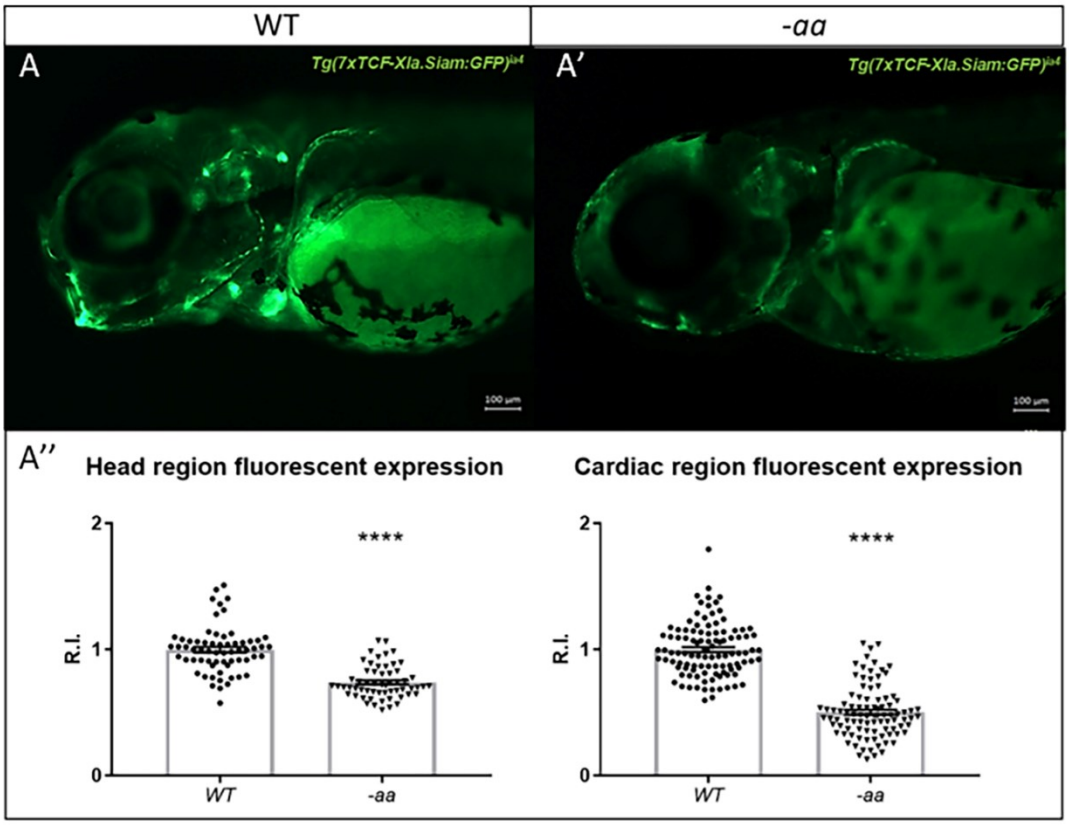

Figure 38: Detection of Wnt/β-catenin dysregulation using a Wnt/ β-catenin-specific transgenic line.

A-A'-A'': Wnt/ β-catenin signalling pathway dysregulation was observed using a Wnt/ β-catenin-specific transgenic line *Tg(7xTCF-Xla.Siam:EGFP)ia4*, underlining a downregulation of this pathway in both head and cardiac region. Embryos are displayed at 3 dpf, in lateral view. Sample size for head region: n=64±6; Sample size for cardiac region: n=104±10. R.I: Relative Ratio. ****=p<0.0001. Test: Unpaired t-test.

4.2.12. Increased cell death events in the cardiac region of –aa mutated larvae

We decided to check the possible presence of cell death events induced by the *lgals3a* depletion in the cardiac region. Acridine Orange (AO) staining can mark DNA or RNA inside the cells due to its ability to pass through membranes strongly labelling global cell death events. We detected a strong increase in the number of dead cells through their fluorescence signal in the cardiac region (**Figure 39 A''**) of mutated zebrafish at larval stage (**Figure 39 A'**), compared to WT ones (**Figure 39 A**), suggesting a fundamental role of Galectin-3 protein in the regulation and control of this phenomenon.

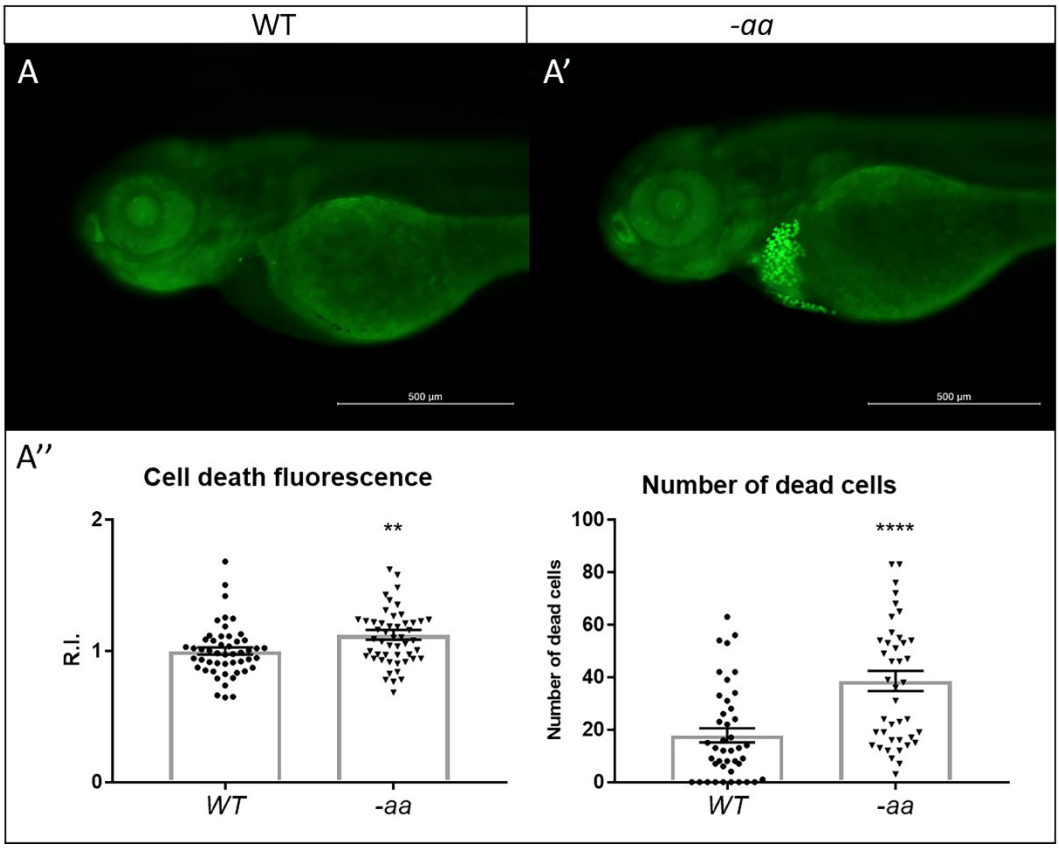

Figure 39: Cell death events in the cardiac region of *lgals3a* mutant larvae.
A-A'-A'': *–aa* mutant larvae presented a statistically significant increase in the number of dead cells and in their fluorescence in the cardiac region. Embryos are displayed at 3 dpf, in lateral view. The sample size for fluorescent expression: n= 50±1; the number of dead cells: n=42. R.R: Relative Ratio. **=p<0.01; ****=p<0.0001. Test: Unpaired t-test.

4.2.13. TGF-β SMAD2/3 signalling dysregulation and inflammatory response on -aa mutated larvae

In our *lgals3a* mutant larvae, the TGF-β signalling pathway was observed to be significantly downregulated by qPCR analysis of *smad2* and *smad3* pathway member expressions (**Figure 40 A**), confirming the hypothesis that lower levels of Galectin-3 protein can induce dysregulation of this pathway (Blanda et al., 2020; Xiao et al., 2020). In addition, we observed in our model the inflammatory factors *tnfα* and *il6* gene expressions were downregulated in a qPCR analysis at the larval stage, underling that these two genes, directly correlated with inflammation phenomena, could have some connection and be related to Galectin-3 protein expression changes in zebrafish as in humans (Alturfan et al., 2014) (**Figure 40 B**). In fact, both TNF-α and IL-6 levels are controlled directly by Galectin-3 (Alturfan et al., 2014) and are mainly produced and secreted by macrophages, which expression and activation was demonstrated to be also related to Galectin-3 presence in the tissue (Silverman et al., 2012; Lu et al., 2020), possibly explaining their dysregulation in our model.

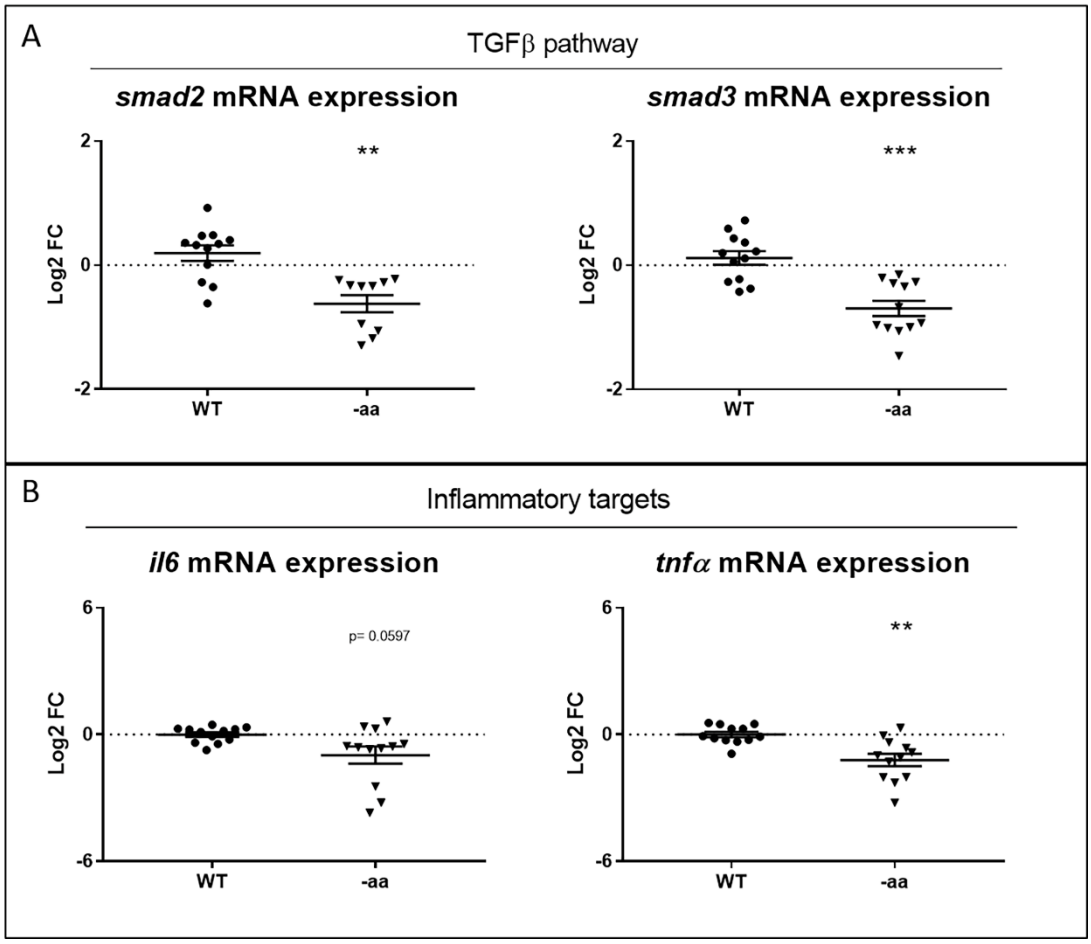

Figure 40: TGF-β signalling, *tnfα* and *il6* gene expressions dysregulation in mutant zebrafish larvae.

A: qPCR analysis detected significant dysregulation of TGF-β signalling in *lgals3a* mutants. Each point on the graph corresponds to a pool of 30 embryos of the same genotype. Sample size: n=12±2. Log2 FC: Log2 Fold Change. *=p<0.05; **=p<0.01; ***=p<0.001. Test: Unpaired t-test. B: qPCR analysis detected significant dysregulation of *tnfα* and *il6* gene expressions in *lgals3a* mutants. Each point on the graph corresponds to a pool of 30 embryos of the same genotype. Sample size: n=12±2. Log2 FC: Log2 Fold Change. **=p<0.01. Test: Unpaired t-test

Interestingly, both inflammatory targets, although still downregulated by the absence of Lgals3a protein expression in our model, did not show the same dysregulation in 1-year-old adult mutant hearts as in larvae, showing no differences if compared to WT controls (**Figure 41**).

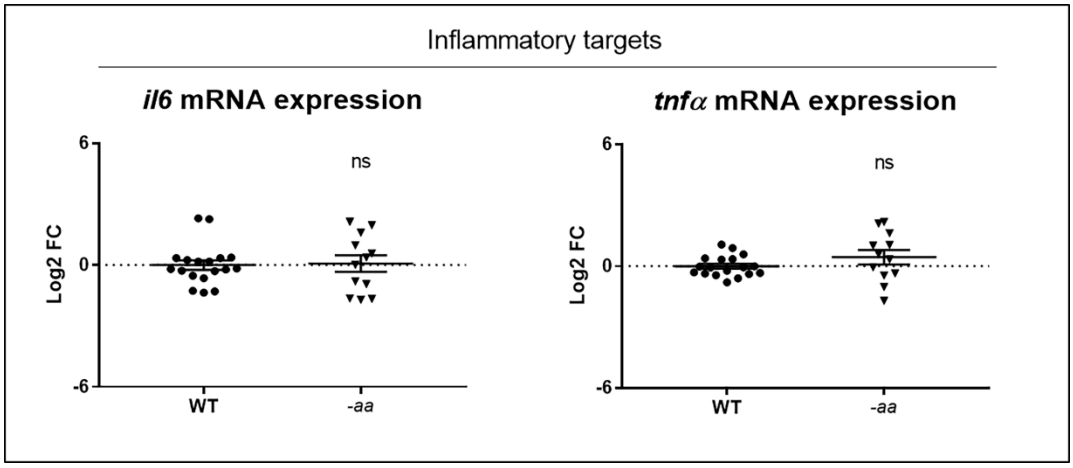

Figure 41: tnfα and il6 gene expressions analysis in mutant zebrafish hearts.
qPCR analysis did not detect any significant dysregulation of *tnfα* and *il6* gene expressions in the hearts of *lgals3a* mutant adults. Each point on the graph corresponds to a pool of hearts of adult zebrafish of the same genotype. Sample size: n=12. Log2 FC: Log2 Fold Change. Ns= not significant. Test: Unpaired t-test.

Although these results made us think that an inflammatory response in the absence of half of the Lgasl3 protein could be hardly detectable at the whole-body level, considering also its previously demonstrated pro-inflammatory role (Cason et al., 2021), we thought that an inflammatory response might still occur in the cardiac region of *lgals3a* mutant animals, since the absence of galectin can cause desmosome instability and thus cell damages. Therefore, we decided to check the possible presence of inflammatory processes in the cardiac area, using an anti-L-plastin antibody as a marker for the detection of inflammatory cells. This immunostaining revealed a two-fold increase of L-plastin-positive cells in the cardiac region of *lgals3a* mutants compared to controls (**Figure 42 A-B-C**).

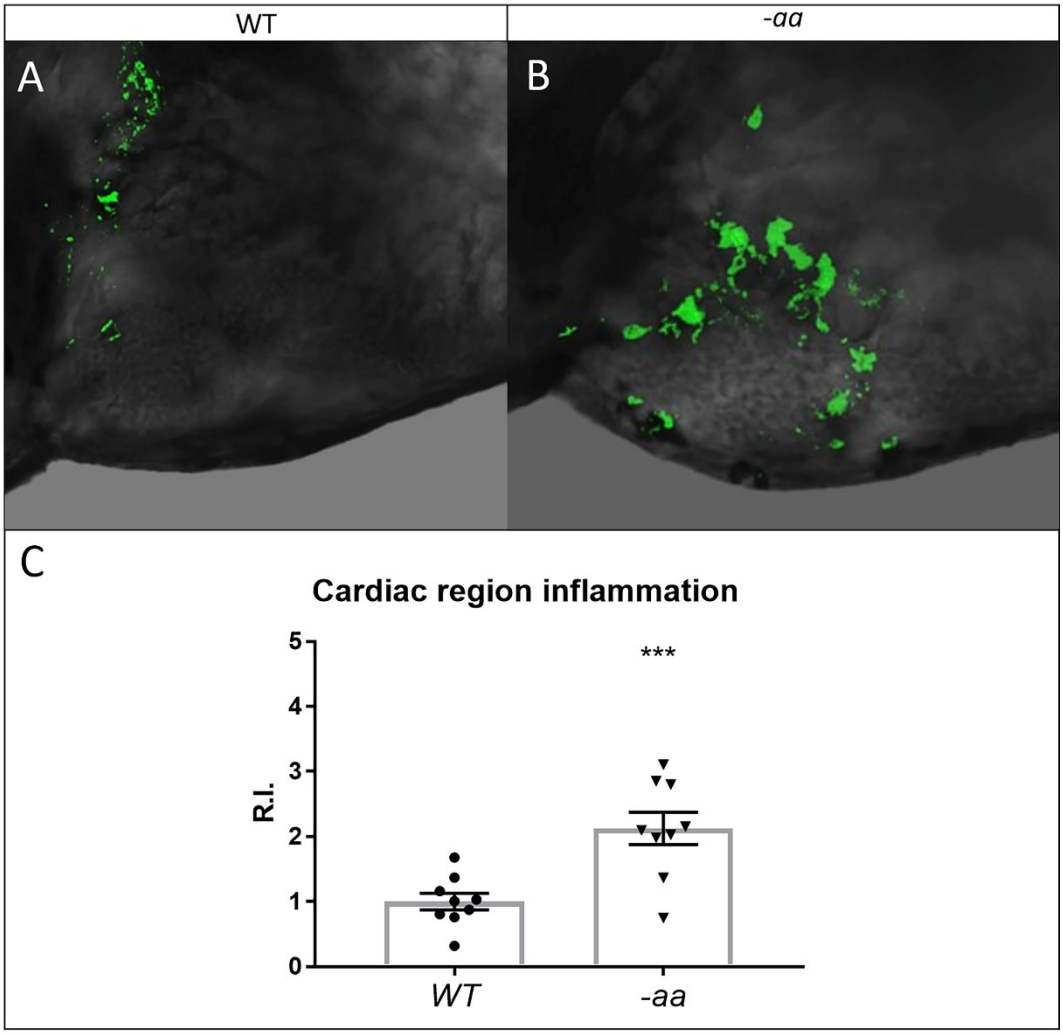

Figure 42: Inflammatory response in larval hearts of *lgals3a* mutants.

A-B-C: Cells expressing the inflammatory marker L-plastin are more abundant in -aa mutant hearts (B), compared to WT (A) in a statistically significant way (C). Cardiac regions of 3 dpf embryos are displayed in lateral view, anterior to the left. Sample size: n=9. R.I.: Relative Intensity. ***=p<0.001. Test: Unpaired t-test.

5. DISCUSSION

5.1. Stable *dsp*-KO zebrafish lines

The Desmoplakin gene, known to be one of the causative genes and directly involved in the pathogenesis of AC in humans (Pilichou et al., 2016), in zebrafish presents two orthologues, *dspa* and *dspb*. The generation of stable KO zebrafish lines for these duplicated *dsp* genes and the subsequent characterization at larval and adult stages confirmed zebrafish as a suitable model to investigate the pathogenesis and progression of AC. Initially, we decided to focus our attention on three main genotypes, -aa, -bb, and -ab lines, representing a condition that resembles human heterozygosity, although the –ab line turned out to be the best one, with the balanced silencing of a single allele for each copy of the gene. This choice was also related to the very low fitness and ability to reach adulthood of the double homozygous line –aabb, making the production of larvae for further studies very difficult, although it seemed a very attractive model to recapitulate severe AC phenotypes. We confirmed the actual presence of the mutations in the target genes by sequencing analysis, while by qPCR analysis, instead, we observed, in mutants, alterations in the expression of both *dsp* mRNAs, probably due to Nonsense-Mediated mRNA Decay (NMD). The absence of Dspa and Dspb proteins in –aa and -bb lines, as well as the balanced reduction of both (55%) in the -ab model, was detected by Western Blot analysis. Therefore, the deficiency of both Dsp mRNA and protein levels confirms that these genetic lesions alter the mRNA sequence triggering NMD, leading also to the predicted formation of a premature stop codon and of a truncated protein in both lines. These preliminary results made us hypothesize that the desmosome structure could have been damaged in our model as in humans (Basso et al., 2006), prompting us to continue our investigations. Structural changes in the heart, including pericardial effusion and/or hemopericardium, alterations in heart morphology, and circulation problems, were documented in around 30% of mutated fish, with a cardiac phenotype penetrance resembling the human one. These cardiac defects were also associated with growth retardation. A clear bradycardic phenotype was found in mutant larvae at all developmental stages analyzed (2, 3, 5, and 7 dpf), with a significant increase in

mortality in the first month of life if compared to healthy controls. This morphological analysis validated our *dsp* zebrafish lines as good models to reproduce alterations in the cardiac structure due to cell-cell junction instability, as in AC (Basso et al., 2006). We continued the characterization of our Dsp mutants zebrafish searching for alterations in the expression of Wnt/β-catenin, Hippo/YAP-TAZ, and TGF-β signalling pathways, known to be involved in heart development, morphogenesis, and remodelling (Brade et al., 2006; Biernacka et al., 2011; Chen et al., 2020), and investigating whether these were dysregulated like in other AC conditions (Garcia-Gras et al., 2006; Chen et al., 2014; Maione et al., 2021). In particular, the expression of two Wnt/β-catenin signaling target genes, *ccnd1,* and *myca*, indicated a down-regulation trend of this pathway, as previously shown also in other AC models (Garcia-Gras et al., 2006; Giuliodori et al., 2018); this downregulation was also confirmed *in vivo* by a GFP-based Wnt biosensor (Moro et al., 2013) expressed in our –ab mutant line. Interestingly, YAP-TAZ signaling showed instead a global upregulation, according to the analyzed pathway members *ccn2a* and *ccn2b*, meaning that the Hippo cascade was switched off. In humans Hippo cascade is normally activated under AC-like conditions (Chen et al., 2014), downregulating the transcription activity of YAP and TAZ. In addition, also the third candidate pathway, TGF-β, usually upregulated in AC (Maione et al., 2021; Frangogiannis, 2022), did not show the same dysregulation as in humans, being slightly downregulated. These unexpected results can be explained by the fact that this was a whole-body analysis and not heart-specific, due to the very early stage of development that did not allow the surgical isolation of the heart tissues, so some results could be attenuated or even changed. At this stage of development, we can therefore state that all these three pathways already began to be dysregulated as a result of desmosome instability (Chen et al., 2014; Lorenzon et al., 2017; Austin et al., 2019; Sattar et al., 2019; Yousefi et al., 2020), although the one consistently down-regulated across many AC models, including ours, was Wnt/β-catenin signalling, proving to be an extremely robust marker for AC. In the overall analysis of the results obtained during this first phase of the characterization, it was possible to note that -ab larvae present, as said before, the most promising combination of alleles in reproducing the human heterozygous condition but also more severe morphological characteristics found in AC patients, among the lines analyzed, thus

focusing our attention from this moment onwards only on them. A more detailed observation of possible structural alterations of the heart chambers in –ab zebrafish larvae was easily performed by taking advantage of a myocardial-specific transgene *Tg(tg:EGFP-myl7:EGFP)ia300* (Porazzi et al., 2012). Fluorescent mutant larvae showed statistically significant enlargement of both heart chambers, underling a prominent cardiac dilation phenotype, already observed in human patients (Corrado et al., 2017). This feature underlined the vulnerability of the myocardium already at this early stage of development in mutant larvae, likely being unable to support the contraction and the mechanical stress usually tolerated by a normal heart. In addition, the presence of undergoing inflammatory processes in mutant larvae was suggested by the detection of an increased number of L-Plastin-positive cells in the cardiac region, if compared to controls. This marker, expressed in peripheral blood T lymphocytes, neutrophils, monocytes, B-lymphocytes, and myeloid cells, is an actin-binding protein that plays a role in the activation of T-cells in response to co-stimulation through TCR/CD3 and CD2 or CD28, modulating also the cell surface expression of IL2RA/CD25 and CD69. Certainly, this inflammatory phenotype should be further investigated, to assess the validity of Dsp zebrafish models in recapitulating inflammatory aspects of human AC (Basso et al., 1996), and evaluate these mechanisms as potential therapeutic targets. Furthermore, we analyzed the possible effect of physical training on disease onset and progression on –ab mutants. First, we assessed that –ab mutated larvae, with respect to WT controls, showed a statistically significant reduction in normal motor activity and response to external stimuli, especially in the relaxing phase when they restarted to swim. A birefringence analysis of the skeletal muscle excluded a potential involvement of skeletal muscle in this phenotype, due to fiber disorganization, pointing toward heart problems as the root cause of these problems. Therefore, mutant larvae were subjected to an intensive training protocol together with WT controls, making them grow in a dense medium that requires greater effort to reach food or just move. The mortality of the trained mutant larvae was higher than both resting mutants and trained and untrained wild-type controls, suggesting that cardiac problems can affect, as demonstrated before, the movement of the mutant larvae but, if intensely trained, provoked an acceleration of the progression of the disease and SCD. After these promising results in the larval characterization, the analysis continued at the

adult stages. We validated the dysregulation of Wnt/β-catenin, Hippo/YAP-TAZ, and TGF-β signaling pathways, already observed at the larval stage, in hearts of adult fish, identifying, also in this case, specific alterations but with some differences resembling better the human condition. While Wnt/β-catenin maintained the same dysregulation, although with a sharper reduction of expression if compared to larval analysis, as expected, the other two signalling pathways showed a different modulation, compared to the larval stage. Specifically, Hippo/YAP-TAZ expression presented, as predicted, a downregulation (Chen et al., 2014), as testified by the two deregulated target genes *ccn2a* and *ccn2b*. This result confirmed our hypothesis that in the larval experiments the outcome could have been affected by the whole-body analysis, while at the adult stage the study was specifically centred on surgically isolated heart tissues. Lastly, the TGF-β signaling pathway surprisingly remained downregulated as in larvae. The well-known ability of zebrafish to regenerate cardiac tissue could explain this peculiar modulation of TGF-β, there being no need for scar formation and/or fibrotic substitution (Poss et al., 2002). As the next step, we focused our attention on a deeper morphological analysis of the heart's possible abnormalities, observing that in 1-year-old mutant – ab zebrafish a statistically significant dilation was evident, compared to wild-type controls, telling us that, as in humans, this could be a progressive disease, getting worse over the years (Nava et al., 2000; Corrado et al., 2017). Therefore, we proceeded with Transmission Electron Microscopy (TEM) analysis of the cardiac tissue, finding that in both 3-month-old and 6-month-old mutant hearts the desmosomes appeared “pale”, disorganized, and delocalized, with a significantly increased distance in the extracellular space at 6 months. Heart sections of 3-, 6- and 9-month-old mutant fish were then analyzed using the Haematoxylin and Eosin staining. At 3 months of age, no differences were seen between WT and mutated heart, so we deduced that it was probably too early to observe structural changes, although through TEM analysis we knew that desmosomes were already severely damaged. Instead, histological analysis of 6-month-old mutated zebrafish heart revealed mild rarefaction of cardiomyocytes, thinning of the myocardial layer, age-related alterations in the distribution and organization of the trabeculae network, an abnormal shape of the ventricle, with the presence of initial vessels dilation and adipose infiltration. In the 9-month-old mutated fish heart, the phenotypic condition

observed in the 6-month-old heart was getting worse, including more dilated vessels inside the myocardial layer, and an evident adipose infiltration starting from the epicardium towards the endocardium. These results confirmed that in zebrafish AC is a progressive disease as in humans, with similar morphological alterations at the cardiac level, possibly related also to the same changes in the signaling pathways analyzed (Garcia-Gras et al., 2006; Chen et al., 2014; Pilichou et al., 2016; Maione et al., 2021; Frangogiannis, 2022). The training protocol applied to larvae was also carried out in adult fish, using a homemade swim tunnel connected to an electric pump. Interestingly, we observed phenotypic similarities between 6-month-old trained fish and 9-month-old resting ones, corroborating the idea that an intensive training protocol can exacerbate/anticipate cardiac alterations, like in humans (James et al., 2013). On the other hand, three additional months of training did not induce a worsening of the condition, suggesting the reaching of maximum damage and/or the activation of regenerative processes (Poss et al., 2002), counteracting a further aggravation of the zebrafish heart state. Electrophysiology studies in zebrafish can pave the way for understanding better this cardiac phenotype, deciphering new aspects of the disease, and discovering new modulators of it. Moreover, after validating the role of intensive physical exercise in AC in our zebrafish model, we aim also to better clarify the involvement of sex hormones in the progression of the disease, having already observed in humans a correlation between gender and penetrance of AC, although we did not observe until now differences due to gender in our model (James et al., 2013; Rigato et al., 2013; Choudhary et al., 2016). Then, next to the completion of the characterization of this model at both larval and adult stages, the question we asked ourselves was if a pharmacological treatment could rescue, totally or partially, the observed AC phenotype. One of the more constant links between human and zebrafish AC phenotypes, which we thought could be an interesting pharmacological target also in our model, was the peculiar Wnt/β-catenin signaling pathway dysregulation. The SB216763 molecule, an agonist of this pathway, was identified by Asimaki and colleagues in 2014 as a potential therapeutic drug in a *jup*-KI AC zebrafish model (Asimaki et al., 2014) and confirmed also by our group in a transient *dsp*-KD zebrafish model of AC (Giuliodori et al., 2018). Therefore, we decided to evaluate the pharmacological effect of this drug also in our stable *dsp* mutant line,

implemented with a Wnt-responsive reporter (*Tg(7xTCF-Xla.Siam: EGFP)ia4*) (Moro et al., 2013) that confirmed a total rescue of the pathway expression after the treatment. In addition, this drug rescued in mutant larvae the cardiac abnormalities and developmental parameters previously described, including body length and eye size. Interestingly, the bradycardic phenotype was also ameliorated in 5 dpf mutant larvae. The analysis of the survival rate after SB216763 pharmacological treatment indicated an improvement in the mutant line fitness. Of note, the mortality rate, observed after methylcellulose-induced training, was also rescued after drug exposure. Overall, these results in a stable KO model, corroborated by the previous evidence from Asimaki's and Giuliodori's studies, points at Wnt/β-catenin signaling modulation as a possible future therapeutic target to treat AC patients (Asimaki et al., 2014; Giuliodori et al., 2018). Thus, in conclusion, the generation and validation of the first stable *dsp*-KO zebrafish line, demostrating at both larval and adult stages a wide spectrum of AC-like phenotypes, represent the strengths of this project. Moreover, a multi-pathway analysis identified a very similar modulation during the progression of the disease. Specifically, the Wnt/β-catenin signalling, dysregulated in this novel AC model, has been identified as a possible general pharmacological target to try to rescue AC phenotypes independently of the causative gene, opening the way to test SB216763 or even other Wnt-specific drugs in human. The idea is to further investigate and identify additional targets and drugs to modulate other dysregulated signalling pathways in AC, such as Hippo/YAP-TAZ, to increase the number of therapeutic approaches that in the future could be applied in human patients. This multi-drug screening, performed in adult mutant fish after the first identification at the larval stage, could be additionally relevant to see how selected drugs can act at different stages of the disease.

5.2. Stable *lgals3a*-KO zebrafish line

It is known that not only desmosomal proteins are involved in the onset and progression of AC (Pilichou et al., 2016). Indeed, non-desmosomal genes have been identified as mutated in 1-3% of AC patients, with *LGALS3* that has been recently linked to the disease (Cason et al., 2021). Specifically, rare genetic variants of this

gene were found in 4% of patients in a cohort of 150 AC cases. Moreover, the myocardial tissue of patients with AC at concealed and acute stages of the disease showed alterations in *LGALS3* expression; in parallel, Dsg2-mutated transgenic mice, with phenotypic signs of AC, presented dysregulation of this gene expression (Cason et al., 2021). These premises have prompted us to investigate more deeply the role of this gene in the pathogenesis of the disease, trying to understand whether it can be considered an AC causative gene or only a modulatory one. As already discussed for *dsp*, also *lgals3* is duplicated in zebrafish, presenting two orthologues, *lgals3a* and *lgals3b*; considering the expression of these genes at the cardiac level and their potential involvement in cardiac diseases, we initially considered both of them in the generation of our model (Hoorntje et al., 2017). Therefore, we generated two KO zebrafish lines for both *lgals3* genes and we checked the presence of the deletions in the targeted regions by sequencing and electrophoretic gel analysis. However, trying to stabilize these lines, we immediately found a serious fertility problem in the *lgals3b* line, with the homozygous female fish that produced a very low number of fertilized eggs among the few non-degenerate one, while the zebrafish *lgals3b* males had instead a normal spermatogenesis. We explained these findings by the already demonstrated expression of *LGALS3* gene in ovary cells in human samples (Shimada et al., 2020). In addition, Gal-3 expression was found downregulated in the endometrium of women with endometriosis-associated infertility, suggesting a possible connection between this dysregulation and infertility problems (Yang et al., 2016). Even in mouse models, Gal-3 was demonstrated to be expressed in the endometrium and involved in embryo implantation, showing that, if KD, it was leading to a decrease in the percentage of implanted embryos (Yang et al., 2012). *lgals3b* in zebrafish was demonstrated to be highly expressed in oocyte and ovary in a tissue-specific analysis, differently from *lgals3a*, suggesting that the role in the fertility and reproduction could be conserved in the *b* orthologues in zebrafish (Ahmed et al., 2004; Heiden et al., 2008). Therefore, considering all these issues in the *lgals3b* line and the strong similarity between Lgals3a and Lgals3b zebrafish proteins with the human one, although being both expressed in the heart tissue, we decided to focus our analysis only on the *a* member. Moreover, a work by Chen and colleagues (Chen et al., 2021) underlined a strong relationship between Lgals3a and its counterpart in humans,

observing in a *lgals3a*-KD zebrafish model a clear developmental and cardiac involvement of this specific orthologue (Chen et al., 2021). From a genetic point of view, our *lgals3a*-KO mutant line displayed only a halved reduction of the total Lgals3 protein expression, due to the ablation of the expression of the *lgals3a* member, with the WT form of the *b* one. The choice of this heterozygous genetic combination was partially constrained by the previously mentioned effects on reproduction and fertility of *lgals3b* mutations, but also to mimic the heterozygous condition presents in human AC patients, although, as in the other *dsp*-KO AC zebrafish model, the double heterozygous model would be probably the best condition. Therefore, we started the characterization of the *lgals3a*-KO mutant line. As in *dsp*-KO lines, an mRNA/protein expression analysis validated the effect of the inserted mutation in our model. Specifically, in the presence of the 4-nt deletion in the *lgals3a* gene, we noted a strong decrease in the related mRNA expression, confirming that the Nonsense-Mediated mRNA Decay (NMD) mechanism is present also in this model. These findings demonstrate that *lgals3a* gene mutation in our stable zebrafish line affects the levels of the mutated mRNA, which would lead to the generation of shortened proteins that are likely to be destroyed or rendered ineffective. Due to the absence of functional antibodies against Lgals3 proteins that work in zebrafish, we decided to investigate possible indirect alterations in the expression of the Dsp desmosomal protein. Interestingly, we noticed a statistically significant reduction of the Dsp protein expression (29%), not severe as the one observed in the *–ab dsp*-KO zebrafish line (65% reduction), but still worthy of consideration. Focusing on the Western Blot results, we deduced in an indirect way that mutations in *lgals3a* gene cause the formation of a not functional protein, as predicted, and that its absence destabilizes the desmosome structure, confirming the findings described by Cason and colleagues (Cason et al., 2021). These data will be verified by an ongoing TEM analysis on adult *lgals3a* mutated zebrafish hearts, to see directly possible "pale", delocalized, and disorganized desmosome structures also in this model. We continued the characterization trying to observe a possible cardiac involvement of this gene, as already discussed in literature (Oz et al., 2017; Blanda et al., 2020). We found out a clear cardiac phenotype characterized by heart morphological abnormalities, such as structurally dilated heart associated with hemopericardium and/or pericardial

effusion. In addition, a significant growth retardation was observed, coupled with clear bradycardic phenotype at all stages of development analysed. The mortality analysis revealed a milder increased in mortality compared to the *dsp* mutant zebrafish line, but still showing some interesting signs of the disease. By exploiting a transgenic mutated zebrafish line *Tg(tg:EGFP-myl7:EGFP)ia300* (Porazzi et al., 2012), specifically designed to fluorescently label the myocardium, facilitating its observation, we detected an overt dilation of the heart chambers at larval stage. We confirmed this pathological phenotype also in mutant 1-year old adult hearts manually extracted, detecting a statistically significant dilation of the ventricle, that presented a double size compared to WT controls, confirming that the disease was present ad larval stage, becoming more severe during the life of the fish, as in humans (Nava et al., 2000; Basso et al., 2011; Corrado et al., 2017). We can conclude this first part of the characterization underling that *lgals3* depletion, even if only in a heterozygous condition, is causative of a cardiomyocyte instability, due to its involvement in intercellular interaction and desmosome stabilization in our model, as demonstrated by Western Blot analysis and cardiac morphological characterization previously presented (Jiang et al., 2014). This phenotyping of the cardiac abnormalities was completed with a motor behaviour analysis that showed a statistically significant reduction of the total distance swum and in the response to external light and dark stimuli by mutant larvae. Most of the differences were observed specifically in the second part of the light phases of the experiment, underlining difficulties in restarting to swim after stressing conditions, when compared with controls. This result told us that, after a birefringence analysis of the skeletal muscle that excluded potential fibres disorganization, the differences in the motor responses are likely due to heart problems and bradycardia, the latter being one of the first signs of these cardiac difficulties in zebrafish. In addition to these promising results, we investigated also Wnt/β-catenin and Hippo/YAP-TAZ signalling pathways expression, known to be involved in the cardiac remodelling, development, and morphogenesis in healthy conditions, and related to AC pathogenesis if dysregulated (Garcia-Gras et al., 2006; Dobaczewski et al., 2011; Chen et al., 2014, 2020; Sattar et al., 2019). At the larval stage, the mRNAs levels of the two target genes *ccnd1* and *myca*, which expression is controlled by the Wnt/β-catenin pathway, showed a statistically significant down-regulation as

expected (Garcia-Gras et al., 2006; Lombardi et al., 2011; Chelko et al., 2016). Gal-3 mutations in fact can affect the Wnt/β-catenin signalling pathway in several ways: as already discussed for the *dsp* model, by the destabilization of cell-cell interactions and desmosomal structures, but also by its interaction with GSK3-β, an enzyme involved in the degradation of β-catenin, as already described in the introduction (Peifer et al., 1994; Yost et al., 1996; Song et al., 2009; Cason et al., 2021). We confirmed this result using again a Wnt/β-catenin reporter line *Tg(7xTCF-Xla.Siam:EGFP)ia4* (Moro et al., 2013). Fluorescent mutant larvae showed statistically significant downregulation of the pathway expression in both head and cardiac region, validating the qPCR analysis of the target genes discussed before. The dysregulation of the Hippo/YAP-TAZ signalling pathway was verified by expression levels of target genes *ccn2a* and *ccn2b*, observed to be downregulated. This result told us that the cell membrane instability caused by Gal-3 mutation provoked the Hippo cascade activation, the phosphorylation of the YAP effector factor, and the subsequent reduction of its transcriptional activity as expected, because it was not able anymore to enter the nucleus to activate the transcription of its target genes (Chen et al., 2014). This last result was different from the one obtained in the *dsp* zebrafish lines at the larval stage, probably because Gal-3 could be differently expressed and dysregulated in other tissues, being a pleiotropic protein. After this multi-signalling pathways study, we moved to the analysis of the already demonstrated anti-apoptotic/necroptotic activity of Gal-3 in the cardiac tissue (Cecchinelli et al., 2006; Al-Salam et al., 2021), as well as its possible involvement in the inflammatory response. We observed in our model a statistically significant increase in the number of cells that are dying in the cardiac region, if compared to WT, confirming the link between these processes and Gal-3 presence/absence. This result was already observed both in human patients (Narula et al., 1996; Gill et al., 2002) and *lgals3a*-KD zebrafish model (Chen et al., 2021), confirming our findings and underling that inhibition of *lgals3a* expression can significantly promote cell death events in cardiomyocytes, with the normal expression of this gene during zebrafish embryo development possibly playing an anti-cardiomyocyte cell death activity, slowing down the progression of the disease. Further studies and experiments need to be done to understand better if we are looking at apoptosis, necrosis, or necroptosis and if they lead to a controlled or

uncontrolled death, fundamental information to comprehend its involvement in the disease. Until now, we know that cardiac cell death is ongoing in the presence of a non-functional Lgals3a protein, aggravating the cardiomyocyte condition and causing an accelerated progression of cardiac degeneration. Moreover, in our mutant larvae, the TGF-β signalling pathway was observed to be significantly downregulated, confirming the pro-fibrotic activity of this protein and that lower levels of it induce downregulation of this pathway (Blanda et al., 2020; Xiao et al., 2020; Cason et al., 2021). As we already described before, in the cardiac tissue there are several reasons underlying a possible dysregulation of the TGF-β signalling pathway (Biernacka et al., 2011; Dobaczewski et al., 2011), knowing that it is strictly connected with fibrogenesis and scar formation (Biernacka et al., 2011). Therefore, we can hypothesize that fibrotic substitution is not occurring in our model, and in general in the case of the lower level of Gal-3 protein could be difficult to detect. Besides, zebrafish are well known to have a strong regeneration ability at the cardiac level, making it even more difficult to detect this kind of changes in the tissue, regardless of the pathological condition (Poss et al., 2002). Further analysis of histological sections of adult mutant hearts is necessary to corroborate such a hypothesis. Concerning the analysis of the inflammation process, the literature tells that LGALS3 is a pro-inflammatory factor and, if inhibited pharmacologically or genetically, inflammation and fibrosis decrease (Yu et al., 2013; Slack et al., 2021). However, we observed a strong inflammatory response in our model, even with a halved Lgals3 expression. Indeed, it is known that Gal-3 is able to modulate the expression of inflammatory cells and markers expressions, such as macrophages, TNF-α and Il-6 (Lee et al., 2005; Silverman et al., 2012; Alturfan et al., 2014; Askevold et al., 2014; Schmidt-Arras and Rose-John, 2016; Chen et al., 2020; Cason et al., 2021), but it is also involved in the stabilization of cell-cell interactions (Jiang et al., 2014). This double ability to influence and stimulate the inflammatory response needs to be further studied, to understand better its role in this process. More in detail, *tnfα* gene expression was significantly downregulated in mutant larval whole body's qPCR analysis. This inflammatory factor is mainly produced and secreted by macrophages that are activated and stimulated by the Gal-3 protein (Lu et al., 2020; Cason et al., 2021), possibly explaining its downregulation in our model together with its direct

regulation by Gal-3 protein itself (Alturfan et al., 2014). Another inflammatory marker, *il6*, was observed downregulated in our model. This factor is one of the most well-characterized and central cytokines involved in cardiovascular diseases (Askevold et al., 2014), mediating myocardial remodelling, cardiomyocyte apoptosis, and reduction of myocardial contractility by inducing the recruitment of inflammatory cells in injured myocardium (Lee et al., 2005). IL-6 comes from a wide range of sources among which macrophages (Schmidt-Arras and Rose-John, 2016), regulated indirectly by Gal-3 as described before, and was also connected with upregulated expression of Lgals3 protein in the microenvironment of human neuroblastoma, possibly explaining its downregulation in our model (Silverman et al., 2012; Alturfan et al., 2014). The idea is to use a macrophage-fluorescent zebrafish line *Tg(mpeg1:EGFP)* (gl22Tg) and a pan-leukocyte-fluorescent zebrafish line *Tg(lysC:DsRed2)* (nz50Tg) to follow the macrophage-specific movement and activation, as well as the global immune response, in the absence of Lgals3a protein expression. We plan to use a drug called TD139, which is a selective inhibitor of Galectin-3 activity, to pharmacologically mimic the genetic condition of Lgals3a depletion, present in our model, in the above-mentioned transgenic lines. These studies should help to clarify if the dysregulation of Gal-3 could be relevant in the inflammatory processes that characterize several cardiac diseases, including AC. Surprisingly, these two inflammatory factors did not present anymore a downregulation pattern in 1-year-old adult mutant zebrafish heart, as in larvae. We tried to explain this change knowing that these two factors, while controlled by Gal-3, are also stimulated and controlled by other players such as T lymphocytes, natural killer (NK) cells, B cells, vascular endothelial cells (ECs), smooth muscle cells (SMCs) and fibroblasts (Parameswaran and Patial, 2010; Schmidt-Arras and Rose-John, 2016). Therefore, assuming the possible presence of an inflammatory response and the subsequent overexpression of these factors by other inflammatory cells, counteracting the downregulation due to Gal-3 halve expression, we can explain the observed not dysregulated condition, different from the one detected at the larval stage. This hypothesis has to be validated by immunohistochemistry analysis of inflammatory response in sections of adult mutant hearts, although it could be challenging to see due to its probably acute and not chronic pattern (Henderson and Sethi, 2009). For this reason, we

chose to investigate first the possible presence of an inflammatory process in the cardiac region of mutated larvae. Interestingly, we found a significant increase in the presence of L-Plastin-positive inflammatory cells in the cardiac region of mutant larvae, if compared to the WT ones. These results told us that Lgals3 is certainly involved in the development and remarkable increase of the inflammatory response in the cardiac tissue (Papaspyridonos et al., 2008; Henderson and Sethi, 2009), likely trough macrophages activation and recruitment and apoptotic/necropoptic stimuli. Lgals3 downregulation could mitigate these events, reducing also inflammatory factors expressions such as TNF-α and IL-6; nonetheless, this reduction appears not prominent in our model, where the inflammatory response is still present. We believe that the observed inflammation in the cardiac region is mainly due to the instability in the cardiomyocyte cell-to-cell junctions, supposing that Lgals3 has a double role if dysregulated, both causing and mitigating the inflammatory response. This result will be crucial to understand the multiple roles of this protein in cardiac disorders, which change depending on its levels of expression, considering that Lgals3 can be found upregulated during inflammatory acute phases of the disease, but also mutated or not functional anymore in AC patients (Cason et al., 2021). Therefore, in conclusion, this *lgals3a-KO* zebrafish model appears a suitable system to study common aspects of cardiac disease pathogenesis, such as inflammation and cell death phenomena, and is fundamental to better understand Lgals3 modulatory role in diseases with cardiac involvement such as AC. Moreover, we confirmed the direct contribution of this protein in the stabilization of the cell-cell junctions and tissue integrity, suggesting that it could be also one of the main triggers of cardiac diseases, being a causative gene by itself. Its involvement also in the dysregulation of signalling pathways directly connected with cardiac tissue regeneration and remodelling corroborates this idea. We do not know yet if, alone, it is able to cause AC when mutated, but our data undoubtedly connected this gene with the disease pathogenesis in general, making it a possible biomarker for different steps of the diseases, due to its variable expression during the disease progression. Moreover, by modulating its expression, which is “phase-dependent”, it will be possible to cure or even prevent the onset and the progression of the disease.

REFERENCES

Ahmed, H., Du, S.-J., O'Leary, N., and Vasta, G. R. (2004). Biochemical and molecular characterization of galectins from zebrafish (Danio rerio): notochord-specific expression of a prototype galectin during early embryogenesis. *Glycobiology* 14, 219–232. doi: 10.1093/glycob/cwh032.

Akdis, D., Saguner, A. M., Shah, K., Wei, C., Medeiros-Domingo, A., von Eckardstein, A., et al. (2017). Sex hormones affect outcome in arrhythmogenic right ventricular cardiomyopathy/dysplasia: from a stem cell derived cardiomyocyte-based model to clinical biomarkers of disease outcome. *Eur Heart J* 38, 1498–1508. doi: 10.1093/eurheartj/ehx011.

Alcalai, R., Metzger, S., Rosenheck, S., Meiner, V., and Chajek-Shaul, T. (2003). A recessive mutation in desmoplakin causes arrhythmogenic right ventricular dysplasia, skin disorder, and woolly hair. *J Am Coll Cardiol* 42, 319–327. doi: 10.1016/s0735-1097(03)00628-4.

Al-Sabeq, B., Krahn, A. D., Conacher, S., Klein, G. J., and Laksman, Z. (2014). Arrhythmogenic right ventricular cardiomyopathy with recessive inheritance related to a new homozygous desmocollin-2 mutation. *Can J Cardiol* 30, 696.e1–3. doi: 10.1016/j.cjca.2014.01.014.

Al-Salam, S., Hashmi, S., Jagadeesh, G. S., and Tariq, S. (2020). Galectin-3: A Cardiomyocyte Antiapoptotic Mediator at 24-Hour Post Myocardial Infarction. *Cell Physiol Biochem* 54, 287–302. doi: 10.33594/000000220.

Al-Salam, S., Jagadeesh, G. S., Sudhadevi, M., Tageldeen, H., and Yasin, J. (2021). Galectin-3 Possesses Anti-Necroptotic and Anti-Apoptotic Effects in Cisplatin-Induced Acute Tubular Necrosis. *Cell Physiol Biochem* 55, 344–363. doi: 10.33594/000000381.

Alturfan, A. A., Basar, I., Emekli-Alturfan, E., Ayan, F., Koldas, L., and Emekli, N. (2014). Galectin-3 and plasma cytokines in patients with acute myocardial infarction. *Lab Med* 45, 336–341. doi: 10.1309/LM3JZKBDA7D4QFOC.

Argüeso, P., Mauris, J., and Uchino, Y. (2015). Galectin-3 as a regulator of the epithelial junction: Implications to wound repair and cancer. *Tissue Barriers* 3, e1026505. doi: 10.1080/21688370.2015.1026505.

Armstrong, D. K., McKenna, K. E., Purkis, P. E., Green, K. J., Eady, R. A., Leigh, I. M., et al. (1999). Haploinsufficiency of desmoplakin causes a striate subtype of palmoplantar keratoderma. *Hum Mol Genet* 8, 143–148. doi: 10.1093/hmg/8.1.143.

Arunachalam, M., Raja, M., Vijayakumar, C., Malaiammal, P., and Mayden, R. L. (2013). Natural history of zebrafish (Danio rerio) in India. *Zebrafish* 10, 1–14. doi: 10.1089/zeb.2012.0803.

Asimaki, A., Kapoor, S., Plovie, E., Karin Arndt, A., Adams, E., Liu, Z., et al. (2014). Identification of a new modulator of the intercalated disc in a zebrafish model of arrhythmogenic cardiomyopathy. *Sci Transl Med* 6, 240ra74. doi: 10.1126/scitranslmed.3008008.

Asimaki, A., Syrris, P., Wichter, T., Matthias, P., Saffitz, J. E., and McKenna, W. J. (2007). A novel dominant mutation in plakoglobin causes arrhythmogenic right ventricular cardiomyopathy. *Am J Hum Genet* 81, 964–973. doi: 10.1086/521633.

Askevold, E. T., Gullestad, L., Dahl, C. P., Yndestad, A., Ueland, T., and Aukrust, P. (2014). Interleukin-6 signaling, soluble glycoprotein 130, and inflammation in heart failure. *Curr Heart Fail Rep* 11, 146–155. doi: 10.1007/s11897-014-0185-9.

Austin, K. M., Trembley, M. A., Chandler, S. F., Sanders, S. P., Saffitz, J. E., Abrams, D. J., et al. (2019). Molecular mechanisms of arrhythmogenic cardiomyopathy. *Nat Rev Cardiol* 16, 519–537. doi: 10.1038/s41569-019-0200-7.

Awad, M. M., Calkins, H., and Judge, D. P. (2008). Mechanisms of disease: molecular genetics of arrhythmogenic right ventricular dysplasia/cardiomyopathy. *Nat Clin Pract Cardiovasc Med* 5, 258–267. doi: 10.1038/ncpcardio1182.

Barboni, E. A., Bawumia, S., Henrick, K., and Hughes, R. C. (2000). Molecular modeling and mutagenesis studies of the N-terminal domains of galectin-3: evidence for participation with the C-terminal carbohydrate recognition domain in oligosaccharide binding. *Glycobiology* 10, 1201–1208. doi: 10.1093/glycob/10.11.1201.

Basso, C., Bauce, B., Corrado, D., and Thiene, G. (2011). Pathophysiology of arrhythmogenic cardiomyopathy. *Nat Rev Cardiol* 9, 223–233. doi: 10.1038/nrcardio.2011.173.

Basso, C., Corrado, D., Marcus, F. I., Nava, A., and Thiene, G. (2009). Arrhythmogenic right ventricular cardiomyopathy. *Lancet* 373, 1289–1300. doi: 10.1016/S0140-6736(09)60256-7.

Basso, C., Czarnowska, E., Della Barbera, M., Bauce, B., Beffagna, G., Wlodarska, E. K., et al. (2006). Ultrastructural evidence of intercalated disc remodelling in arrhythmogenic right ventricular cardiomyopathy: an electron microscopy investigation on endomyocardial biopsies. *Eur Heart J* 27, 1847–1854. doi: 10.1093/eurheartj/ehl095.

Basso, C., Thiene, G., Corrado, D., Angelini, A., Nava, A., and Valente, M. (1996). Arrhythmogenic right ventricular cardiomyopathy. Dysplasia, dystrophy, or myocarditis? *Circulation* 94, 983–991. doi: 10.1161/01.cir.94.5.983.

Bass-Zubek, A. E., Hobbs, R. P., Amargo, E. V., Garcia, N. J., Hsieh, S. N., Chen, X., et al. (2008). Plakophilin 2: a critical scaffold for PKC alpha that

regulates intercellular junction assembly. *J Cell Biol* 181, 605–613. doi: 10.1083/jcb.200712133.

Bauce, B., Nava, A., Beffagna, G., Basso, C., Lorenzon, A., Smaniotto, G., et al. (2010). Multiple mutations in desmosomal proteins encoding genes in arrhythmogenic right ventricular cardiomyopathy/dysplasia. *Heart Rhythm* 7, 22–29. doi: 10.1016/j.hrthm.2009.09.070.

Beffagna, G., De Bortoli, M., Nava, A., Salamon, M., Lorenzon, A., Zaccolo, M., et al. (2007). Missense mutations in desmocollin-2 N-terminus, associated with arrhythmogenic right ventricular cardiomyopathy, affect intracellular localization of desmocollin-2 in vitro. *BMC Med Genet* 8, 65. doi: 10.1186/1471-2350-8-65.

Beffagna, G., Occhi, G., Nava, A., Vitiello, L., Ditadi, A., Basso, C., et al. (2005). Regulatory mutations in transforming growth factor-beta3 gene cause arrhythmogenic right ventricular cardiomyopathy type 1. *Cardiovasc Res* 65, 366–373. doi: 10.1016/j.cardiores.2004.10.005.

Bennett, R. G., Haqqani, H. M., Berruezo, A., Della Bella, P., Marchlinski, F. E., Hsu, C.-J., et al. (2019). Arrhythmogenic Cardiomyopathy in 2018-2019: ARVC/ALVC or Both? *Heart Lung Circ* 28, 164–177. doi: 10.1016/j.hlc.2018.10.013.

Benslimane, F. M., Zakaria, Z. Z., Shurbaji, S., Abdelrasool, M. K. A., Al-Badr, M. A. H. I., Al Absi, E. S. K., et al. (2020). Cardiac function and blood flow hemodynamics assessment of zebrafish (Danio rerio) using high-speed video microscopy. *Micron* 136, 102876. doi: 10.1016/j.micron.2020.102876.

Ben-Ze'ev, A., Shtutman, M., and Zhurinsky, J. (2000). The integration of cell adhesion with gene expression: the role of beta-catenin. *Exp Cell Res* 261, 75–82. doi: 10.1006/excr.2000.5045.

Bierkamp, C., Mclaughlin, K. J., Schwarz, H., Huber, O., and Kemler, R. (1996). Embryonic heart and skin defects in mice lacking plakoglobin. *Dev Biol* 180, 780–785. doi: 10.1006/dbio.1996.0346.

Biernacka, A., Dobaczewski, M., and Frangogiannis, N. G. (2011). TGF-β signaling in fibrosis. *Growth Factors* 29, 196–202. doi: 10.3109/08977194.2011.595714.

Blanda, V., Bracale, U. M., Di Taranto, M. D., and Fortunato, G. (2020). Galectin-3 in Cardiovascular Diseases. *IJMS* 21, 9232. doi: 10.3390/ijms21239232.

Bomma, C., Rutberg, J., Tandri, H., Nasir, K., Roguin, A., Tichnell, C., et al. (2004). Misdiagnosis of arrhythmogenic right ventricular dysplasia/cardiomyopathy. *J Cardiovasc Electrophysiol* 15, 300–306. doi: 10.1046/j.1540-8167.2004.03429.x.

Bondue, A., Arbustini, E., Bianco, A., Ciccarelli, M., Dawson, D., De Rosa, M., et al. (2018). Complex roads from genotype to phenotype in dilated cardiomyopathy: scientific update from the Working Group of Myocardial Function of the European Society of Cardiology. *Cardiovasc Res* 114, 1287–1303. doi: 10.1093/cvr/cvy122.

Boopathy, G. T. K., and Hong, W. (2019). Role of Hippo Pathway-YAP/TAZ Signaling in Angiogenesis. *Front Cell Dev Biol* 7, 49. doi: 10.3389/fcell.2019.00049.

Boscher, C., Zheng, Y. Z., Lakshminarayan, R., Johannes, L., Dennis, J. W., Foster, L. J., et al. (2012). Galectin-3 protein regulates mobility of N-cadherin and GM1 ganglioside at cell-cell junctions of mammary carcinoma cells. *J Biol Chem* 287, 32940–32952. doi: 10.1074/jbc.M112.353334.

Bowley, G., Kugler, E., Wilkinson, R., Lawrie, A., van Eeden, F., Chico, T. J. A., et al. (2022). Zebrafish as a tractable model of human cardiovascular disease. *Br J Pharmacol* 179, 900–917. doi: 10.1111/bph.15473.

Brade, T., Männer, J., and Kühl, M. (2006). The role of Wnt signalling in cardiac development and tissue remodelling in the mature heart. *Cardiovasc Res* 72, 198–209. doi: 10.1016/j.cardiores.2006.06.025.

Burlacu, A. (2003). Regulation of apoptosis by Bcl-2 family proteins. *J Cell Mol Med* 7, 249–257. doi: 10.1111/j.1582-4934.2003.tb00225.x.

Cabral, R. M., Liu, L., Hogan, C., Dopping-Hepenstal, P. J. C., Winik, B. C., Asial, R. A., et al. (2010). Homozygous mutations in the 5' region of the JUP gene result in cutaneous disease but normal heart development in children. *J Invest Dermatol* 130, 1543–1550. doi: 10.1038/jid.2010.7.

Calore, M., Lorenzon, A., De Bortoli, M., Poloni, G., and Rampazzo, A. (2015). Arrhythmogenic cardiomyopathy: a disease of intercalated discs. *Cell Tissue Res* 360, 491–500. doi: 10.1007/s00441-014-2015-5.

Carvajal-Huerta, L. (1998). Epidermolytic palmoplantar keratoderma with woolly hair and dilated cardiomyopathy. *J Am Acad Dermatol* 39, 418–421. doi: 10.1016/s0190-9622(98)70317-2.

Cason, M., Celeghin, R., Marinas, M. B., Beffagna, G., Della Barbera, M., Rizzo, S., et al. (2021). Novel pathogenic role for galectin-3 in early disease stages of arrhythmogenic cardiomyopathy. *Heart Rhythm* 18, 1394–1403. doi: 10.1016/j.hrthm.2021.04.006.

Cecchinelli, B., Lavra, L., Rinaldo, C., Iacovelli, S., Gurtner, A., Gasbarri, A., et al. (2006). Repression of the antiapoptotic molecule galectin-3 by homeodomain-interacting protein kinase 2-activated p53 is required for p53-induced apoptosis. *Mol Cell Biol* 26, 4746–4757. doi: 10.1128/MCB.00959-05.

Celeghin, R., Cipriani, A., Bariani, R., Bueno Marinas, M., Cason, M., Bevilacqua, M., et al. (2022). Filamin-C variant-associated cardiomyopathy: A pooled analysis of individual patient data to evaluate the clinical profile and risk of sudden cardiac death. *Heart Rhythm* 19, 235–243. doi: 10.1016/j.hrthm.2021.09.029.

Centelles, J. J. (2012). General aspects of colorectal cancer. *ISRN Oncol* 2012, 139268. doi: 10.5402/2012/139268.

Chelko, S. P., Asimaki, A., Andersen, P., Bedja, D., Amat-Alarcon, N., DeMazumder, D., et al. (2016). Central role for GSK3β in the pathogenesis of arrhythmogenic cardiomyopathy. *JCI Insight* 1, 85923. doi: 10.1172/jci.insight.85923.

Chen, K., Fan, Y., Gu, J., Han, Z., Wang, Y., Gao, L., et al. (2021). Effect of lgals3a on embryo development of zebrafish. *Transgenic Res* 30, 739–750. doi: 10.1007/s11248-021-00276-5.

Chen, S. N., Gurha, P., Lombardi, R., Ruggiero, A., Willerson, J. T., and Marian, A. J. (2014). The hippo pathway is activated and is a causal mechanism for adipogenesis in arrhythmogenic cardiomyopathy. *Circ Res* 114, 454–468. doi: 10.1161/CIRCRESAHA.114.302810.

Chen, X., Bonne, S., Hatzfeld, M., van Roy, F., and Green, K. J. (2002). Protein binding and functional characterization of plakophilin 2. Evidence for its diverse roles in desmosomes and beta -catenin signaling. *J Biol Chem* 277, 10512–10522. doi: 10.1074/jbc.M108765200.

Chen, X., Li, Y., Luo, J., and Hou, N. (2020). Molecular Mechanism of Hippo-YAP1/TAZ Pathway in Heart Development, Disease, and Regeneration. *Front Physiol* 11, 389. doi: 10.3389/fphys.2020.00389.

Chitaev, N. A., Leube, R. E., Troyanovsky, R. B., Eshkind, L. G., Franke, W. W., and Troyanovsky, S. M. (1996). The binding of plakoglobin to desmosomal cadherins: patterns of binding sites and topogenic potential. *J Cell Biol* 133, 359–369. doi: 10.1083/jcb.133.2.359.

Choudhary, N., Tompkins, C., Polonsky, B., McNitt, S., Calkins, H., Mark Estes, N. A., et al. (2016). Clinical Presentation and Outcomes by Sex in Arrhythmogenic Right Ventricular Cardiomyopathy: Findings from the North American ARVC Registry. *J Cardiovasc Electrophysiol* 27, 555–562. doi: 10.1111/jce.12947.

Clevers, H., and Nusse, R. (2012). Wnt/β-catenin signaling and disease. *Cell* 149, 1192–1205. doi: 10.1016/j.cell.2012.05.012.

Coonar, A. S., Protonotarios, N., Tsatsopoulou, A., Needham, E. W., Houlston, R. S., Cliff, S., et al. (1998). Gene for arrhythmogenic right ventricular cardiomyopathy with diffuse nonepidermolytic palmoplantar keratoderma and woolly hair (Naxos disease) maps to 17q21. *Circulation* 97, 2049–2058. doi: 10.1161/01.cir.97.20.2049.

Corrado, D., Basso, C., and Judge, D. P. (2017). Arrhythmogenic Cardiomyopathy. *Circ Res* 121, 784–802. doi: 10.1161/CIRCRESAHA.117.309345.

Corrado, D., Basso, C., Pavei, A., Michieli, P., Schiavon, M., and Thiene, G. (2006). Trends in sudden cardiovascular death in young competitive athletes after implementation of a preparticipation screening program. *JAMA* 296, 1593–1601. doi: 10.1001/jama.296.13.1593.

Corrado, D., Basso, C., Rizzoli, G., Schiavon, M., and Thiene, G. (2003). Does sports activity enhance the risk of sudden death in adolescents and young adults? *J Am Coll Cardiol* 42, 1959–1963. doi: 10.1016/j.jacc.2003.03.002.

Corrado, D., Basso, C., Thiene, G., McKenna, W. J., Davies, M. J., Fontaliran, F., et al. (1997). Spectrum of clinicopathologic manifestations of arrhythmogenic right ventricular cardiomyopathy/dysplasia: a multicenter study. *J Am Coll Cardiol* 30, 1512–1520. doi: 10.1016/s0735-1097(97)00332-x.

Corrado, D., Fontaine, G., Marcus, F. I., McKenna, W. J., Nava, A., Thiene, G., et al. (2000). Arrhythmogenic right ventricular dysplasia/cardiomyopathy: need for an international registry. Study Group on Arrhythmogenic Right Ventricular Dysplasia/Cardiomyopathy of the Working Groups on Myocardial and Pericardial Disease and Arrhythmias of the European Society of Cardiology and of the Scientific Council on Cardiomyopathies of the World Heart Federation. *Circulation* 101, E101-106. doi: 10.1161/01.cir.101.11.e101.

Corrado, D., Perazzolo Marra, M., Zorzi, A., Beffagna, G., Cipriani, A., Lazzari, M. D., et al. (2020). Diagnosis of arrhythmogenic cardiomyopathy: The Padua criteria. *Int J Cardiol* 319, 106–114. doi: 10.1016/j.ijcard.2020.06.005.

Corrado, D., and Thiene, G. (2006). Arrhythmogenic right ventricular cardiomyopathy/dysplasia: clinical impact of molecular genetic studies. *Circulation* 113, 1634–1637. doi: 10.1161/CIRCULATIONAHA.105.616490.

Corrado, D., Thiene, G., Nava, A., Rossi, L., and Pennelli, N. (1990). Sudden death in young competitive athletes: clinicopathologic correlations in 22 cases. *Am J Med* 89, 588–596. doi: 10.1016/0002-9343(90)90176-e.

Cox, M. G. P. J., van der Zwaag, P. A., van der Werf, C., van der Smagt, J. J., Noorman, M., Bhuiyan, Z. A., et al. (2011). Arrhythmogenic right ventricular dysplasia/cardiomyopathy: pathogenic desmosome mutations in index-patients predict outcome of family screening: Dutch arrhythmogenic right ventricular dysplasia/cardiomyopathy genotype-phenotype follow-up study. *Circulation* 123, 2690–2700. doi: 10.1161/CIRCULATIONAHA.110.988287.

Dahm, R., and Geisler, R. (2006). Learning from small fry: the zebrafish as a genetic model organism for aquaculture fish species. *Mar Biotechnol (NY)* 8, 329–345. doi: 10.1007/s10126-006-5139-0.

Dawson, K., Aflaki, M., and Nattel, S. (2013). Role of the Wnt-Frizzled system in cardiac pathophysiology: a rapidly developing, poorly understood area with enormous potential. *J Physiol* 591, 1409–1432. doi: 10.1113/jphysiol.2012.235382.

de Jong, S., van Veen, T. A. B., van Rijen, H. V. M., and de Bakker, J. M. T. (2011). Fibrosis and cardiac arrhythmias. *J Cardiovasc Pharmacol* 57, 630–638. doi: 10.1097/FJC.0b013e318207a35f.

Delmar, M., and McKenna, W. J. (2010). The cardiac desmosome and arrhythmogenic cardiomyopathies: from gene to disease. *Circ Res* 107, 700–714. doi: 10.1161/CIRCRESAHA.110.223412.

Delva, E., Tucker, D. K., and Kowalczyk, A. P. (2009). The desmosome. *Cold Spring Harb Perspect Biol* 1, a002543. doi: 10.1101/cshperspect.a002543.

Derynck, R., and Budi, E. H. (2019). Specificity, versatility, and control of TGF-β family signaling. *Sci Signal* 12, eaav5183. doi: 10.1126/scisignal.aav5183.

Dobaczewski, M., Chen, W., and Frangogiannis, N. G. (2011). Transforming growth factor (TGF)-β signaling in cardiac remodeling. *J Mol Cell Cardiol* 51, 600–606. doi: 10.1016/j.yjmcc.2010.10.033.

Dominguez, F., Zorio, E., Jimenez-Jaimez, J., Salguero-Bodes, R., Zwart, R., Gonzalez-Lopez, E., et al. (2020). Clinical characteristics and determinants of the phenotype in TMEM43 arrhythmogenic right ventricular cardiomyopathy type 5. *Heart Rhythm* 17, 945–954. doi: 10.1016/j.hrthm.2020.01.035.

Dumic, J., Dabelic, S., and Flögel, M. (2006). Galectin-3: an open-ended story. *Biochim Biophys Acta* 1760, 616–635. doi: 10.1016/j.bbagen.2005.12.020.

Elliott, P., Andersson, B., Arbustini, E., Bilinska, Z., Cecchi, F., Charron, P., et al. (2008). Classification of the cardiomyopathies: a position statement from the European Society Of Cardiology Working Group on Myocardial and Pericardial Diseases. *Eur Heart J* 29, 270–276. doi: 10.1093/eurheartj/ehm342.

Eshkind, L., Tian, Q., Schmidt, A., Franke, W. W., Windoffer, R., and Leube, R. E. (2002). Loss of desmoglein 2 suggests essential functions for early embryonic development and proliferation of embryonal stem cells. *Eur J Cell Biol* 81, 592–598. doi: 10.1078/0171-9335-00278.

Estigoy, C. B., Pontén, F., Odeberg, J., Herbert, B., Guilhaus, M., Charleston, M., et al. (2009). Intercalated discs: multiple proteins perform multiple functions in non-failing and failing human hearts. *Biophys Rev* 1, 43. doi: 10.1007/s12551-008-0007-y.

Ferrigno, O., Lallemand, F., Verrecchia, F., L'Hoste, S., Camonis, J., Atfi, A., et al. (2002). Yes-associated protein (YAP65) interacts with Smad7 and potentiates its inhibitory activity against TGF-beta/Smad signaling. *Oncogene* 21, 4879–4884. doi: 10.1038/sj.onc.1205623.

Fontaine, G., Fontaliran, F., and Frank, R. (1998). Arrhythmogenic right ventricular cardiomyopathies: clinical forms and main differential diagnoses. *Circulation* 97, 1532–1535. doi: 10.1161/01.cir.97.16.1532.

Fontaine, G., Frank, R., Guiraudon, G., Pavie, A., Tereau, Y., Chomette, G., et al. (1984). [Significance of intraventricular conduction disorders observed in arrhythmogenic right ventricular dysplasia]. *Arch Mal Coeur Vaiss* 77, 872–879.

Franceschetti, A. T., Reinhart, V., and Schnyder, U. W. (1972). [Meleda disease]. *J Genet Hum* 20, 267–296.

Frangogiannis, N. G. (2022). Transforming growth factor-β in myocardial disease. *Nat Rev Cardiol* 19, 435–455. doi: 10.1038/s41569-021-00646-w.

Frank, R., Fontaine, G., Vedel, J., Mialet, G., Sol, C., Guiraudon, G., et al. (1978). [Electrocardiology of 4 cases of right ventricular dysplasia inducing arrhythmia]. *Arch Mal Coeur Vaiss* 71, 963–972.

Fressart, V., Duthoit, G., Donal, E., Probst, V., Deharo, J.-C., Chevalier, P., et al. (2010). Desmosomal gene analysis in arrhythmogenic right ventricular dysplasia/cardiomyopathy: spectrum of mutations and clinical impact in practice. *Europace* 12, 861–868. doi: 10.1093/europace/euq104.

Frigeri, L. G., Zuberi, R. I., and Liu, F. T. (1993). Epsilon BP, a beta-galactoside-binding animal lectin, recognizes IgE receptor (Fc epsilon RI) and activates mast cells. *Biochemistry* 32, 7644–7649. doi: 10.1021/bi00081a007.

Fukumori, T., Takenaka, Y., Oka, N., Yoshii, T., Hogan, V., Inohara, H., et al. (2004). Endogenous galectin-3 determines the routing of CD95 apoptotic signaling pathways. *Cancer Res* 64, 3376–3379. doi: 10.1158/0008-5472.CAN-04-0336.

Gagnon, J. A., Valen, E., Thyme, S. B., Huang, P., Akhmetova, L., Ahkmetova, L., et al. (2014). Efficient mutagenesis by Cas9 protein-mediated oligonucleotide insertion and large-scale assessment of single-guide RNAs. *PLoS One* 9, e98186. doi: 10.1371/journal.pone.0098186.

Gallicano, G. I., Kouklis, P., Bauer, C., Yin, M., Vasioukhin, V., Degenstein, L., et al. (1998). Desmoplakin is required early in development for assembly of desmosomes and cytoskeletal linkage. *J Cell Biol* 143, 2009–2022. doi: 10.1083/jcb.143.7.2009.

Gandjbakhch, E., Charron, P., Fressart, V., Lorin de la Grandmaison, G., Simon, F., Gary, F., et al. (2011). Plakophilin 2A is the dominant isoform in human heart tissue: consequences for the genetic screening of arrhythmogenic right

ventricular cardiomyopathy. *Heart* 97, 844–849. doi: 10.1136/hrt.2010.205880.

Garcia-Gras, E., Lombardi, R., Giocondo, M. J., Willerson, J. T., Schneider, M. D., Khoury, D. S., et al. (2006). Suppression of canonical Wnt/beta-catenin signaling by nuclear plakoglobin recapitulates phenotype of arrhythmogenic right ventricular cardiomyopathy. *J Clin Invest* 116, 2012–2021. doi: 10.1172/JCI27751.

Garrod, D., and Chidgey, M. (2008). Desmosome structure, composition and function. *Biochim Biophys Acta* 1778, 572–587. doi: 10.1016/j.bbamem.2007.07.014.

Garrod, D. R., Berika, M. Y., Bardsley, W. F., Holmes, D., and Tabernero, L. (2005). Hyper-adhesion in desmosomes: its regulation in wound healing and possible relationship to cadherin crystal structure. *J Cell Sci* 118, 5743–5754. doi: 10.1242/jcs.02700.

Genge, C. E., Lin, E., Lee, L., Sheng, X., Rayani, K., Gunawan, M., et al. (2016). The Zebrafish Heart as a Model of Mammalian Cardiac Function. *Rev Physiol Biochem Pharmacol* 171, 99–136. doi: 10.1007/112_2016_5.

Gerull, B., Heuser, A., Wichter, T., Paul, M., Basson, C. T., McDermott, D. A., et al. (2004). Mutations in the desmosomal protein plakophilin-2 are common in arrhythmogenic right ventricular cardiomyopathy. *Nat Genet* 36, 1162–1164. doi: 10.1038/ng1461.

Gerull, B., Kirchner, F., Chong, J. X., Tagoe, J., Chandrasekharan, K., Strohm, O., et al. (2013). Homozygous founder mutation in desmocollin-2 (DSC2) causes arrhythmogenic cardiomyopathy in the Hutterite population. *Circ Cardiovasc Genet* 6, 327–336. doi: 10.1161/CIRCGENETICS.113.000097.

Gessert, S., and Kühl, M. (2010). The multiple phases and faces of wnt signaling during cardiac differentiation and development. *Circ Res* 107, 186–199. doi: 10.1161/CIRCRESAHA.110.221531.

Giardoglou, P., and Beis, D. (2019). On Zebrafish Disease Models and Matters of the Heart. *Biomedicines* 7, E15. doi: 10.3390/biomedicines7010015.

Gill, C., Mestril, R., and Samali, A. (2002). Losing heart: the role of apoptosis in heart disease--a novel therapeutic target? *FASEB J* 16, 135–146. doi: 10.1096/fj.01-0629com.

Giuliodori, A., Beffagna, G., Marchetto, G., Fornetto, C., Vanzi, F., Toppo, S., et al. (2018). Loss of cardiac Wnt/β-catenin signalling in desmoplakin-deficient AC8 zebrafish models is rescuable by genetic and pharmacological intervention. *Cardiovasc Res* 114, 1082–1097. doi: 10.1093/cvr/cvy057.

Glickman, N. S., and Yelon, D. (2002). Cardiac development in zebrafish: coordination of form and function. *Semin Cell Dev Biol* 13, 507–513. doi: 10.1016/s1084952102001040.

Goodwin, J. F. (1982). The frontiers of cardiomyopathy. *Br Heart J* 48, 1–18. doi: 10.1136/hrt.48.1.1.

Green, K. J., and Simpson, C. L. (2007). Desmosomes: new perspectives on a classic. *J Invest Dermatol* 127, 2499–2515. doi: 10.1038/sj.jid.5701015.

Groeneweg, J. A., Bhonsale, A., James, C. A., te Riele, A. S., Dooijes, D., Tichnell, C., et al. (2015). Clinical Presentation, Long-Term Follow-Up, and Outcomes of 1001 Arrhythmogenic Right Ventricular Dysplasia/Cardiomyopathy Patients and Family Members. *Circ Cardiovasc Genet* 8, 437–446. doi: 10.1161/CIRCGENETICS.114.001003.

Gross, A., Pack, L. A. P., Schacht, G. M., Kant, S., Ungewiss, H., Meir, M., et al. (2018). Desmoglein 2, but not desmocollin 2, protects intestinal epithelia from injury. *Mucosal Immunol* 11, 1630–1639. doi: 10.1038/s41385-018-0062-z.

Grossmann, K. S., Grund, C., Huelsken, J., Behrend, M., Erdmann, B., Franke, W. W., et al. (2004). Requirement of plakophilin 2 for heart morphogenesis and cardiac junction formation. *J Cell Biol* 167, 149–160. doi: 10.1083/jcb.200402096.

Hatzfeld, M. (1999). The armadillo family of structural proteins. *Int Rev Cytol* 186, 179–224. doi: 10.1016/s0074-7696(08)61054-2.

Hatzfeld, M. (2007). Plakophilins: Multifunctional proteins or just regulators of desmosomal adhesion? *Biochim Biophys Acta* 1773, 69–77. doi: 10.1016/j.bbamcr.2006.04.009.

Haywood, A. F. M., Merner, N. D., Hodgkinson, K. A., Houston, J., Syrris, P., Booth, V., et al. (2013). Recurrent missense mutations in TMEM43 (ARVD5) due to founder effects cause arrhythmogenic cardiomyopathies in the UK and Canada. *Eur Heart J* 34, 1002–1011. doi: 10.1093/eurheartj/ehs383.

Heallen, T., Zhang, M., Wang, J., Bonilla-Claudio, M., Klysik, E., Johnson, R. L., et al. (2011). Hippo pathway inhibits Wnt signaling to restrain cardiomyocyte proliferation and heart size. *Science* 332, 458–461. doi: 10.1126/science.1199010.

Heiden, T. C. K., Struble, C. A., Rise, M. L., Hessner, M. J., Hutz, R. J., and Carvan, M. J. (2008). Molecular targets of 2,3,7,8-tetrachlorodibenzo-p-dioxin (TCDD) within the zebrafish ovary: insights into TCDD-induced endocrine disruption and reproductive toxicity. *Reprod Toxicol* 25, 47–57. doi: 10.1016/j.reprotox.2007.07.013.

Heldin, C.-H., and Moustakas, A. (2016). Signaling Receptors for TGF-β Family Members. *Cold Spring Harb Perspect Biol* 8, a022053. doi: 10.1101/cshperspect.a022053.

Henderson, N. C., and Sethi, T. (2009). The regulation of inflammation by galectin-3. *Immunol Rev* 230, 160–171. doi: 10.1111/j.1600-065X.2009.00794.x.

Heuser, A., Plovie, E. R., Ellinor, P. T., Grossmann, K. S., Shin, J. T., Wichter, T., et al. (2006). Mutant desmocollin-2 causes arrhythmogenic right ventricular cardiomyopathy. *Am J Hum Genet* 79, 1081–1088. doi: 10.1086/509044.

Hoorntje, E. T., Te Rijdt, W. P., James, C. A., Pilichou, K., Basso, C., Judge, D. P., et al. (2017). Arrhythmogenic cardiomyopathy: pathology, genetics, and concepts in pathogenesis. *Cardiovasc Res* 113, 1521–1531. doi: 10.1093/cvr/cvx150.

Howe, K., Clark, M. D., Torroja, C. F., Torrance, J., Berthelot, C., Muffato, M., et al. (2013). The zebrafish reference genome sequence and its relationship to the human genome. *Nature* 496, 498–503. doi: 10.1038/nature12111.

Hu, Y., and Pu, W. T. (2014). Hippo activation in arrhythmogenic cardiomyopathy. *Circ Res* 114, 402–405. doi: 10.1161/CIRCRESAHA.113.303114.

Huber, O. (2003). Structure and function of desmosomal proteins and their role in development and disease. *Cell Mol Life Sci* 60, 1872–1890. doi: 10.1007/s00018-003-3050-7.

Hurley, I. A., Mueller, R. L., Dunn, K. A., Schmidt, E. J., Friedman, M., Ho, R. K., et al. (2007). A new time-scale for ray-finned fish evolution. *Proc Biol Sci* 274, 489–498. doi: 10.1098/rspb.2006.3749.

Ippel, H., Miller, M. C., Vértesy, S., Zheng, Y., Cañada, F. J., Suylen, D., et al. (2016). Intra- and intermolecular interactions of human galectin-3: assessment by full-assignment-based NMR. *Glycobiology* 26, 888–903. doi: 10.1093/glycob/cww021.

James, C. A., Bhonsale, A., Tichnell, C., Murray, B., Russell, S. D., Tandri, H., et al. (2013). Exercise increases age-related penetrance and arrhythmic risk in arrhythmogenic right ventricular dysplasia/cardiomyopathy-associated desmosomal mutation carriers. *J Am Coll Cardiol* 62, 1290–1297. doi: 10.1016/j.jacc.2013.06.033.

James, C. A., Jongbloed, J. D. H., Hershberger, R. E., Morales, A., Judge, D. P., Syrris, P., et al. (2021). International Evidence Based Reappraisal of Genes Associated With Arrhythmogenic Right Ventricular Cardiomyopathy Using the Clinical Genome Resource Framework. *Circ Genom Precis Med* 14, e003273. doi: 10.1161/CIRCGEN.120.003273.

Jiang, K., Rankin, C. R., Nava, P., Sumagin, R., Kamekura, R., Stowell, S. R., et al. (2014). Galectin-3 regulates desmoglein-2 and intestinal epithelial intercellular adhesion. *J Biol Chem* 289, 10510–10517. doi: 10.1074/jbc.M113.538538.

Joe, A. W. B., Yi, L., Natarajan, A., Le Grand, F., So, L., Wang, J., et al. (2010). Muscle injury activates resident fibro/adipogenic progenitors that facilitate myogenesis. *Nat Cell Biol* 12, 153–163. doi: 10.1038/ncb2015.

Kaplan, S. R., Gard, J. J., Carvajal-Huerta, L., Ruiz-Cabezas, J. C., Thiene, G., and Saffitz, J. E. (2004). Structural and molecular pathology of the heart in Carvajal syndrome. *Cardiovasc Pathol* 13, 26–32. doi: 10.1016/S1054-8807(03)00107-8.

Kimmel, C. B., Ballard, W. W., Kimmel, S. R., Ullmann, B., and Schilling, T. F. (1995). Stages of embryonic development of the zebrafish. *Dev Dyn* 203, 253–310. doi: 10.1002/aja.1002030302.

Kuwabara, I., and Liu, F. T. (1996). Galectin-3 promotes adhesion of human neutrophils to laminin. *J Immunol* 156, 3939–3944.

Lee, P., Peng, H., Gelbart, T., Wang, L., and Beutler, E. (2005). Regulation of hepcidin transcription by interleukin-1 and interleukin-6. *Proc Natl Acad Sci U S A* 102, 1906–1910. doi: 10.1073/pnas.0409808102.

Leung, C. L., Green, K. J., and Liem, R. K. H. (2002). Plakins: a family of versatile cytolinker proteins. *Trends Cell Biol* 12, 37–45. doi: 10.1016/s0962-8924(01)02180-8.

Li, M., Andersson-Lendahl, M., Sejersen, T., and Arner, A. (2013). Knockdown of desmin in zebrafish larvae affects interfilament spacing and mechanical properties of skeletal muscle. *J Gen Physiol* 141, 335–345. doi: 10.1085/jgp.201210915.

Li, Y.-J., Wei, Z.-M., Meng, Y.-X., and Ji, X.-R. (2005). Beta-catenin up-regulates the expression of cyclinD1, c-myc and MMP-7 in human pancreatic cancer: relationships with carcinogenesis and metastasis. *World J Gastroenterol* 11, 2117–2123. doi: 10.3748/wjg.v11.i14.2117.

Libro, R., Bramanti, P., and Mazzon, E. (2016). The role of the Wnt canonical signaling in neurodegenerative diseases. *Life Sci* 158, 78–88. doi: 10.1016/j.lfs.2016.06.024.

Lieschke, G. J., and Currie, P. D. (2007). Animal models of human disease: zebrafish swim into view. *Nat Rev Genet* 8, 353–367. doi: 10.1038/nrg2091.

Lin, Y.-N., Ibrahim, A., Marbán, E., and Cingolani, E. (2021). Pathogenesis of arrhythmogenic cardiomyopathy: role of inflammation. *Basic Res Cardiol* 116, 39. doi: 10.1007/s00395-021-00877-5.

Link, V., Shevchenko, A., and Heisenberg, C.-P. (2006). Proteomics of early zebrafish embryos. *BMC Dev Biol* 6, 1. doi: 10.1186/1471-213X-6-1.

Liu, F. T., Hsu, D. K., Zuberi, R. I., Kuwabara, I., Chi, E. Y., and Henderson, W. R. (1995). Expression and function of galectin-3, a beta-galactoside-binding

lectin, in human monocytes and macrophages. *Am J Pathol* 147, 1016–1028.

Liu, L., Sakai, T., Sano, N., and Fukui, K. (2004). Nucling mediates apoptosis by inhibiting expression of galectin-3 through interference with nuclear factor kappaB signalling. *Biochem J* 380, 31–41. doi: 10.1042/BJ20031300.

Lombardi, R., da Graca Cabreira-Hansen, M., Bell, A., Fromm, R. R., Willerson, J. T., and Marian, A. J. (2011). Nuclear plakoglobin is essential for differentiation of cardiac progenitor cells to adipocytes in arrhythmogenic right ventricular cardiomyopathy. *Circ Res* 109, 1342–1353. doi: 10.1161/CIRCRESAHA.111.255075.

Lopez-Ayala, J. M., Pastor-Quirante, F., Gonzalez-Carrillo, J., Lopez-Cuenca, D., Sanchez-Munoz, J. J., Oliva-Sandoval, M. J., et al. (2015). Genetics of myocarditis in arrhythmogenic right ventricular dysplasia. *Heart Rhythm* 12, 766–773. doi: 10.1016/j.hrthm.2015.01.001.

Lorenzon, A., Calore, M., Poloni, G., De Windt, L. J., Braghetta, P., and Rampazzo, A. (2017). Wnt/β-catenin pathway in arrhythmogenic cardiomyopathy. *Oncotarget* 8, 60640–60655. doi: 10.18632/oncotarget.17457.

Lorenzon, A., Pilichou, K., Rigato, I., Vazza, G., De Bortoli, M., Calore, M., et al. (2015). Homozygous Desmocollin-2 Mutations and Arrhythmogenic Cardiomyopathy. *Am J Cardiol* 116, 1245–1251. doi: 10.1016/j.amjcard.2015.07.037.

Lu, H.-Y., Shih, C.-M., Huang, C.-Y., Wu, A. T. H., Cheng, T.-M., Mi, F.-L., et al. (2020). Galectin-3 Modulates Macrophage Activation and Contributes Smooth Muscle Cells Apoptosis in Abdominal Aortic Aneurysm Pathogenesis. *Int J Mol Sci* 21, E8257. doi: 10.3390/ijms21218257.

Lubos, N., van der Gaag, S., Gerçek, M., Kant, S., Leube, R. E., and Krusche, C. A. (2020). Inflammation shapes pathogenesis of murine arrhythmogenic cardiomyopathy. *Basic Res Cardiol* 115, 42. doi: 10.1007/s00395-020-0803-5.

Lucon-Xiccato, T., Bella, L., Mainardi, E., Baraldi, M., Bottarelli, M., Sandonà, D., et al. (2021). An Automated Low-Cost Swim Tunnel for Measuring Swimming Performance in Fish. *Zebrafish* 18, 231–234. doi: 10.1089/zeb.2020.1975.

MacDonald, B. T., Tamai, K., and He, X. (2009). Wnt/beta-catenin signaling: components, mechanisms, and diseases. *Dev Cell* 17, 9–26. doi: 10.1016/j.devcel.2009.06.016.

Maione, A. S., Stadiotti, I., Pilato, C. A., Perrucci, G. L., Saverio, V., Catto, V., et al. (2021). Excess TGF-β1 Drives Cardiac Mesenchymal Stromal Cells to a Pro-Fibrotic Commitment in Arrhythmogenic Cardiomyopathy. *Int J Mol Sci* 22, 2673. doi: 10.3390/ijms22052673.

Maisch, B., Noutsias, M., Ruppert, V., Richter, A., and Pankuweit, S. (2012). Cardiomyopathies: classification, diagnosis, and treatment. *Heart Fail Clin* 8, 53–78. doi: 10.1016/j.hfc.2011.08.014.

Mallat, Z., Tedgui, A., Fontaliran, F., Frank, R., Durigon, M., and Fontaine, G. (1996). Evidence of apoptosis in arrhythmogenic right ventricular dysplasia. *N Engl J Med* 335, 1190–1196. doi: 10.1056/NEJM199610173351604.

Marcus, F. I., Fontaine, G. H., Guiraudon, G., Frank, R., Laurenceau, J. L., Malergue, C., et al. (1982). Right ventricular dysplasia: a report of 24 adult cases. *Circulation* 65, 384–398. doi: 10.1161/01.cir.65.2.384.

Marcus, F. I., McKenna, W. J., Sherrill, D., Basso, C., Bauce, B., Bluemke, D. A., et al. (2010). Diagnosis of arrhythmogenic right ventricular cardiomyopathy/dysplasia: proposed modification of the task force criteria. *Circulation* 121, 1533–1541. doi: 10.1161/CIRCULATIONAHA.108.840827.

Marcus, F. I., Zareba, W., Calkins, H., Towbin, J. A., Basso, C., Bluemke, D. A., et al. (2009). Arrhythmogenic right ventricular cardiomyopathy/dysplasia clinical presentation and diagnostic evaluation: results from the North American Multidisciplinary Study. *Heart Rhythm* 6, 984–992. doi: 10.1016/j.hrthm.2009.03.013.

Maron, B. J., Towbin, J. A., Thiene, G., Antzelevitch, C., Corrado, D., Arnett, D., et al. (2006). Contemporary definitions and classification of the cardiomyopathies: an American Heart Association Scientific Statement from the Council on Clinical Cardiology, Heart Failure and Transplantation Committee; Quality of Care and Outcomes Research and Functional Genomics and Translational Biology Interdisciplinary Working Groups; and Council on Epidemiology and Prevention. *Circulation* 113, 1807–1816. doi: 10.1161/CIRCULATIONAHA.106.174287.

Martin, E. D., Moriarty, M. A., Byrnes, L., and Grealy, M. (2009). Plakoglobin has both structural and signalling roles in zebrafish development. *Dev Biol* 327, 83–96. doi: 10.1016/j.ydbio.2008.11.036.

Mayosi, B. M., Fish, M., Shaboodien, G., Mastantuono, E., Kraus, S., Wieland, T., et al. (2017). Identification of Cadherin 2 (CDH2) Mutations in Arrhythmogenic Right Ventricular Cardiomyopathy. *Circ Cardiovasc Genet* 10, e001605. doi: 10.1161/CIRCGENETICS.116.001605.

Mazurek, N., Conklin, J., Byrd, J. C., Raz, A., and Bresalier, R. S. (2000). Phosphorylation of the beta-galactoside-binding protein galectin-3 modulates binding to its ligands. *J Biol Chem* 275, 36311–36315. doi: 10.1074/jbc.M003831200.

McCartan, C., Mason, R., Jayasinghe, S. R., and Griffiths, L. R. (2012). Cardiomyopathy classification: ongoing debate in the genomics era. *Biochem Res Int* 2012, 796926. doi: 10.1155/2012/796926.

McKenna, W. J., Thiene, G., Nava, A., Fontaliran, F., Blomstrom-Lundqvist, C., Fontaine, G., et al. (1994). Diagnosis of arrhythmogenic right ventricular dysplasia/cardiomyopathy. Task Force of the Working Group Myocardial and Pericardial Disease of the European Society of Cardiology and of the Scientific Council on Cardiomyopathies of the International Society and Federation of Cardiology. *Br Heart J* 71, 215–218. doi: 10.1136/hrt.71.3.215.

McKoy, G., Protonotarios, N., Crosby, A., Tsatsopoulou, A., Anastasakis, A., Coonar, A., et al. (2000). Identification of a deletion in plakoglobin in arrhythmogenic right ventricular cardiomyopathy with palmoplantar keratoderma and woolly hair (Naxos disease). *Lancet* 355, 2119–2124. doi: 10.1016/S0140-6736(00)02379-5.

Meeker, N. D., Hutchinson, S. A., Ho, L., and Trede, N. S. (2007). Method for isolation of PCR-ready genomic DNA from zebrafish tissues. *Biotechniques* 43, 610, 612, 614. doi: 10.2144/000112619.

Mehul, B., Bawumia, S., and Hughes, R. C. (1995). Cross-linking of galectin 3, a galactose-binding protein of mammalian cells, by tissue-type transglutaminase. *FEBS Lett* 360, 160–164. doi: 10.1016/0014-5793(95)00100-n.

Menon, R. P., and Hughes, R. C. (1999). Determinants in the N-terminal domains of galectin-3 for secretion by a novel pathway circumventing the endoplasmic reticulum-Golgi complex. *Eur J Biochem* 264, 569–576. doi: 10.1046/j.1432-1327.1999.00671.x.

Merner, N. D., Hodgkinson, K. A., Haywood, A. F. M., Connors, S., French, V. M., Drenckhahn, J.-D., et al. (2008). Arrhythmogenic right ventricular cardiomyopathy type 5 is a fully penetrant, lethal arrhythmic disorder caused by a missense mutation in the TMEM43 gene. *Am J Hum Genet* 82, 809–821. doi: 10.1016/j.ajhg.2008.01.010.

Merritt, A. J., Berika, M. Y., Zhai, W., Kirk, S. E., Ji, B., Hardman, M. J., et al. (2002). Suprabasal desmoglein 3 expression in the epidermis of transgenic mice results in hyperproliferation and abnormal differentiation. *Mol Cell Biol* 22, 5846–5858. doi: 10.1128/MCB.22.16.5846-5858.2002.

Mertens, C., Kuhn, C., and Franke, W. W. (1996). Plakophilins 2a and 2b: constitutive proteins of dual location in the karyoplasm and the desmosomal plaque. *J Cell Biol* 135, 1009–1025. doi: 10.1083/jcb.135.4.1009.

Mia, M. M., and Singh, M. K. (2019). The Hippo Signaling Pathway in Cardiac Development and Diseases. *Front Cell Dev Biol* 7, 211. doi: 10.3389/fcell.2019.00211.

Milting, H., Klauke, B., Christensen, A. H., Müsebeck, J., Walhorn, V., Grannemann, S., et al. (2015). The TMEM43 Newfoundland mutation p.S358L causing ARVC-5 was imported from Europe and increases the

stiffness of the cell nucleus. *Eur Heart J* 36, 872–881. doi: 10.1093/eurheartj/ehu077.

Moon, B. K., Lee, Y. J., Battle, P., Jessup, J. M., Raz, A., and Kim, H. R. (2001). Galectin-3 protects human breast carcinoma cells against nitric oxide-induced apoptosis: implication of galectin-3 function during metastasis. *Am J Pathol* 159, 1055–1060. doi: 10.1016/S0002-9440(10)61780-4.

Moriarty, M. A., Ryan, R., Lalor, P., Dockery, P., Byrnes, L., and Grealy, M. (2012). Loss of plakophilin 2 disrupts heart development in zebrafish. *Int J Dev Biol* 56, 711–718. doi: 10.1387/ijdb.113390mm.

Moro, E., Vettori, A., Porazzi, P., Schiavone, M., Rampazzo, E., Casari, A., et al. (2013). Generation and application of signaling pathway reporter lines in zebrafish. *Mol Genet Genomics* 288, 231–242. doi: 10.1007/s00438-013-0750-z.

Nagar, B., Overduin, M., Ikura, M., and Rini, J. M. (1996). Structural basis of calcium-induced E-cadherin rigidification and dimerization. *Nature* 380, 360–364. doi: 10.1038/380360a0.

Nangia-Makker, P., Nakahara, S., Hogan, V., and Raz, A. (2007). Galectin-3 in apoptosis, a novel therapeutic target. *J Bioenerg Biomembr* 39, 79–84. doi: 10.1007/s10863-006-9063-9.

Narula, J., Haider, N., Virmani, R., DiSalvo, T. G., Kolodgie, F. D., Hajjar, R. J., et al. (1996). Apoptosis in myocytes in end-stage heart failure. *N Engl J Med* 335, 1182–1189. doi: 10.1056/NEJM199610173351603.

Nava, A., Bauce, B., Basso, C., Muriago, M., Rampazzo, A., Villanova, C., et al. (2000). Clinical profile and long-term follow-up of 37 families with arrhythmogenic right ventricular cardiomyopathy. *J Am Coll Cardiol* 36, 2226–2233. doi: 10.1016/s0735-1097(00)00997-9.

Nava, A., Canciani, B., Buja, G., Martini, B., Daliento, L., Scognamiglio, R., et al. (1988). Electrovectorcardiographic study of negative T waves on precordial leads in arrhythmogenic right ventricular dysplasia: relationship with right ventricular volumes. *J Electrocardiol* 21, 239–245. doi: 10.1016/0022-0736(88)90098-2.

Neben, C. L., and Merrill, A. E. (2015). Signaling Pathways in Craniofacial Development: Insights from Rare Skeletal Disorders. *Curr Top Dev Biol* 115, 493–542. doi: 10.1016/bs.ctdb.2015.09.005.

Newlaczyl, A. U., and Yu, L.-G. (2011). Galectin-3--a jack-of-all-trades in cancer. *Cancer Lett* 313, 123–128. doi: 10.1016/j.canlet.2011.09.003.

Nio-Kobayashi, J. (2017). Tissue- and cell-specific localization of galectins, β-galactose-binding animal lectins, and their potential functions in health and disease. *Anat Sci Int* 92, 25–36. doi: 10.1007/s12565-016-0366-6.

Nirmala, J. G., and Lopus, M. (2020). Cell death mechanisms in eukaryotes. *Cell Biol Toxicol* 36, 145–164. doi: 10.1007/s10565-019-09496-2.

Norgett, E. E., Hatsell, S. J., Carvajal-Huerta, L., Cabezas, J. C., Common, J., Purkis, P. E., et al. (2000). Recessive mutation in desmoplakin disrupts desmoplakin-intermediate filament interactions and causes dilated cardiomyopathy, woolly hair and keratoderma. *Hum Mol Genet* 9, 2761–2766. doi: 10.1093/hmg/9.18.2761.

North, A. J., Bardsley, W. G., Hyam, J., Bornslaeger, E. A., Cordingley, H. C., Trinnaman, B., et al. (1999). Molecular map of the desmosomal plaque. *J Cell Sci* 112 (Pt 23), 4325–4336. doi: 10.1242/jcs.112.23.4325.

Nuber, U. A., Schäfer, S., Schmidt, A., Koch, P. J., and Franke, W. W. (1995). The widespread human desmocollin Dsc2 and tissue-specific patterns of synthesis of various desmocollin subtypes. *Eur J Cell Biol* 66, 69–74.

Ortiz-Genga, M. F., Cuenca, S., Dal Ferro, M., Zorio, E., Salgado-Aranda, R., Climent, V., et al. (2016). Truncating FLNC Mutations Are Associated With High-Risk Dilated and Arrhythmogenic Cardiomyopathies. *J Am Coll Cardiol* 68, 2440–2451. doi: 10.1016/j.jacc.2016.09.927.

Oz, F., Onur, I., Elitok, A., Ademoglu, E., Altun, I., Bilge, A. K., et al. (2017). Galectin-3 correlates with arrhythmogenic right ventricular cardiomyopathy and predicts the risk of ventricular -arrhythmias in patients with implantable defibrillators. *Acta Cardiol* 72, 453–459. doi: 10.1080/00015385.2017.1335371.

Pahnke, A., Conant, G., Huyer, L. D., Zhao, Y., Feric, N., and Radisic, M. (2016). The role of Wnt regulation in heart development, cardiac repair and disease: A tissue engineering perspective. *Biochem Biophys Res Commun* 473, 698–703. doi: 10.1016/j.bbrc.2015.11.060.

Papaspyridonos, M., McNeill, E., de Bono, J. P., Smith, A., Burnand, K. G., Channon, K. M., et al. (2008). Galectin-3 is an amplifier of inflammation in atherosclerotic plaque progression through macrophage activation and monocyte chemoattraction. *Arterioscler Thromb Vasc Biol* 28, 433–440. doi: 10.1161/ATVBAHA.107.159160.

Parameswaran, N., and Patial, S. (2010). Tumor necrosis factor-α signaling in macrophages. *Crit Rev Eukaryot Gene Expr* 20, 87–103. doi: 10.1615/critreveukargeneexpr.v20.i2.10.

Patrianakos, A. P., Protonotarios, N., Nyktari, E., Pagonidis, K., Tsatsopoulou, A., Parthenakis, F. I., et al. (2012). Arrhythmogenic right ventricular cardiomyopathy/dysplasia and troponin release. Myocarditis or the “hot phase” of the disease? *Int J Cardiol* 157, e26-28. doi: 10.1016/j.ijcard.2011.09.017.

Pauls, S., Zecchin, E., Tiso, N., Bortolussi, M., and Argenton, F. (2007). Function and regulation of zebrafish nkx2.2a during development of pancreatic islet and ducts. *Dev Biol* 304, 875–890. doi: 10.1016/j.ydbio.2007.01.024.

Peifer, M., Pai, L. M., and Casey, M. (1994). Phosphorylation of the Drosophila adherens junction protein Armadillo: roles for wingless signal and zeste-white 3 kinase. *Dev Biol* 166, 543–556. doi: 10.1006/dbio.1994.1336.

Pilichou, K., Lazzarini, E., Rigato, I., Celeghin, R., De Bortoli, M., Perazzolo Marra, M., et al. (2017). Large Genomic Rearrangements of Desmosomal Genes in Italian Arrhythmogenic Cardiomyopathy Patients. *Circ Arrhythm Electrophysiol* 10, e005324. doi: 10.1161/CIRCEP.117.005324.

Pilichou, K., Nava, A., Basso, C., Beffagna, G., Bauce, B., Lorenzon, A., et al. (2006). Mutations in desmoglein-2 gene are associated with arrhythmogenic right ventricular cardiomyopathy. *Circulation* 113, 1171–1179. doi: 10.1161/CIRCULATIONAHA.105.583674.

Pilichou, K., Remme, C. A., Basso, C., Campian, M. E., Rizzo, S., Barnett, P., et al. (2009). Myocyte necrosis underlies progressive myocardial dystrophy in mouse dsg2-related arrhythmogenic right ventricular cardiomyopathy. *J Exp Med* 206, 1787–1802. doi: 10.1084/jem.20090641.

Pilichou, K., Thiene, G., Bauce, B., Rigato, I., Lazzarini, E., Migliore, F., et al. (2016). Arrhythmogenic cardiomyopathy. *Orphanet J Rare Dis* 11, 33. doi: 10.1186/s13023-016-0407-1.

Porazzi, P., Marelli, F., Benato, F., de Filippis, T., Calebiro, D., Argenton, F., et al. (2012). Disruptions of global and JAGGED1-mediated notch signaling affect thyroid morphogenesis in the zebrafish. *Endocrinology* 153, 5645–5658. doi: 10.1210/en.2011-1888.

Poss, K. D., Wilson, L. G., and Keating, M. T. (2002). Heart regeneration in zebrafish. *Science* 298, 2188–2190. doi: 10.1126/science.1077857.

Postlethwait, J. H., Yan, Y. L., Gates, M. A., Horne, S., Amores, A., Brownlie, A., et al. (1998). Vertebrate genome evolution and the zebrafish gene map. *Nat Genet* 18, 345–349. doi: 10.1038/ng0498-345.

Protonotarios, A., Anastasakis, A., Panagiotakos, D. B., Antoniades, L., Syrris, P., Vouliotis, A., et al. (2016). Arrhythmic risk assessment in genotyped families with arrhythmogenic right ventricular cardiomyopathy. *Europace* 18, 610–616. doi: 10.1093/europace/euv061.

Protonotarios, N., Tsatsopoulou, A., Patsourakos, P., Alexopoulos, D., Gezerlis, P., Simitsis, S., et al. (1986). Cardiac abnormalities in familial palmoplantar keratosis. *Br Heart J* 56, 321–326. doi: 10.1136/hrt.56.4.321.

Qadri, S., Anttonen, O., Viikilä, J., Seppälä, E. H., Myllykangas, S., Alastalo, T.-P., et al. (2017). Case reports of two pedigrees with recessive arrhythmogenic right ventricular cardiomyopathy associated with

homozygous Thr335Ala variant in DSG2. *BMC Med Genet* 18, 86. doi: 10.1186/s12881-017-0442-3.

Quarta, G., Syrris, P., Ashworth, M., Jenkins, S., Zuborne Alapi, K., Morgan, J., et al. (2012). Mutations in the Lamin A/C gene mimic arrhythmogenic right ventricular cardiomyopathy. *Eur Heart J* 33, 1128–1136. doi: 10.1093/eurheartj/ehr451.

Rampazzo, A., Nava, A., Malacrida, S., Beffagna, G., Bauce, B., Rossi, V., et al. (2002). Mutation in human desmoplakin domain binding to plakoglobin causes a dominant form of arrhythmogenic right ventricular cardiomyopathy. *Am J Hum Genet* 71, 1200–1206. doi: 10.1086/344208.

Rayment, N. B., Haven, A. J., Madden, B., Murday, A., Trickey, R., Shipley, M., et al. (1999). Myocyte loss in chronic heart failure. *J Pathol* 188, 213–219. doi: 10.1002/(SICI)1096-9896(199906)188:2<213::AID-PATH348>3.0.CO;2-5.

Report of the WHO/ISFC task force on the definition and classification of cardiomyopathies (1980). *Br Heart J* 44, 672–673. doi: 10.1136/hrt.44.6.672.

Richardson, P., McKenna, W., Bristow, M., Maisch, B., Mautner, B., O'Connell, J., et al. (1996). Report of the 1995 World Health Organization/International Society and Federation of Cardiology Task Force on the Definition and Classification of cardiomyopathies. *Circulation* 93, 841–842. doi: 10.1161/01.cir.93.5.841.

Rigato, I., Bauce, B., Rampazzo, A., Zorzi, A., Pilichou, K., Mazzotti, E., et al. (2013). Compound and digenic heterozygosity predicts lifetime arrhythmic outcome and sudden cardiac death in desmosomal gene-related arrhythmogenic right ventricular cardiomyopathy. *Circ Cardiovasc Genet* 6, 533–542. doi: 10.1161/CIRCGENETICS.113.000288.

Risato, G., Celeghin, R., Brañas Casas, R., Dinarello, A., Zuppardo, A., Vettori, A., et al. (2022). Hyperactivation of Wnt/β-catenin and Jak/Stat3 pathways in human and zebrafish foetal growth restriction models: Implications for pharmacological rescue. *Front Cell Dev Biol* 10, 943127. doi: 10.3389/fcell.2022.943127.

Rizzo, S., Lodder, E. M., Verkerk, A. O., Wolswinkel, R., Beekman, L., Pilichou, K., et al. (2012). Intercalated disc abnormalities, reduced Na(+) current density, and conduction slowing in desmoglein-2 mutant mice prior to cardiomyopathic changes. *Cardiovasc Res* 95, 409–418. doi: 10.1093/cvr/cvs219.

Ruparelia, A. A., Oorschot, V., Vaz, R., Ramm, G., and Bryson-Richardson, R. J. (2014). Zebrafish models of BAG3 myofibrillar myopathy suggest a toxic gain of function leading to BAG3 insufficiency. *Acta Neuropathol* 128, 821–833. doi: 10.1007/s00401-014-1344-5.

Sanger, F., Nicklen, S., and Coulson, A. R. (1977). DNA sequencing with chain-terminating inhibitors. *Proc Natl Acad Sci U S A* 74, 5463–5467. doi: 10.1073/pnas.74.12.5463.

Sano, H., Hsu, D. K., Yu, L., Apgar, J. R., Kuwabara, I., Yamanaka, T., et al. (2000). Human galectin-3 is a novel chemoattractant for monocytes and macrophages. *J Immunol* 165, 2156–2164. doi: 10.4049/jimmunol.165.4.2156.

Sattar, Y., Abdullah, H. M., Neisani Samani, E., Myla, M., and Ullah, W. (2019). Arrhythmogenic Right Ventricular Cardiomyopathy/Dysplasia: An Updated Review of Diagnosis and Management. *Cureus* 11, e5381. doi: 10.7759/cureus.5381.

Schäfer, S., Koch, P. J., and Franke, W. W. (1994). Identification of the ubiquitous human desmoglein, Dsg2, and the expression catalogue of the desmoglein subfamily of desmosomal cadherins. *Exp Cell Res* 211, 391–399. doi: 10.1006/excr.1994.1103.

Schmidt-Arras, D., and Rose-John, S. (2016). IL-6 pathway in the liver: From physiopathology to therapy. *J Hepatol* 64, 1403–1415. doi: 10.1016/j.jhep.2016.02.004.

Sciacchitano, S., Lavra, L., Morgante, A., Ulivieri, A., Magi, F., De Francesco, G. P., et al. (2018). Galectin-3: One Molecule for an Alphabet of Diseases, from A to Z. *Int J Mol Sci* 19, E379. doi: 10.3390/ijms19020379.

Sehnert, A. J., and Stainier, D. Y. R. (2002). A window to the heart: can zebrafish mutants help us understand heart disease in humans? *Trends Genet* 18, 491–494. doi: 10.1016/s0168-9525(02)02766-x.

Sen-Chowdhry, S., Syrris, P., Prasad, S. K., Hughes, S. E., Merrifield, R., Ward, D., et al. (2008). Left-dominant arrhythmogenic cardiomyopathy: an under-recognized clinical entity. *J Am Coll Cardiol* 52, 2175–2187. doi: 10.1016/j.jacc.2008.09.019.

Shi, X., Chen, R., Zhang, Y., Yun, J., Brand-Arzamendi, K., Liu, X., et al. (2018). Zebrafish heart failure models: opportunities and challenges. *Amino Acids* 50, 787–798. doi: 10.1007/s00726-018-2578-7.

Shimada, C., Xu, R., Al-Alem, L., Stasenko, M., Spriggs, D. R., and Rueda, B. R. (2020). Galectins and Ovarian Cancer. *Cancers (Basel)* 12, E1421. doi: 10.3390/cancers12061421.

Silverman, A. M., Nakata, R., Shimada, H., Sposto, R., and DeClerck, Y. A. (2012). A galectin-3-dependent pathway upregulates interleukin-6 in the microenvironment of human neuroblastoma. *Cancer Res* 72, 2228–2238. doi: 10.1158/0008-5472.CAN-11-2165.

Simpson, M. A., Mansour, S., Ahnood, D., Kalidas, K., Patton, M. A., McKenna, W. J., et al. (2009). Homozygous mutation of desmocollin-2 in

arrhythmogenic right ventricular cardiomyopathy with mild palmoplantar keratoderma and woolly hair. *Cardiology* 113, 28–34. doi: 10.1159/000165696.

Slack, R. J., Mills, R., and Mackinnon, A. C. (2021). The therapeutic potential of galectin-3 inhibition in fibrotic disease. *Int J Biochem Cell Biol* 130, 105881. doi: 10.1016/j.biocel.2020.105881.

Song, S., Mazurek, N., Liu, C., Sun, Y., Ding, Q. Q., Liu, K., et al. (2009). Galectin-3 mediates nuclear beta-catenin accumulation and Wnt signaling in human colon cancer cells by regulation of glycogen synthase kinase-3beta activity. *Cancer Res* 69, 1343–1349. doi: 10.1158/0008-5472.CAN-08-4153.

Stappenbeck, T. S., Lamb, J. A., Corcoran, C. M., and Green, K. J. (1994). Phosphorylation of the desmoplakin COOH terminus negatively regulates its interaction with keratin intermediate filament networks. *J Biol Chem* 269, 29351–29354.

Sygitowicz, G., Maciejak-Jastrzębska, A., and Sitkiewicz, D. (2021). The Diagnostic and Therapeutic Potential of Galectin-3 in Cardiovascular Diseases. *Biomolecules* 12, 46. doi: 10.3390/biom12010046.

Syrris, P., Ward, D., Evans, A., Asimaki, A., Gandjbakhch, E., Sen-Chowdhry, S., et al. (2006). Arrhythmogenic right ventricular dysplasia/cardiomyopathy associated with mutations in the desmosomal gene desmocollin-2. *Am J Hum Genet* 79, 978–984. doi: 10.1086/509122.

Taylor, M., Graw, S., Sinagra, G., Barnes, C., Slavov, D., Brun, F., et al. (2011). Genetic variation in titin in arrhythmogenic right ventricular cardiomyopathy-overlap syndromes. *Circulation* 124, 876–885. doi: 10.1161/CIRCULATIONAHA.110.005405.

Thiene, G. (2015). The research venture in arrhythmogenic right ventricular cardiomyopathy: a paradigm of translational medicine. *Eur Heart J* 36, 837–846. doi: 10.1093/eurheartj/ehu493.

Thiene, G., Corrado, D., and Basso, C. (2004). Cardiomyopathies: is it time for a molecular classification? *Eur Heart J* 25, 1772–1775. doi: 10.1016/j.ehj.2004.07.026.

Thiene, G., Corrado, D., and Basso, C. (2007). Arrhythmogenic right ventricular cardiomyopathy/dysplasia. *Orphanet J Rare Dis* 2, 45. doi: 10.1186/1750-1172-2-45.

Thiene, G., Corrado, D., Nava, A., Rossi, L., Poletti, A., Boffa, G. M., et al. (1991). Right ventricular cardiomyopathy: is there evidence of an inflammatory aetiology? *Eur Heart J* 12 Suppl D, 22–25. doi: 10.1093/eurheartj/12.suppl_d.22.

Thiene, G., Nava, A., Corrado, D., Rossi, L., and Pennelli, N. (1988). Right ventricular cardiomyopathy and sudden death in young people. *N Engl J Med* 318, 129–133. doi: 10.1056/NEJM198801213180301.

Tiso, N., Stephan, D. A., Nava, A., Bagattin, A., Devaney, J. M., Stanchi, F., et al. (2001). Identification of mutations in the cardiac ryanodine receptor gene in families affected with arrhythmogenic right ventricular cardiomyopathy type 2 (ARVD2). *Hum Mol Genet* 10, 189–194. doi: 10.1093/hmg/10.3.189.

Tzavlaki, K., and Moustakas, A. (2020). TGF-β Signaling. *Biomolecules* 10, 487. doi: 10.3390/biom10030487.

Uezumi, A., Ito, T., Morikawa, D., Shimizu, N., Yoneda, T., Segawa, M., et al. (2011). Fibrosis and adipogenesis originate from a common mesenchymal progenitor in skeletal muscle. *J Cell Sci* 124, 3654–3664. doi: 10.1242/jcs.086629.

Uhl, H. S. M. (1952). A previously undescribed congenital malformation of the heart: almost total absence of the myocardium of the right ventricle. *Bull Johns Hopkins Hosp* 91, 197–209.

Valente, M., Calabrese, F., Thiene, G., Angelini, A., Basso, C., Nava, A., et al. (1998). In vivo evidence of apoptosis in arrhythmogenic right ventricular cardiomyopathy. *Am J Pathol* 152, 479–484.

van der Zwaag, P. A., van Rijsingen, I. A. W., Asimaki, A., Jongbloed, J. D. H., van Veldhuisen, D. J., Wiesfeld, A. C. P., et al. (2012). Phospholamban R14del mutation in patients diagnosed with dilated cardiomyopathy or arrhythmogenic right ventricular cardiomyopathy: evidence supporting the concept of arrhythmogenic cardiomyopathy. *Eur J Heart Fail* 14, 1199–1207. doi: 10.1093/eurjhf/hfs119.

van Hengel, J., Calore, M., Bauce, B., Dazzo, E., Mazzotti, E., De Bortoli, M., et al. (2013). Mutations in the area composita protein αT-catenin are associated with arrhythmogenic right ventricular cardiomyopathy. *Eur Heart J* 34, 201–210. doi: 10.1093/eurheartj/ehs373.

van Tintelen, J. P., Van Gelder, I. C., Asimaki, A., Suurmeijer, A. J. H., Wiesfeld, A. C. P., Jongbloed, J. D. H., et al. (2009). Severe cardiac phenotype with right ventricular predominance in a large cohort of patients with a single missense mutation in the DES gene. *Heart Rhythm* 6, 1574–1583. doi: 10.1016/j.hrthm.2009.07.041.

Vornanen, M., and Hassinen, M. (2016). Zebrafish heart as a model for human cardiac electrophysiology. *Channels (Austin)* 10, 101–110. doi: 10.1080/19336950.2015.1121335.

Warren, K. S., and Fishman, M. C. (1998). "Physiological genomics": mutant screens in zebrafish. *Am J Physiol* 275, H1-7. doi: 10.1152/ajpheart.1998.275.1.H1.

Xiao, M., Zhang, M., Bie, M., Wang, X., Guo, J., and Xiao, H. (2020). Galectin-3 Induces Atrial Fibrosis by Activating the TGF-β1/Smad Pathway in Patients with Atrial Fibrillation. *Cardiology* 145, 446–455. doi: 10.1159/000506072.

Xie, J., Wang, Y., Ai, D., Yao, L., and Jiang, H. (2022). The role of the Hippo pathway in heart disease. *FEBS J* 289, 5819–5833. doi: 10.1111/febs.16092.

Yang, H., Lei, C., and Zhang, W. (2012). Expression of galectin-3 in mouse endometrium and its effect during embryo implantation. *Reprod Biomed Online* 24, 116–122. doi: 10.1016/j.rbmo.2011.09.003.

Yang, H., Yin, J., Ficarrotta, K., Hsu, S. H., Zhang, W., and Cheng, C. (2016). Aberrant expression and hormonal regulation of Galectin-3 in endometriosis women with infertility. *J Endocrinol Invest* 39, 785–791. doi: 10.1007/s40618-016-0435-7.

Yang, R. Y., Hill, P. N., Hsu, D. K., and Liu, F. T. (1998). Role of the carboxyl-terminal lectin domain in self-association of galectin-3. *Biochemistry* 37, 4086–4092. doi: 10.1021/bi971409c.

Yang, R. Y., Hsu, D. K., and Liu, F. T. (1996). Expression of galectin-3 modulates T-cell growth and apoptosis. *Proc Natl Acad Sci U S A* 93, 6737–6742. doi: 10.1073/pnas.93.13.6737.

Yoshii, T., Fukumori, T., Honjo, Y., Inohara, H., Kim, H.-R. C., and Raz, A. (2002). Galectin-3 phosphorylation is required for its anti-apoptotic function and cell cycle arrest. *J Biol Chem* 277, 6852–6857. doi: 10.1074/jbc.M107668200.

Yost, C., Torres, M., Miller, J. R., Huang, E., Kimelman, D., and Moon, R. T. (1996). The axis-inducing activity, stability, and subcellular distribution of beta-catenin is regulated in Xenopus embryos by glycogen synthase kinase 3. *Genes Dev* 10, 1443–1454. doi: 10.1101/gad.10.12.1443.

Yousefi, F., Shabaninejad, Z., Vakili, S., Derakhshan, M., Movahedpour, A., Dabiri, H., et al. (2020). TGF-β and WNT signaling pathways in cardiac fibrosis: non-coding RNAs come into focus. *Cell Commun Signal* 18, 87. doi: 10.1186/s12964-020-00555-4.

Yu, L., Ruifrok, W. P. T., Meissner, M., Bos, E. M., van Goor, H., Sanjabi, B., et al. (2013). Genetic and pharmacological inhibition of galectin-3 prevents cardiac remodeling by interfering with myocardial fibrogenesis. *Circ Heart Fail* 6, 107–117. doi: 10.1161/CIRCHEARTFAILURE.112.971168.

Yuan, Z.-Y., Cheng, L.-T., Wang, Z.-F., and Wu, Y.-Q. (2021). Desmoplakin and clinical manifestations of desmoplakin cardiomyopathy. *Chin Med J (Engl)* 134, 1771–1779. doi: 10.1097/CM9.0000000000001581.

Zhao, G., Qiu, Y., Zhang, H. M., and Yang, D. (2019). Intercalated discs: cellular adhesion and signaling in heart health and diseases. *Heart Fail Rev* 24, 115–132. doi: 10.1007/s10741-018-9743-7.

Zhou, Q., Li, L., Zhao, B., and Guan, K.-L. (2015). The hippo pathway in heart development, regeneration, and diseases. *Circ Res* 116, 1431–1447. doi: 10.1161/CIRCRESAHA.116.303311.

Zorzi, A., Cipriani, A., Bariani, R., Pilichou, K., Corrado, D., and Bauce, B. (2021). Role of Exercise as a Modulating Factor in Arrhythmogenic Cardiomyopathy. *Curr Cardiol Rep* 23, 57. doi: 10.1007/s11886-021-01489-0.

Zorzi, A., Rigato, I., Pilichou, K., Perazzolo Marra, M., Migliore, F., Mazzotti, E., et al. (2016). Phenotypic expression is a prerequisite for malignant arrhythmic events and sudden cardiac death in arrhythmogenic right ventricular cardiomyopathy. *Europace* 18, 1086–1094. doi: 10.1093/europace/euv205.